THE IMPACT OF POOR POWER QUALITY AND HARMONICS ON THE PERFORMANCE OF AN ELECTRICAL POWER NETWORK

by

Mfanasibili Stanley Nkonyane

Student No: 20101392

A dissertation submitted in fulfillment of the requirements for the degree of Master of Engineering in the Department of Electrical Power Engineering
Faculty of Engineering and Built Environment

Supervisor: Dr. E.E. Ojo

Co-Supervisor**:** Dr. B.S. Rigby

2019

ABSTRACT

Poor power quality has a negative impact on electrical protection systems, rotating machines, transformers, control circuits, electronics, and power electronics equipment. The demand from industries to use power electronics equipment leads to more poor power quality issues – especially relating to harmonics. Determining the level of harmonics in an electrical network has become a necessity, as most electrical equipment are susceptible to harmonics. Previously, electrical networks on the customer side consisted mostly of direct current and induction motors, which resulted in simple networks that were easy to model using various types of simulation software. Today's electrical network is considered complex due to power electronic equipment such as variable frequency drives (VFDs), uninterruptible power supplies (UPSs), switch mode power supplies (SMPSs) and other electronics equipment. Power electronic equipment are primary source of harmonics and are also susceptible to harmonics. To protect the electrical network infrastructure, it is very important to identify the level of harmonics content in an electrical network, so that solutions can be developed to minimise the harmonic level to acceptable limits – as determined by power quality or harmonics standards.

This dissertation presents an analysis of the performance of an island electrical network for an offshore crude-oil drilling ship. A real-time digital simulator was used as a systematic analytical tool to study the level of harmonics in a reduced-scale electrical network model, used to represent the real drilling ship power network. The study objective was to evaluate the behaviour of the power network when direct on line (DOL) starters and variable frequency drives are used to run induction motors coupled with mechanical loads. The waveforms from a limited number of field measurements on the actual network are compared to those obtained from the reduced-scale real-time simulation model of the plant.

The study reviews the theory and literature of power quality, generators, transformers, variable frequency drives, and induction machines, and focuses on poor power quality as contributed to by harmonics. The investigation was based on 12 pulse rectifiers for all variable speed drives, which are standard for drilling ships and other offshore installations – as they offer advantages in reducing the fifth and seventh harmonics.

Both the field measurements and real-time simulation results in the dissertation indicate the presence of similar harmonic waveforms, and with comparable frequencies – but with different amplitudes. Unfortunately, the simulation results could not be closely matched to the field results, as most operating parameters that are needed for better representation of the plant in the simulation model, could not be obtained within the limited time available for field measurements. Nevertheless, the model developed could be used with a greater degree of accuracy to demonstrate the level of harmonics for an offshore drilling ship power network, provided all operating conditions' parameters are available.

DECLARATION OF ORIGINALITY

I, Mfanasibili Stanley Nkonyane, declare that the work hereby submitted for the degree of Master of Engineering at Durban University of Technology (DUT) is my own particular work and has not been beforehand submitted by me at another University for any degree. Where utilization has been made of the work of others, it has been appropriately recognized in the text and included in the lists of references.

This research was conducted at Durban University of Technology under the supervision of Dr. B.S. Rigby.

Submitted by:

Mfanasibili Nkonyane _____ _____

(BTech, SMSAIEE, MIEEE) Signature Date

APPROVED FOR FINAL SUBMISSION

Supervisor: Evans Ojo _____ _____

(BEng, MScEng, PhD, SAIMechE) Signature Date

Co-Supervisor: Bruce Rigby _____ _____

(BScEng, MScEng, PhD, MIEEE) Signature Date

DEDICATION

This dissertation is dedicated to my late mentor and brother, Kozana David Mokebe *and my late friend and brother,* Msawenkosi Jacob Masuku.

ACKNOWLEDGEMENTS

I would like to thank Dr. Rigby for supervising this work during my entire study period. Dr. Rigby provided guidance, advice and constant support and he put additional time and energy to horn my technical and writing skills.

The VSD modeling approach was derived from Mr. Chenal Palhad work. I would like to extend my thanks to Chenal for his valuable support, patience and sacrifices in assisting me with the VSD simulation model.

I would like to thank Durban University of Technology for allowing unrestricted use of their RTDS™ Technologies real-time digital simulator.

I would also like to thank the staff at Durban University of Technology, especially Brigitte Marie Le Breton and Regina Naidoo for their support during the course of my study.

I would like to thank ENSCO DS6 management for allowing the use of their electrical network as a case study.

A special thanks to Nkosinamandla Mvelase (Bozza) for editing and proof reading this work.

Finally, I wish to thank my family and friends for their understanding, patience, love, support and personal sacrifices each of you had to make during the years of my studies. To my daughters: Sphesihle, Slindokuhle and Thandokuhle, I know it has been a difficult period not seeing your father while other kids were enjoying quality time with their fathers.

Table of Contents

List of Figures

List of Tables

Acronyms

AC	Alternating Current
ABS	The American Bureau of Shipping
CSI	Current Source Inverter
DC	Direct Current
DOL	Direct On Line
EMC	Electromagnetic Compatibility
IEC	The International Electro-technical Commission
IEEE	The Institute of Electrical and Electronics Engineers Association
PCC	Point of Common Coupling
PQM	Power Quality Meter
RMS	Root Mean Square
SABS	The South African Bureau of Standards
SCR	Short-Circuit Ratio
SMPS	Switch Mode Power Supply
SPWM	Sinusoidal Pulse-Width Modulation
THD	Total Harmonic Distortion
VSI	Voltage Source Inverter

CHAPTER ONE

Introduction

1.1 General Background

Security of supply is critical for offshore crude-oil drillships, due to the nature and risks associated with crude-oil drilling and exploration activities. The power network of a drillship consists of various power electronics equipment due to drilling process requirements and the advantages offered by semi-conductor components. Historically, there have been numerous accidents on-board offshore drillships, and investigations into the real causes have yielded inconclusive results. Malfunctioning of equipment on offshore oil rigs often results in catastrophic failures that could lead to loss of lives - as it happened with the Deepwater Horizon in 2010 and the Piper Alpha incident in 1988.

Power electronics equipment are the main contributor of harmonics into the electrical network and causes poor power quality issues. Acceptable power quality allows electrical equipment to operate correctly without being damaged and stressed – while poor power quality causes electrical equipment to malfunction, become unreliable, and to get damaged. Malfunctioning of the measuring instruments used to detect gases from an open crude-oil well can result in the release of dangerous and explosive gases from the sea-bed, with disastrous consequences. Most previous studies indicate that malfunctioning of electrical equipment on an offshore drillship are due to poor power quality, as the electrical network does not adhere to any of the power quality standards given that it is not connected to a national grid.

The complex electrical network of an offshore installation results in complex power quality issues that provide challenges to electrical engineers. Harmonics are not healthy for any power network and need to be eliminated and managed, as their presence in an electrical network poses problems due to:

(i) electromechanical resonance that produces vibrations, noise and fatigue failure of mechanical components;
(ii) additional heating of cables, transformers and motors;
(iii) interference with communications and electronics circuits;
(iv) electrical resonance – resulting in potentially dangerous voltages and currents;
(v) Harmonics, which also causes errors in power calculations and nuisance tripping of protective devices.

Harmonics studies are complex in nature and require good knowledge of the mechanics and operations of electrical network parameters and loads.

In order to study the behaviour of complex electrical networks, simulation tools are used. Simulation can be thought of as a process of determining the behaviour of a physical system using mathematical models of that system – instead of via measurements on the system itself. The challenges presented by the complex electrical network have resulted in fast development of simulation tools. The two types of simulation tools used are the traditional method of simulation and real-time simulation. Both types have proven to be effective and efficient tools for identifying power quality issues. Nevertheless, real-time simulation is gaining widespread usage as it offers superior capabilities compared to traditional power simulation tools. The advantage of real-time simulation is that it allows the mathematical models to predict the behaviour of the power network under study in real-time.

This dissertation describes power quality issues – especially harmonics and the impact of poor power quality – on a drillship electrical network. This chapter presents the problem statement, the aim and objectives of the research, and also the study layout.

1.2 The Research Problem

The complexity of offshore operations for crude-oil drilling and exploration requires the usage of electrical adjustable frequency drives and other power electronics equipment. Variable frequency drives are standard equipment on-board a drillship and they generate harmonics that are harmful to the electrical

power network. As a result, their operations can potentially degrade the quality of electric power, resulting in loss of operational capability and equipment failure – with subsequent down-time. There are also various safety concerns.

Poor power quality in a drilling ship power network can cause premature equipment failure or malfunction as recorded in the ship computerised maintenance management system. There are other known disastrous events like the Piper Alpha disaster in 1988, the BP's Deepwater Horizon in 2010, and recently the explosion on the Chevron Nigeria Limited oil rig in 2012. Most root-cause analysis performed on electrical equipment is inconclusive – as the findings are based on safety and do not interrogate the impact of power quality on failures.

1.3 Aim and Objectives

1.3.1 Aim

The aim of this study was to develop a simplified offshore drillship electrical power network model – for the purpose of studying harmonics.

1.3.2 Objectives

The research objectives of this study were to:

- Investigate the content of harmonics on an offshore drillship power network, by taking field measurements using a power quality meter.
- Develop a simplified drillship electrical power network model for the purpose of harmonic studies.
- Recommend the adoption of harmonic limitation measures based on current standards.

1.4 Research Methodology

The research work undertaken comprises theory, field measurements and simulation. The methodology discussed below was applied in order to address the research objectives:

- The case study adopted was based on a drillship electrical network and field measurements were taken at various locations –, i.e. the 690V drilling system, 440V system and 230V system.
- A comprehensive review of issues related to harmonics, as generated by non-linear loads and various models, was undertaken.
- A model of a simplified representation of the drillship electrical network was developed and documented.
- The RTDS Real-Time simulator using RSCAD software, was used to simulate the simplified representation of the drillship electrical network, and measurements were taken on the simulation.
- A systematic approach methodology was developed to model the network, to take field measurements, and to assess and analyse the measurements.

The details of how the research was conducted are shown in a schematic diagram presented in Appendix I.

1.5 Dissertation Contributions

Due to the impact of poor power quality on an electrical network and the challenges imposed on electrical components, the output of this study will assist offshore installation operators to understand the impacts of harmonics on their electrical network and to encourage them to adhere to existing harmonics standards.

The research used small-time step modelling and a detailed real-time model was developed that can be duplicated for other offshore installation electrical networks. The custom-developed real-time model can be used to simulate various variable frequency drives integrated into an electrical network.

The final contribution is that the knowledge obtained from this study will assist operators to improve the design of new offshore installations and to adhere to standards.

1.6 Dissertation Layout

Chapter One provides an introduction and background to the study. The aim and objectives of the study are also presented.

Chapter Two provides the literature review in connection with the field of interest, which covers power quality and power electronics.

Chapter Three presents the theory of operation of the real-time simulation model of an electrical network consisting of induction motors and variable speed drive models, which are utilised in this study. The chapter then presents the development of the real-time model used for this study.

Chapter Four presents the results and discussion in connection with field measurements and simulation results.

Chapter Five provides the conclusions and recommendations of the study, which were derived from the results obtained in Chapter Four.

CHAPTER TWO

Literature Review

2.1 General Background

The main aim of this dissertation was to develop a model to study harmonics on a drilling ship electrical network. The reliability and stability of any electric power system is critical, especially for an island network where any instability can cause a blackout that is detrimental to a drillship due to the hazards associated with drilling operations. A drillship electrical network comprises linear and non-linear loads, causing power quality issues. Harmonic distortions cause poor power quality, and are a cause for concern for the stability and reliability of an electrical power system. There have been significant developments on standards and guidelines to address poor power quality issues, especially harmonics, in an electrical network.

The fundamentals of power quality are presented in this chapter, in order to explain the causes of harmonics and their impact on an electrical network. This literature study was undertaken to review models for induction motors and variable speed drives and transformers under harmonic polluted environments. Since harmonics in an island network are the main focus of this dissertation, the sources of harmonics are also presented. Finally, the chapter discusses the characteristics and modelling approaches of an induction motor, and of the selected variable speed drive.

2.2 Harmonic Standards

The main roles of power quality standards are to provide guidelines, recommendations and limits, in order to help assure compatibility between end-use equipment and the system where it is applied [1, 2, 3]. In a regular power network, in order for the power network to adhere to these power quality standards, the utility has to supply voltage that is within the tolerances and permissible voltage levels established by the standards, so that the life-span of the customer equipment is not reduced [4, 5, 6]. End-users are also

monitored and policed by the standards, so that the current drawn by the customer plant is within the limits set out by these standards, and such that it does not impact on the levels of voltage quality on the utility network [4, 5].

The utility and the end-user have shared responsibility, although power quality issues ultimately impact the end-user. The point of common coupling (PCC) between the utility and the end-user is the utility metering point, depending on the type of supply required by the customer. In low voltage supply, the PCC is the secondary side of the transformer. The following standards are guidelines for power quality especially harmonics:

- The Institute of Electrical and Electronics Engineers Standards Association (IEEE SA), developed the IEEE 519 Standard (Recommended Practices and Requirements for Harmonic Control in Electrical Power Systems), which provides limits for both the utility and end-user. The utility must control the harmonic voltage distortion within the limits that it can supply to the customer, while the end-user must control the harmonic current injected into the system. This study is based on the IEEE 519 standard.
- The International Electro-technical Commission (IEC) developed the Electromagnetic Compatibility (EMC) standards, to monitor and control power quality problems. The South African Bureau of Standards (SABS) is in partnership with IEC.
- The American Bureau of Shipping (ABS) Guidance Notes for Control of Harmonics in Electrical Power Systems has been developed specifically for on-board ships and the electrical power systems of offshore installations in order to raise awareness of the potential risks associated with harmonics.

The recommended harmonic indices by IEEE [4] are:

- Individual-harmonic and total-harmonic voltage distortion.
- Individual-harmonic and total-harmonic current distortion.
- Depth of notches, total notch area, and distortion of bus voltage by commutation notches (low-voltages).

This study uses indices of individual-harmonic and total-harmonic distortions of both current and voltage. The required characteristics of harmonic indices are that they should be simple, physically meaningful, and have strong correlations to the severity of the harmonic effects [4].

The acceptable limits for current harmonics listed in Table 2.1 are taken from the IEEE 519 standard, and are based on the size of the load with respect to the power system. I_{SC}/I_L is a short circuit ratio (SCR) that measures the size of the end-user plant relative to the capacity of the utility supply network at the end-user point of common coupling [2]. The short circuit ratio is also a factor that determines the sensitivity of a power system to injected harmonic currents. The load current, I_L, is calculated as the average of the maximum demand over a twelve-month period [2, 4]. The maximum allowable current distortion limit is the amount of harmonic current that the customer is permitted to draw from the utility supply. In case of non-islanded power networks, limits are set to police the utility so that it supplies power that is within the allowable limits at the point of common coupling. The SCR limits the size of the end-user's plant in terms of the total injected harmonic currents at the point of common coupling, where the customer's load connects to other customers [7].

Table 2.1 Current distortion limits for systems rated 120V through 69kV [8].

Maximum harmonic current distortion in percent of I_L						
Individual harmonic order (odd harmonics)[a,b]						
I_{SC}/I_L	**3≤h<11**	**11≤h<17**	**17≤h<23**	**23≤h<35**	**35≤h<50**	**TDD**
<20[C]	4.0	2.0	1.5	0.6	0.3	5.0
20<50	7.0	3.5	2.5	1.0	0.5	8.0
50<100	10.0	4.5	4.0	1.5	0.7	12.0
100<1000	12.0	5.5	5.0	2.0	1.0	15.0
>1000	15.0	7.0	6.0	2.5	1.4	20.0

The harmonic voltage distortion on the system will be a function of the total-harmonic current injected and the system impedance at each of the harmonic frequencies [9]. The voltage distortion limits from the IEEE 519 Standard are presented in Table 2.2. Table 2.2 indicates that for low voltage, the maximum individual-harmonic limit is 5 percent and the total harmonic distortion (THD) maximum limit is 8 percent. For the medium voltage range, the maximum individual-harmonic limit is 3 percent and the total harmonic distortion limit is 5 percent [4, 8].

Table 2.2 Voltage distortion limits [8].

Bus voltage V at PCC	**Individual harmonic (%)**	**Total harmonic distortion THD (%)**
$V \leq 1.0$ kV	5.0	8.0
1 kV < $V \leq$ 69 kV	3.0	5.0

Power quality standards must provide guidelines, recommendations and limits, as presented in Table 2.1 and Table 2.2. These limit values must not be exceeded, to ensure compatibility between the end-user equipment and the utility supply.

Where, a = even harmonics limited to 25% of the odd harmonic limits above and b = current distortions that result in a dc offset.

All power generation equipment are limited to these values of current distortion, regardless of actual I_{SC}/I_L.

Where, I_{SC} = maximum short-circuit current at PCC and I_L = maximum demand load current (fundamental frequency component) at the PCC under normal load operating conditions.

2.3 Power Quality

Historically, end-user loads were linear in nature, drawing sinusoidal current from the electrical system with a simple power quality equation. However, due to the recent rapid advancement of power electronics technology, the

characteristics of some loads have changed, resulting in power quality-related disturbances [1, 2]. Non-linear loads such as rectifiers and variable speed drives are used extensively on drilling ships and offshore installation applications, and these loads produce harmonics posing potential risks to the ship's electrical system, if the harmonics are not predicted and controlled [2]. The presence of these non-linear loads in the drilling ship electrical network, changes the characteristics of its voltage and current waveforms and the resultant (distorted) waveforms differ from the pure sinusoidal, constant-amplitude waveforms [9].

Power quality is influenced by the interaction between the power system and the load, as shown in Figure 2.1. As such, power quality refers to the variation of voltage, current and frequency in a power system [1, 10]. Power quality can also be understood to be related to the quality of voltage and current, and most electronics and power electronics equipment are sensitive to voltage disturbances [10]. Power quality has become a strategic issue, as distorted voltage waveforms can degrade the quality and lessen the reliability of a power supply. This results in severe economic consequences because of the reliance of drilling ships on sensitive devices, for example variable speed drives and uninterruptible power supplies.

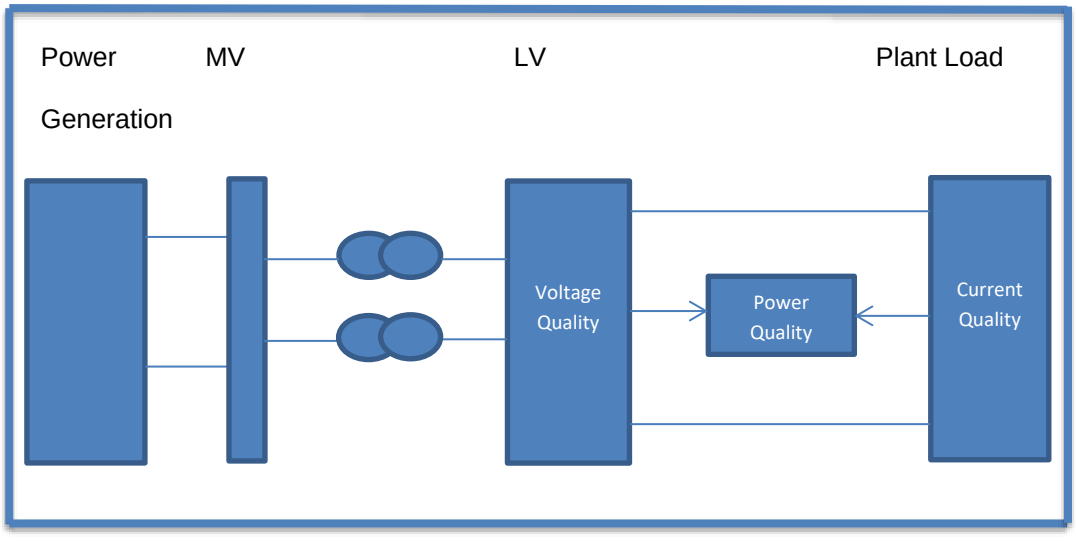

Figure 2.1 Power quality measurements [10].

The sources of poor power quality can be categorised into end-user systems (actual loads, equipment and components) and subsystems of transmission and distribution systems [2]. Electronic and power electronics equipment end-

user systems are sensitive to harmonics, but they are the main sources of harmonics. The point of common coupling is the secondary side of the transformer, and at that point the utility voltage supplied to the end-user must be within limits, and the end-user must ensure that the current drawn by the plant load is within the limits. The two categories of power quality disturbance are shown in Figure 2.2, and are discussed below:

1. Variations are small deviations of voltage or current from the ideal reference value, and are disturbances that can be measured at any instant of time [10, 12].
2. Events are larger deviations that only occur occasionally, and are disturbances that start and end with the crossing of a threshold value [10, 12].

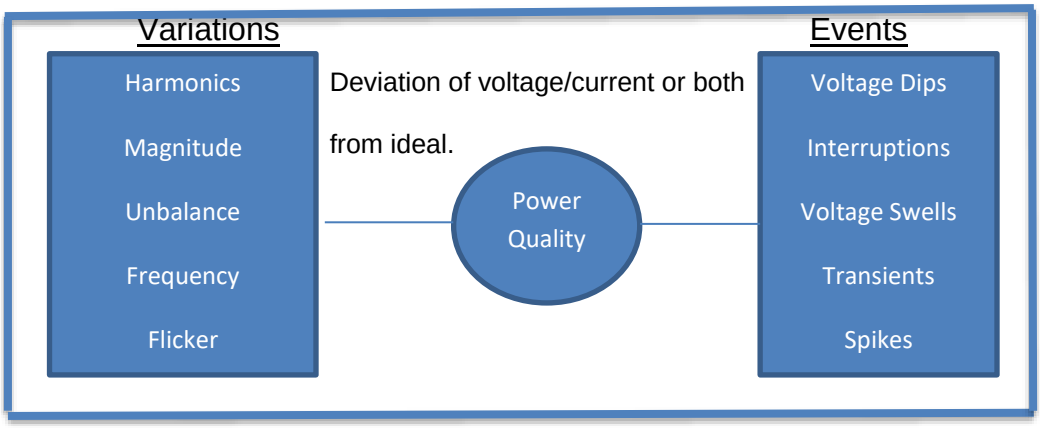

Figure 2.2 Power quality disturbances [12].

Table 2.3 summarises the main power quality disturbances, their causes, and the impact they have on the power network. The utility power supply can have a detrimental effect on the performance and reliability of end-user equipment, if the supply does not adhere to the limits provided by power quality standards [1]. Harmonics generated by non-linear loads affect the drillship power network and the generating units, if left unmonitored [2]. Table 2.3 also indicates that poor power quality results in equipment and component failures, leading to downtimes that affect plant productivity.

Table 2.3 Summary of power quality problems, effects and causes [1].

Power Quality Problems	**Effects**	**Causes**
Harmonics	Nuisance tripping process equipment. Transformer heating and equipment failure.	Mainly due to power electronic switching loads, non-linear loads, and system resonance.
Voltage Flicker	Irritation of human eyes due to visible light fluctuation. Reduces lifespan of electronics and cathode ray tube.	Motor start-up, switching of capacitor banks, arc furnaces and rolling mills.
Voltage Imbalance	Slowing down and heating of induction motors. Uncontrolled negative sequence currents to the compensator.	Mostly due to single-line to ground faults and unbalanced loading.
Voltage Sag	Malfunctioning of loads, equipment shutdown, tripping of relays, and motor contactors in drives.	Remote and parallel faults. Starting of large induction motors.
Transients	Flashovers and equipment damage, insulation failure, component failure, and electronics equipment disoperation.	Nuisance tripping of capacitor banks.
Interruptions	An excessive loss due to industry downtime.	Open circuit faults in cables. Operation of protective devices during fault clearance.

A power quality disturbance manifests in a non-standard voltage, current or frequency deviation that result in a failure or disoperation of end-use equipment [1]. Table 2.4 provides further information regarding the power quality problems presented in Table 2.3, by categorising these power quality problems according to their typical duration and amplitude impact on the system voltage. When sag occurs, the typical voltage range is 0.1 p.u to 0.9 p.u of RMS voltage at the supply frequency for a duration of 0.5 cycles to 30 cycles. Therefore, a “30 percent sag” refers to a sag that results in a voltage dipping by 0.3 p.u of the RMS voltage. A swell occurs when the RMS voltage increases to between 1.1 p.u and 1.8 p.u, at the supply frequency, for 0.5 cycles to 30 cycles.

Table 2.4 Categories of power quality disturbances [1].

Categories	Typical Duration	Typical Voltage
Transients	0.3–50 ms	0–4 p.u
Interruptions	0.5 cycle–3 s	< 0.1 p.u
Sag	0.5–30 cycles	0.1–0.9 p.u
Swell	0.5–30 cycles	1.1–1.8 p.u
Voltage Imbalance	Steady State	0.5–2%
Harmonics	Steady State	0–20 %
Voltage Flicker	Intermittent	0.1–7 %

2.4 Power System Harmonics

A drillship electrical system comprises both linear and non-linear loads. The demands of the drilling and exploration operations require the usage of microprocessors and power electronics devices, such as rectifiers and variable speed drives. Nonlinear loads pollute the electrical system with harmonics by drawing current in abrupt short pulses, rather than in a smooth sinusoidal

manner [14]. The harmonic voltage distortion levels are determined by the system impedance and the frequency characteristics [5]. The harmonic voltage distortion levels do not depend on the sinusoidal supply voltage, but instead are due to the non-sinusoidal currents drawn by nonlinear loads [12]. There are various types of power system harmonics, such as steady-state harmonics, interharmonics and transient harmonics. However, the primary focus of this dissertation is on steady-state harmonics.

2.4.1 Steady State Harmonics

Power system harmonics are defined as sinusoidal voltage and currents at frequencies that are an integer multiple of the fundamental frequency [2]. In this dissertation, the fundamental frequency refers to 60 Hz, which is typically the frequency of electrical systems on drilling ships. Therefore, the harmonic components are referred to by their harmonic number (for example, h = 3 refers to a 180 Hz frequency component and h = 7 refers to a 420 Hz frequency component) [5]. Harmonic pollution in electrical networks is a cause for concern for both utilities and end-users, as the effects of harmonic voltage and current can have disastrous consequences that lead to equipment malfunctioning and premature failures [2, 15].

2.4.2 Characteristic Harmonic

In a six-pulse converter, the characteristic harmonics are the non-triple odd harmonics, for example, the 5^{th}, 7^{th}, 11^{th}, and 13^{th} [4, 14]. A six-pulse rectifier is a building block for higher order rectifier configurations powered by a transformer with several secondary windings, for example 12-pulse, 18-pulse and 24-pulse [17]. The characteristic harmonic (h) formula is derived below. The characteristic harmonics (h) are based on the number of rectifiers (pulse number, q) used in a circuit.

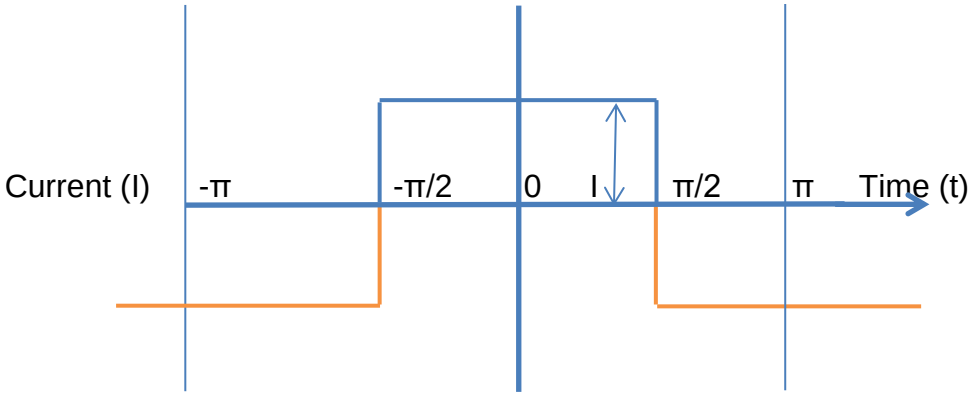

Figure 2.3 Time-domain representation of a square wave [13].

In analyzing the waveform of Figure 2.3, the origin (t = 0) is taken at the centre of the pulse, F($2\pi t$) is shown to be an even function (For example, f(t) = f(-t)). The Fourier series has only cosine terms as shown in Equation 2.2., with the relevant Fourier coefficients (A_n and A_o) that are referenced to a one per-unit DC current. The domain (t) of the square wave function shown in Figure 2.3 is given as follows: $-\pi < t < \pi$.

$$A_0 = \frac{1}{2\pi}\int_{-t}^{t} d(2\pi t) = \frac{1}{2\pi}\int_{-\pi}^{\pi} d(2\pi t) = \frac{1}{p} \tag{2.1}$$

$$A_n = \frac{1}{2\pi}\int_{-\pi}^{\pi} \cos(n\pi t)\, d(\pi t) = \frac{1}{\pi n}\sin\left(\frac{2\pi n}{p}\right) \tag{2.2}$$

Where, A_0 and A_n = the Fourier coefficients of a periodic function (Even symmetry) and t = is the pulse width period (between –π and π in Figure 2.3). The Fourier coefficients are referenced to a one per-unit DC current.

The phase currents can be calculated using a positive rectangular pulse width, $\omega = \frac{2\pi}{p}$, based on the assumption that the system has zero AC system impedance and infinite smoothing inductance [13]. The formula for the positive current pulse is:

$$F_p = \frac{2}{\pi}\left[\begin{array}{l}\frac{\omega}{4}+\sin\left(\frac{\omega}{2}\right)\cos(\omega t)+\frac{1}{2}\sin\left(\frac{2\omega}{2}\right)\cos(2\omega t)+\frac{1}{3}\sin\left(\frac{3\omega}{2}\right)\cos(3\omega t)\\ +\frac{1}{4}\sin\left(\frac{4\omega}{2}\right)\cos(4\omega t)+\ldots\end{array}\right] \quad (2.3)$$

And the formula for the negative pulse is:

$$F_n = \frac{2}{\pi}\left[\begin{array}{l}-\frac{\omega}{4}+\sin\left(\frac{\omega}{2}\right)\cos(\omega t)-\frac{1}{2}\sin\left(\frac{2\omega}{2}\right)\cos(2\omega t)+\frac{1}{3}\sin\left(\frac{3\omega}{2}\right)\cos(3\omega t)\\ -\frac{1}{4}\sin\left(\frac{4\omega}{2}\right)\cos(4\omega t)+\ldots\end{array}\right] \quad (2.4)$$

Where, F_p = positive rectangular pulse width and F_n = negative rectangular pulse width.

The positive and negative square wave periodic pulses are combined together:

$$F = F_p + F_n \quad (2.5)$$

$$F = \frac{4}{\pi}\left[\cos(\omega t)-\frac{1}{3}\cos(3\omega t)+\frac{1}{5}\cos(5\omega t)-\frac{1}{7}\cos(7\omega t)+\ldots\right] \quad (2.6)$$

Where, F = positive sequence harmonic order.

Equation 2.6 is called the 'general equation' and it can be seen that the DC component and even-ordered harmonics have been eliminated [13]. This equation is used to determine the positive sequence harmonic of orders, e.g. n = 1, 5, 9, and negative sequence harmonic of orders, e.g. n = 3, 7 and 11. This is achieved by substituting ω with π, and the resultant square wave of Figure 2.3 can be represented as time-domain and frequency-domain of a square wave.

To determine the harmonic order or characteristic harmonics (h), of three-phase six-pulse rectifiers, $\omega = 2\pi/3$ is substituted in equation (2.6) and the actual DC current is also inserted in the equation. The equation for the AC current in any of the phases in a frequency domain for a star-star connection is:

$$I_a = \frac{2\sqrt{3}}{\pi} I_d \left[\begin{array}{l} \cos(\omega t) - \frac{1}{5}\cos(5\omega t) + \frac{1}{7}\cos(7\omega t) - \frac{1}{11}\cos(11\omega t) + \frac{1}{13}\cos(13\omega t) - \\ \frac{1}{17}\cos(17\omega t) + \frac{1}{19}\cos(19\omega t) \ldots \end{array} \right] \quad (2.7)$$

For a star-delta transformer connection, the Fourier series for the current in one of the phases is:

$$I_a = \frac{2\sqrt{3}}{\pi} I_d \left[\begin{array}{l} \cos(\omega t) + \frac{1}{5}\cos(5\omega t) - \frac{1}{7}\cos(7\omega t) - \frac{1}{11}\cos(11\omega t) \\ + \frac{1}{13}\cos(13\omega t) + \frac{1}{17}\cos(17\omega t) - \frac{1}{19}\cos(19\omega t) \ldots \end{array} \right] \quad (2.8)$$

Where I_a = AC phase current and I_d = DC current.

Equations (2.7) and (2.8) indicate the absence of the third harmonic and other triplen harmonics, and they indicate the presence of harmonics of orders 6k±1 for integer values of k [5, 13]. Therefore, the formula for the harmonic current or voltage components of the AC current or voltage wave is:

$$h = kq \pm 1 \quad (2.9)$$

Where, h = harmonic order, k = any positive integer (1, 2, 3…) and q = pulse number of the rectifier circuit.

The lowest characteristic harmonic from a 6-pulse rectifier is the 5th harmonic, as calculated below using equation 2.1:

$h = kq \pm 1$

h = (1 x 6) $\pm$ 1 ⇒ 5th and 7th harmonics.

The single-harmonic and total-harmonic voltage or current distortions produced by an ideal six-pulse rectifier are higher than the IEEE standard limits [17]. The IEEE standard dictates that any individual-harmonic voltage distortion should not be more than 3 percent and the total-harmonic voltage distortion should not be more than 5 percent [4]. Higher order pulse rectifiers must be used to control or reduce the total-harmonic distortion. Therefore, as the number of pulses increases, the input characteristic improves.

The twelve-pulse configuration consists of two six-pulse rectifiers fed from a transformer with two secondary windings of equal voltage, but phase-shifted by 30° [5, 13]. With both sets of six-pulse rectifiers operating at the same time, the resultant AC current is derived from the Fourier series of the star-star-delta transformer by combining equations (2.7) and (2.8):

$$I_a = 2\left(\frac{2\sqrt{3}}{\pi}\right) I_d \left[\begin{array}{l} \cos(\omega t) - \frac{1}{11}\cos(11\omega t) + \frac{1}{13}\cos(13\omega t) - \frac{1}{23}\cos(23\omega t) \\ + \frac{1}{25}\cos(25\omega t)\ldots \end{array}\right] \qquad (2.10)$$

This Fourier series only contains harmonics of order 12k±1 [5, 13]. Therefore, for a 12-pulse rectifier, the lowest characteristic harmonic is the 11th harmonic:

h = (2 x 6) $\pm$ 1 $\Rightarrow$ 11th and 13th harmonics.

Twelve-pulse configuration rectifiers are the main focus of non-linear loads in this study, as they are the main sources of harmonics in a drillship electrical network.

2.4.3 Harmonic-Producing Loads

Due to the crude-oil drilling process requirements, the power network consists of both linear and nonlinear loads in order to meet the demand of offshore drilling. Nonlinear loads are defined as harmonic current generators that draw non-sinusoidal current from the power network [5].

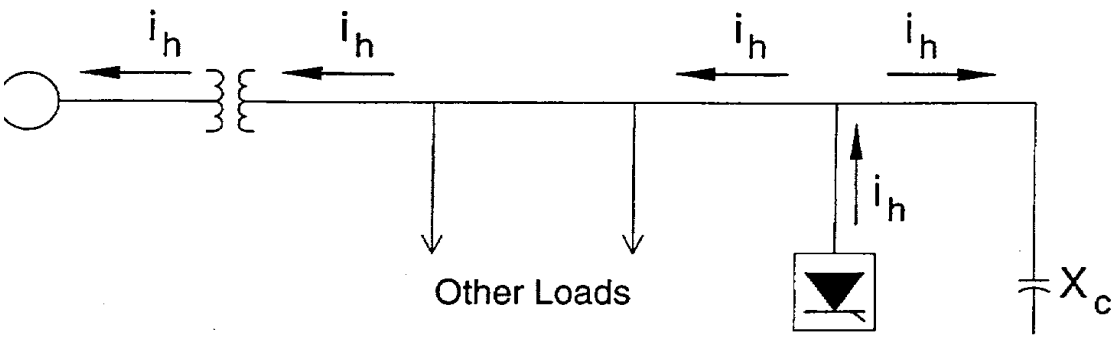

Figure 2.4 Direction of harmonic current [4].

The conventional flow of current is from the source to the load, and Figure 2.4 indicates the flow of the harmonic current (I_h) from the non-linear load to the source and other parts of the power network – affecting other connected loads. The three main categories of nonlinear loads are discussed below.

2.4.3.1 Machines

These are saturable devices that are known sources of harmonics due to their nonlinear characteristics of saturable elements [5, 18]. The harmonics are generated due to tooth ripples in the voltage waveform of rotating machines, variations in air-gap reluctance over synchronous machine pole pitch, flux distortions in the synchronous machine from sudden load changes, non-sinusoidal distribution of the flux in the air gap of synchronous machines, and transformer magnetising currents [4]. Examples of saturable devices are [5]:

- Transformers; and
- Motors (to some extent).

2.4.3.2 Power Electronics

The other traditional sources of harmonics are power electronics devices, such as diodes, transistors and thyristors. These devices generate harmonic currents during switching action and are the building blocks of the following equipment [2, 5]:

- Rectifiers and inverters;
- Switch mode power supplies;
- Variable speed motor drives; and
- Induction heating.

2.4.3.3 Arcing Devices

The other known sources of harmonics are arcing devices like arc furnaces that are utilised for melting and refining processes. Arc furnaces operate at a low power factor, and due to non-linear resistance the current drawn is not directly proportional to the voltage. Therefore, an arc furnace acts as a source

of current harmonics of the second to the seventh order – especially during the meltdown period [18]. Coreless induction furnaces supplied by medium voltage converters generate fixed and variable frequency harmonics [19].

2.4.4 Effects of Harmonic Distortion

The study of harmonics is critical, due to the negative impact of distorted voltage and current waveforms on power networks. The distorted current of a load does not directly affect other loads, but does do so indirectly by causing distortion in the voltage at the point of common coupling [13]. The main effect of voltage and current harmonics is the dielectric thermal or voltage stress causing degradation of insulation of electrical components, resulting in the shortening of their useful life span as specified by the manufactures [2, 4].

The effect of harmonics depends on the affected equipment characteristics. Therefore, the severity of the effect of harmonics imposed on the electrical network equipment cannot be perfectly correlated to harmonic indices, and a case-by-case analysis and good engineering judgement are thus recommended to identify the effects of harmonics [2, 4, 8]. Harmonic currents and voltages from power conversion apparatus produce magnetic and electric fields that will impair the satisfactory performance of communication systems, that, by virtue of their proximity and susceptibility, can be disturbed [2, 4]. The most commonly affected devices on a drilling ship electrical network are presented in Table 2.5.

Table 2.5 Effects of harmonic distortion [2, 4, 5, 8, 13].

Devices	**Effects of harmonics**
Rotating Machinery	• Harmonics cause increased heating due to iron and copper losses at harmonic frequencies. • Harmonic components such as the 5^{th} and 7^{th}, can combine to cause mechanical oscillations in a turbine-generator system and motor-load system. • Harmonic currents further cause harmonic torque, with the positive sequence component aiding shaft rotation and the negative sequence component opposing shaft rotation.
Transformers	• Harmonics cause increased thermal losses at high harmonic frequencies due to skin effect phenomena.
Cables	• Harmonic voltage increases dielectric stress on cables, and decreases the reliability and lifespan of the cable insulation proportion to the crest voltage. • If the cable supplies a nonlinear load, the triplen harmonics in each phase add up cumulatively in the neutral conductor to 173 percent of the phase current – causing overheating and sometimes burn-out of conductors.
Switchgear and Relay	• Harmonic currents cause increased heating and losses in the switchgear and fuses, so reducing their current carrying capability. • Harmonics cause relays to malfunction, and operate slower with high pick-up values.

Electronic Controls	• Some electronic controls are designed to operate or change state at voltage crossings, and harmonic distortion causes shifting in the voltage zero crossing – resulting in malfunctioning.

2.5 Induction Motors

The most-commonly used three-phase electric motors in the industrial, commercial or agricultural sectors are induction motors due to their simple, cheap, reliable, efficient and robust construction, while the squirrel cage-type is the widely used induction machine [22, 23]. The squirrel cage motor comprises a symmetrical three-phase stator winding and a cage rotor with copper or aluminium bars inserted in laminated iron slots. The slots are skewed, for better starting of the motor to run quietly. The ends of the rotor bars are short-circuited [22]. The equivalent circuit of an induction motor is shown in Figure 2.5 (below). The stator winding is represented by the combination of stator winding resistance (R_1) and the leakage reactance (X_1). The mutual flux linking between the stator and the rotor is represented by the unsaturated magnetising reactance (X_m). The rotor bars are represented by the rotor resistance (R_2) and the leakage reactance (X_2).

When a supply (V_Φ) is connected to the stator windings, the current (I_1) flows in the stator winding and produces a rotating magnetic field at a constant synchronous speed (n_s) [22, 23]. The magnitude of the resultant flux (Φ) rotates at constant speed, making one revolution for each cycle of the supply voltage. As the rotating magnetic field cuts the rotor bars, a voltage is induced, so causing current flow as the ends of the conducting rings are joined. The current (I_2) in the rotor bars creates a magnetic field and interacts with the stator rotating magnetic field to produce forces that tend to turn the rotor in the same direction as the rotating magnetic field [23]. The turning forces (torque) produced result in the rotation of the rotor. In induction motors, the rotor rotates at a slower speed than the synchronous speed, so that torque can be produced. The difference between the synchronous speed, determined by the supply frequency (ω_s) and the rotor speed with frequency (ω_r), is called induction motor slip (s).

The formula for synchronous speed is:

$$n_S = \frac{f}{p} \quad \text{revolutions per second,} \tag{2.11}$$

Where, n_s = the speed (synchronous) of the revolution of the rotating magnetic field, f = frequency of the currents in the stator windings and p = pairs of poles.

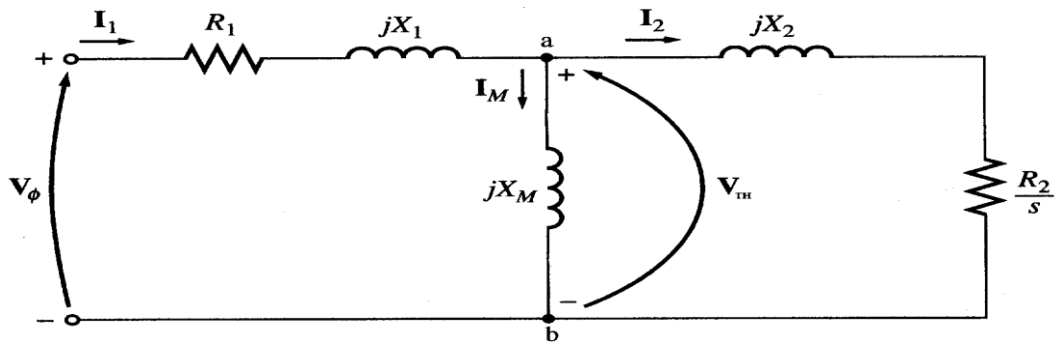

Figure 2.5 Equivalent circuit model of an induction motor [23].

2.5.1 Induction Motor Power and Torque

Figure 2.6 represents the power flow in an induction motor. The input power, P_{in}, is applied to the stator winding to create the rotating magnetic field.

$$P_{in} = \sqrt{3} V_T I_L \cos\theta \tag{2.12}$$

Where, P_{in} = input power applied at the stator winding, V_T = terminal voltage and I_L = supply line current.

The input power minus all the losses (stator copper losses, rotor copper losses and rotational losses) is equal to the mechanical power or output power. The output power is calculated using the following equation:

$$P_{out} = \tau_{load} \omega_m \tag{2.13}$$

Where, P_{out} = mechanical (shaft) power developed, τ_{Load} = shaft torque and ω_m = rotor speed in radians.

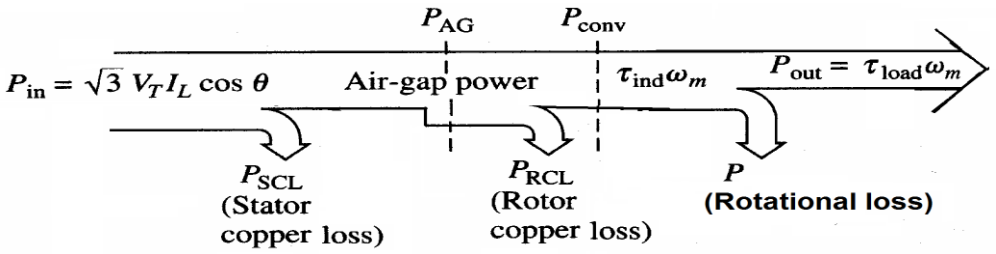

Figure 2.6 Power flow of an induction motor [23].

The stator and rotor resistance are critical parameters of an induction motor behaviour, as they influence the power and torque calculations of the motor. Figure 2.7 represents the torque-speed characteristics of an induction motor, when a direct-on-line starting method is used. The starting torque is on the order of 200 percent of the full-load (motor) torque. As the motor speed increases, the torque reaches maximum torque, known as pull-out torque. As the motor approaches full speed, the torque drops to 100 percent of the full-load torque. Once the motor reaches full speed and at minimum slip, the torque will be 100 percent of the motor-load torque [22, 23]. The use of adjustable frequency drives allows for the control of the starting torque, and starting current is limited to full load current.

From Figure 2.6, the torque equation for an induction motor is determined using the equivalent circuit:

$$\text{Torque,}\quad T = \left(\frac{1}{2\pi ns}\right)\left(\frac{Ir^2 R_2}{s}\right) \tag{2.14}$$

Where, T = torque produced by induction motor, n = rated rotational speed, s = slip, I_r = rotor current and R_2 = rotor resistance.

The full-load torque of a three-phase induction motor is given by the equation:

$$T = \left(\frac{M\left(\frac{N_2}{N_1}\right)^2}{2\pi ns}\right)\left(\frac{s(V_\Phi)^2 R_2}{(R_2)^2 + (sX_2)^2}\right) \tag{2.15}$$

Where, M = the number of phases, N_1 = number of turns on the stator windings, N_2 = number of turns on the rotor windings, R_2 = rotor resistance, X_2 = rotor reactance, s = slip and V_ϕ = rotor voltage.

Under normal conditions the supply voltage is usually constant and the rotor resistance R_2 is unaffected by frequency or slip, and hence remains constant. The torque will be maximum when $\frac{R_2^2}{s} = sX_2^2$.

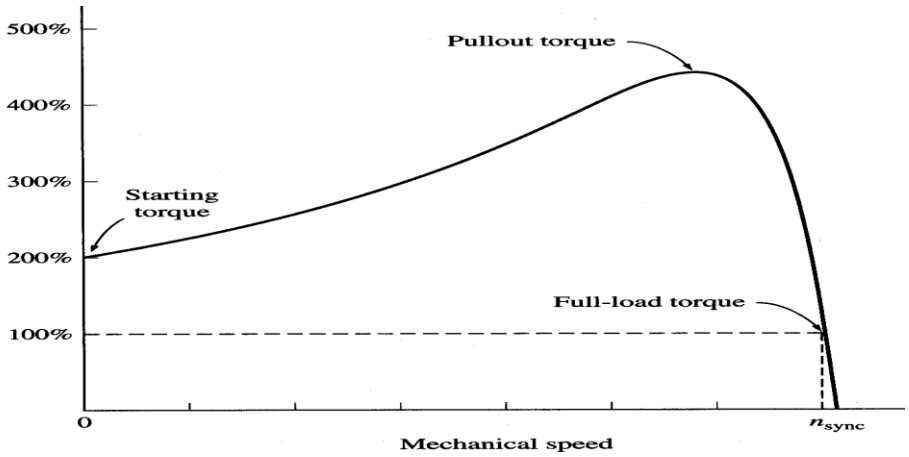

Figure 2.7 Torque-speed characteristics of an induction motor [24].

2.6 Variable Speed Drives

The demand imposed by industrialisation has seen an increase in technological developments that has led to an ever increasing use of electronics devices [25]. The use of variable speed drives with advanced controls utilising microprocessors for process controls is preferred in offshore drilling and other industries. The variable speed drive (VSD) system in Figure 2.8 (below) is the most used motion control system that possesses significant features of high dynamic performance, efficient operation, and increased reliability [26].

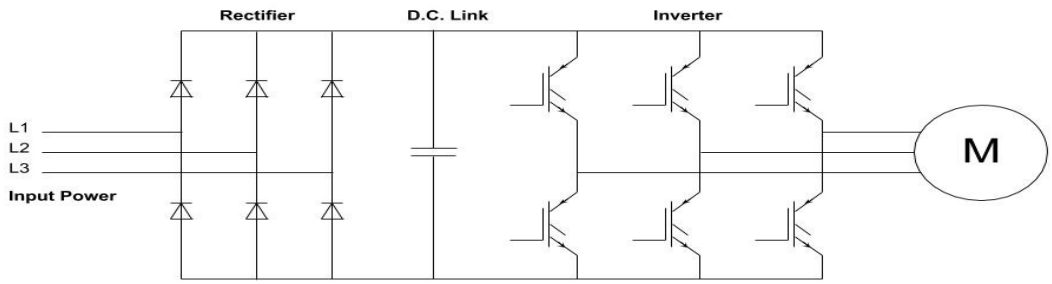

Figure 2.8 Simple variable speed drive diagram.

The conversion of power within the variable speed drives occurs in two stages. The drive comprises three sections: the rectifier, DC link, and inverter. The first power conversion occurs in the rectification stage. The star rectifier and bridge rectifier are the two types of three-phase rectifiers, which are used to convert three-phase AC power into DC voltage. The three-phase bridge rectifiers are most commonly used for high-power applications, because they have the highest possible transformer utilisation factor for a three-phase system [27].

Figure 2.9 (below) indicates that the flow of current through the diodes occurs during the diode conduction times. The conduction sequences are $D_5 – D_6$, $D_6 – D_1$, $D_1 – D_2$, $D_2 – D_3$, $D_3 – D_4$, and $D_4 – D_5$. The pair of diodes that are connected between two supply lines having the highest amount of instantaneous line-to-line voltage, will conduct [27]. Due to the switching characteristics of diodes when AC voltage is applied, the current drawn from the three-phase AC supply is non-sinusoidal. Harmonic currents flow from the non-linear load (rectifier) into the ac supply – adversely affecting other loads in the electrical network. As can be seen, the currents (I_s) drawn from the supply are disjointed, the positive current flow is between 60° and 180° and the negative current flow occurs between 240° and 360°. Therefore, the supply current is distorted and consists of harmonic currents.

In Figure 2.9, the line current (i_a) is represented by the equation,

$$i_a = \frac{\sqrt{3}Vm}{R} \tag{2.16}$$

Where, i_a = phase current drawn by the rectifier, V_m = line voltage and R = resistive load supplied by the diode rectifier.

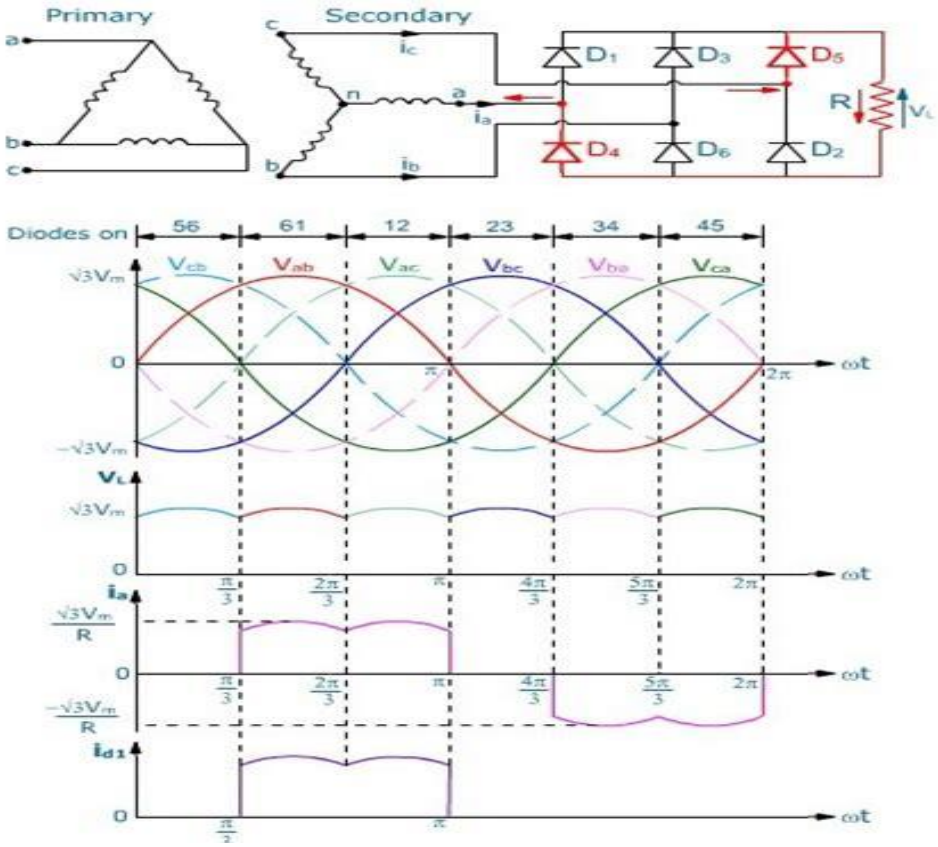

Figure 2.9 Three-phase diode bridge rectifier with waveforms [27].

The drillship electrical network studied in this dissertation consists of both 6-pulse and 12-pulse type rectifiers. The controller on the rectifier is only used for protection and measurement purposes as the diodes themselves are uncontrolled. The second power conversion in the variable speed drive of Figure 2.8 occurs in the inverter section. The inverter produces an AC output waveform from a DC power supply. For sinusoidal AC output waveforms, the magnitude, frequency and phase angle should be controllable. The two types of commonly used topologies are voltage source inverters (VSIs) and current source inverters (CSIs). VSIs are the most widely used [27]. The two types of high-performance AC machine control algorithms that are mostly used within machine-side inverter controllers are field-oriented control, also known as vector control (VC) and direct torque control [26].

The conversion of a fixed and uncontrolled DC input voltage into a variable AC output voltage can be obtained through varying the gain of the inverter. The

inverter gain is defined as the ratio of the AC output voltage to the DC input voltage [27]. The sinusoidal pulse-width-modulation (SPWM) is the most used carrier-based modulating technique. The AC output voltage produced by the voltage source inverter (VSI) of a standard variable speed drive is a three-level waveform, and is also non-sinusoidal; however, its fundamental components behave as such [27]. The AC output voltage waveform consists of harmonic voltages.

2.7 Conclusion

This chapter has presented the literature on power quality and harmonics, illustrating the impact of harmonics in a power system network. It also reviewed information on sources and the effects of harmonics on electrical network equipment.

The chapter further introduced the standards used to monitor and police utilities and consumers in terms of poor power quality. It explained the harmonic current and voltage allowable limits at the point of common coupling. Properties of an induction motor and the characteristics of variable speed drives were briefly discussed, as they are the major load in a drilling ship and their properties are critical to the behaviour of the network.

The next chapter describes the methodology used in the dissertation for investigating the impact of harmonics on the island power network – using a real-time simulator and field measurements to develop a simulation model that will represent an offshore drilling ship power network.

CHAPTER THREE

Real-time simulation modelling

3.1 Introduction

In Chapter Two, the literature related to power quality, specifically harmonics was reviewed and presented. In this chapter, modelling approaches for a drilling ship electrical network are presented. The rationale for this chapter is that harmonics generated by variable speed drives can be evaluated using real-time simulator models.

This chapter reviews the simplified drillship electrical network which comprises two generators, three transformers, three induction motors, a variable speed drive system, and a DC drive system. A real-time simulation model for the drillship electrical network equipment was developed in the simulation package RSCAD, in order to study harmonics on an offshore drillship power network. Therefore, harmonic studies for an offshore drillship power network can be carried out in a realistic laboratory environment.

This chapter also presents the power quality meter (PQM) used for field measurements on an offshore drillship power network. The field measurement results will be compared with the real-time simulation results.

3.2 The Real-Time Simulator

Power system studies can be carried out by using either analogue simulators or by means of digital software simulation packages, with each approach having different capabilities over the other. Analogue simulators operate in real-time; however, they cannot solve large power system networks [29]. They also cannot accurately replicate the parameters, non-linearity and dynamic performance of the actual components in large power systems that they were developed to replicate [26, 28]. Therefore, real-time digital simulators are adapted to model complex power systems and they operate in real-world time [28]. Digital simulation models use the Dommel's general equation method and solve the network responses at every discrete time step so as to provide continuous output conditions that accurately represent real network conditions

[28, 29]. The real-time simulator used for this study was the RTDS Technologies real-time digital simulator (RTDS^{TM}). “The RTDS system combines the advantages of analogue and digital power system simulation methods with realisation of the concept made possible by advances in digital signal processor technology that allowed Dommel’s general solution method to be solved in real-time” [29].

Simulation models of generators, transformers and power electronic converters have been developed within the RSCAD software, which is used for carrying out studies on the real-time digital simulator. The software comprises sub-programs (DRAFT, RUNTIME, TLINE, CABLE and MULTIPLOT) that are used to program, run and control the real-time digital simulator [29]. The detailed models are developed in DRAFT, as large-time step or small-time step sub-systems. Large-time step sub-systems refer to the normal solving capability of the real-time simulator, in which the models are solved at discrete time intervals of 50 microseconds (μs) for traditional components operating at fundamental frequencies (50Hz or 60Hz). Small time sub-systems are used to model power electronic converters that switch in the kilohertz frequency range for which the models are solved at time-step intervals of 1.4 to 2.0 microseconds [29]. Within DRAFT, there are various control system component models that are used to develop the model to test the network and other hardware.

3.3 Overview of the Study System

A reduced-scale representation of an actual drillship electrical network, which is shown in Figure 3.1 (below), was modelled on the RSCAD software so that harmonic waveforms could be measured in real-time. The full drillship electrical network comprises three 11 kilovolts (kV) switchboards, each similar to that shown in Figure 3.1, inter-linked to one another by two bus-couplers. The three 11kV switchboards in the full drillship network supply similar loads to those shown in Figure 3.1, and comprise induction motors, variable speed motor drives, electronics, and other power electronic devices. The total capacity of the drillship generating plant is 52 500 kVA, consisting of six 8 750 kVA diesel generators (two per switchboard).

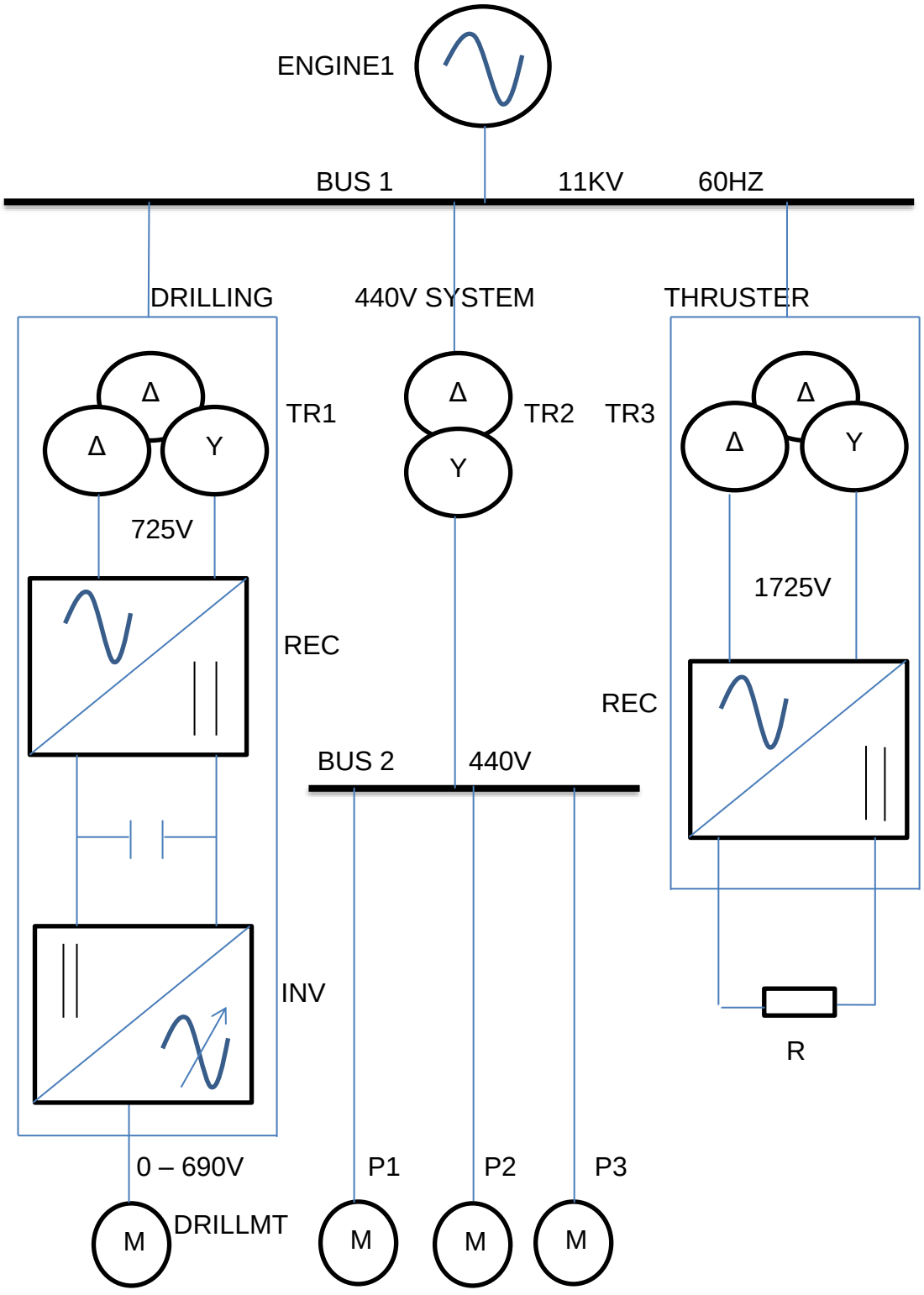

Figure 3.1 Drillship simplified electrical network.

As such, Figure 3.1 represents, in reasonable detail, one switchboard (BUS1) from the full drillship network, supplied by a generator (ENGINE1). The loads on the switchboard are the drilling drive system (DRILLING), the low voltage system (440 V system), and the thruster drive system (THRUSTER). The

drilling drive system comprises a transformer TR1 (11kV/725V/725V), a rectifier (REC), an inverter (INV), and an induction motor (DrillMT) driving a mechanical load. The 440 V system consists of a transformer TR2 (11kV/440V) and a low voltage switchboard (BUS2) that supplies three induction motors (P1, P2 and P3) driving mechanical loads. The induction motors on the low voltage system are started using direct-on-line starting methods. The thruster drive system (THRUSTER) is represented by transformer TR3 (11kV/1725V/1725V) and a rectifier (REC) with a resistive load. The thruster system is represented by a rectifier as the focus of the study is on the low voltage system harmonics.

The starting point for network studies is the development of simulation models, either by using traditional simulation software or real-time simulation software such as RSCAD. Both types of simulation models (traditional and real-time) can be used to represent power system components, with acceptable results. Parameters for electrical equipment are required so that the simulation can be a true representation of the physical system components. The RSCAD models used in this harmonic study were the induction motor model, the transformer model, rectifier model and inverter model.

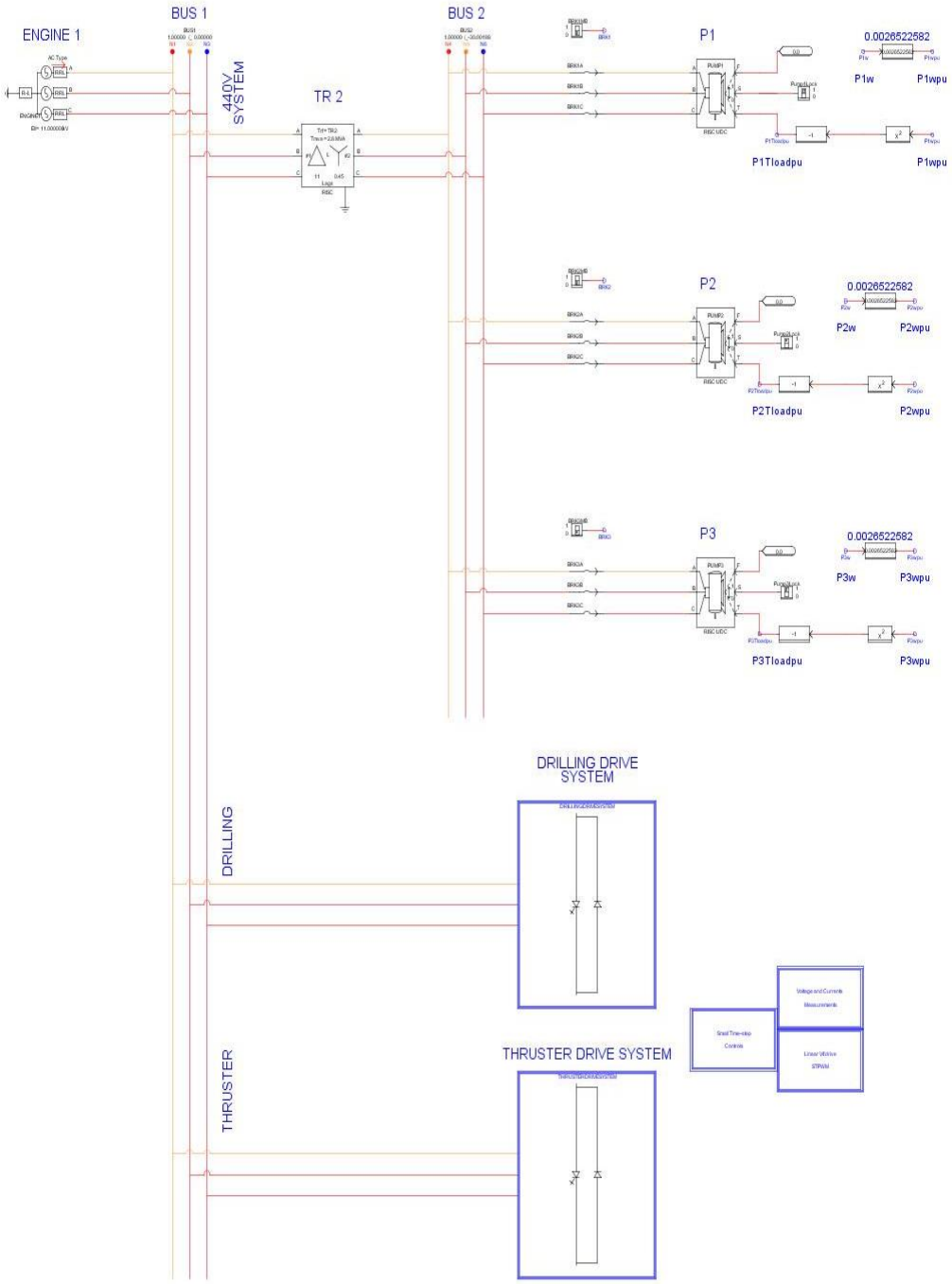

Figure 3.2 Drillship electrical network - RSCAD simulation model.

Figure 3.2 (above) is the simulation model (developed in the RSCAD software) of the simplified drillship network shown in Figure 3.1. The model comprises two small time-step sub-system models that are interfaced with the main, large time-step system model. The components represented within the large time-step system, are source model (ENGINE1), transformer model (TR2), and the three induction motor models (P1, P2 and P3). The two small time-step subsystems in the model are contained in the two hierarchy boxes that are

labelled ‘DRILLING DRIVE SYSTEM’ and ‘THRUSTER DRIVE SYSTEM’ and shown in Figure 3.2, and these contain the models of the drilling drive and thruster systems shown earlier in Figure 3.1. Each of the main components of the RSCAD model shown in Figure 3.2 is discussed in more detail in the subsections that follow.

3.3.1 Generator - Engine 1

The actual generator (ENGINE1) on the drilling ship that feeds the 11kV switchboard is represented by a RSCAD three-phase voltage source model with a grounded neutral wire and without harmonics, as shown in Figure 3.3 (below).

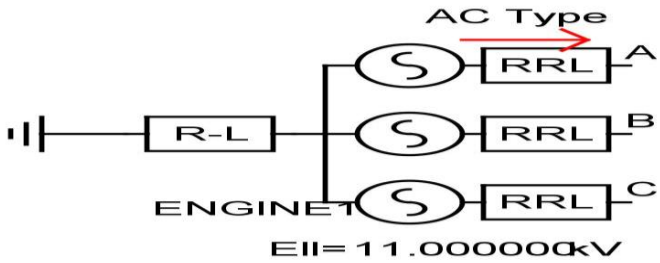

Figure 3.3 Drillship diesel-generator – ENGINE1.

The selected source impedance type for Engine 1 was the R-R//L, and with zero sequence and static impedance included. The actual parameters from the generator manufacturer were used to configure the RSCAD source model, so that it represented the actual drillship generator characteristics as closely as possible, namely a supply frequency 60Hz, output voltage 11 000V, and the power 7 MW. The other source parameters (zero sequence and positive sequence impedances), were calculated based on the actual generator nameplate data:

- Zero sequence impedance = 1.137 Ohms (Ω)
- Zero sequence impedance phase angle = 86.63 degrees (°)
- Positive sequence impedance = 1.979 Ω
- Positive sequence impedance phase angle = 85.94°

Figure 3.4 (below) presents the sliders developed in the RUNTIME to set terminal voltage and the fundamental frequency. The ABCmag slider was used to set the generator terminal voltage at 11 kV, and the Freq slider was used to set the electrical network fundamental frequency at 60 Hz.

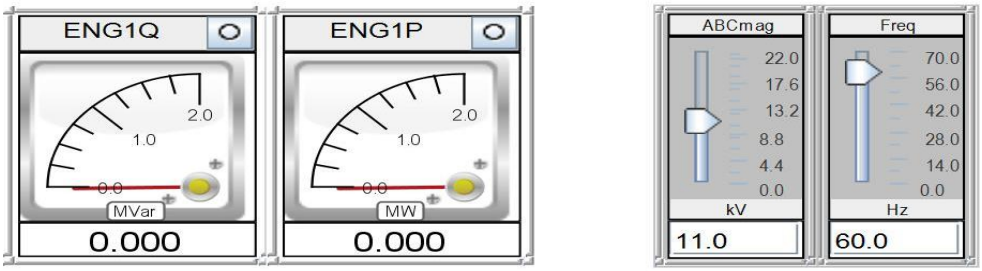

Figure 3.4 ENGINE 1 sliders.

3.3.2 Drilling pumps

All three pumps (P1, P2 and P3) driven by induction motors, use a direct on line (DOL) starting method, and are fed by the 440 V system as indicated in Figure 3.2. Figure 3.5 (below) shows the RSCAD induction motor model used to represent one such motor-pump set in the drillship electrical network, i.e. Pump 1 (P1). Pump 2 (P2) and Pump 3 (P3) were represented using the same induction motor model as is shown in Figure 3.5, with the only difference being the motor power ratings in each case. The mechanical load on all three representations of the pump motors was simulated by activating the three inputs, as shown in Figure 3.5.

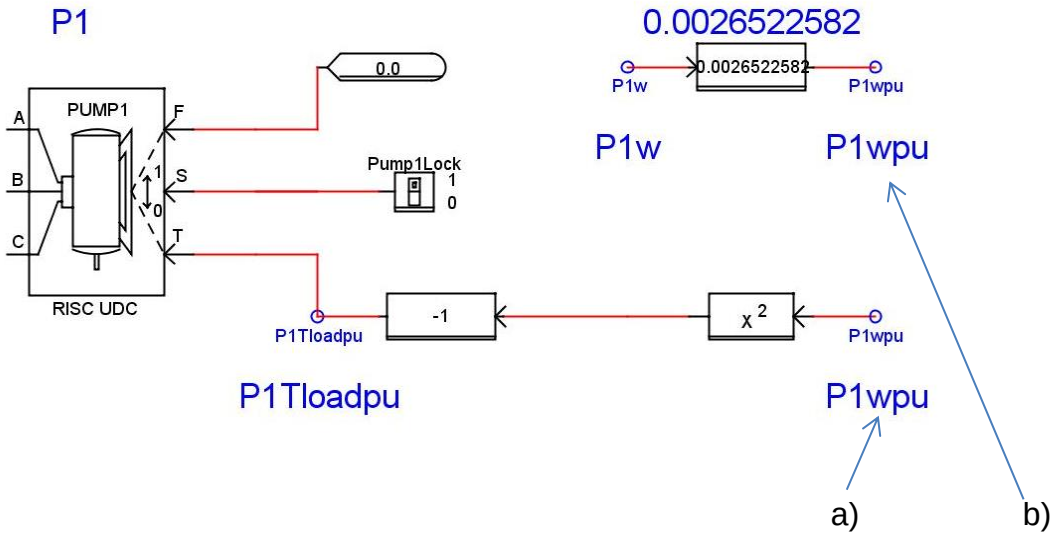

Figure 3.5 Drilling pump motor 1.

The three inputs in Figure 3.5 are the machine speed (F), speed and torque selector switch (S), and mechanical torque (T). Figure 3.6 (below) shows a slider and two switches developed in RUNTIME to control the simulated mechanical load on the motors. The first switch, BRK1MB, controls the Pump 1 circuit breaker to start (close) and stop (open) the motor. The second switch, Pump1Lock, is used to select between speed and torque input. The mechanical speed of the machine model in RSCAD can be made to respond directly to a speed order or the speed can be made vary according to an applied mechanical torque. When the Pump1Lock switch in Figure 3.6 was set to 1 (Lock), the machine model responded to a speed signal in Hertz (Hz) applied at machine speed input F of the machine model.

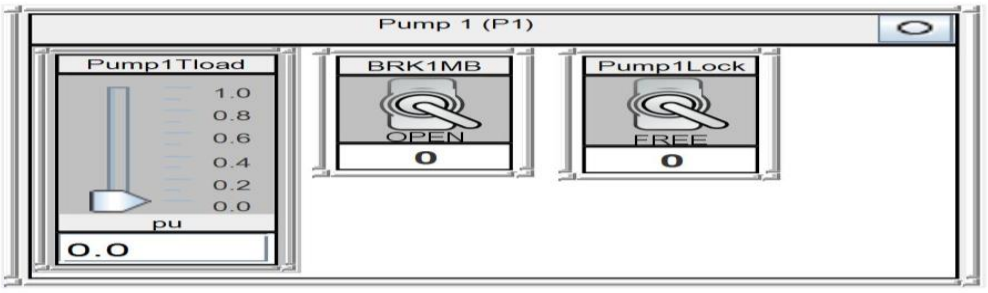

Figure 3.6 Pump 1 control switches created in RUNTIME.

When the switch was set to 0 (Free), the machine model responded to whatever mechanical torque signal was applied at its torque input (T). The control circuit, Figure 3.5 a) and b), was developed in order to represent the induction motor torque-speed relationship shown in the graph in Figure 3.7 (below):

$$T_e = J_m \frac{d\omega}{dt} \quad \left(\text{Assuming } \beta_m \omega \text{ is zero}\right) \tag{3.1}$$

Where, T_e = motor torque, ω = motor rated speed and J_m = rotational inertia of the mechanical system.

$$T_{load} = k\omega^2 \tag{3.2}$$

Therefore, $k = \frac{\omega^2_{\text{rated}}}{T_{\text{load rated}}}$

Where, T_{load} = shaft torque developed and ω_{rated} = rated rotational speed.

In Figure 3.5, the signal T_{loadpu} is the calculated value of the load torque, in per unit, that is applied at the torque input T of the motor model. The required value of T_{loadpu} is calculated from the measured speed P1ω of the motor, according to the desired torque-speed relationship, as follows. The motor speed (P1ω) is converted into per unit (P1ωpu) by multiplying P1ω by the scale factor 0.002652 as shown in Figure 3.5. This scale factor is equal to $\frac{1}{2\pi 60}$, which is the inverse of the speed, $\omega = \frac{4\pi f}{p}$ (radians per second). Figure 3.5 a) shows that the per unit value of speed is squared, as per equation (3.2), and then multiplied by negative one, according to the sign convention of the RSCAD induction motor model, in which negative values of torque applied at the load torque input, T, correspond to operation in motoring mode as required to represent the behaviour of the pumps (P1, P2 and P3) in the drilling ship system.

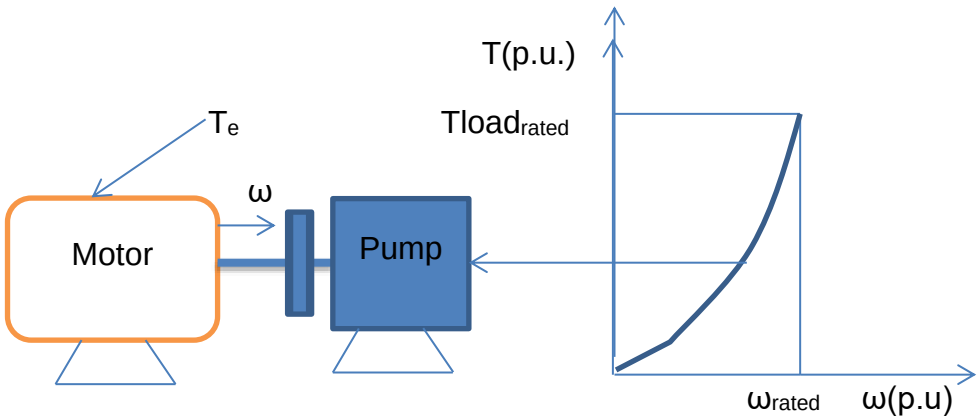

Figure 3.7 Induction machine model control circuit development.

3.3.2.1 Parameterisation of induction machine model

Figure 2.5 in Chapter Two showed the equivalent circuit of an induction motor, with the parameters required for the RSCAD induction machine model shown in Figure 3.5. For the RTDS to truly represent an actual induction motor, electrical parameters, as shown in an equivalent circuit, are inputs into the

simulation as well as mechanical parameters. The RTDS electrical parameters were calculated using the actual motor nameplate data, power, voltage, current, power factor, and rated speed. The other data were from the no load and short-circuit test results. The no load current of the motor was used to calculate the unsaturated magnetising reactance (X_M). The actual motor short-circuit test results were used to calculate the stator leakage reactance (x_a), and the DC resistance test data were used to calculate the stator resistance (r_1) and the first cage rotor resistance (r_2). All the electrical parameters were converted into per unit, as the RTDS parameters are in per unit (p.u).

The driving torque developed by the motor is opposed by the load torque and the moment of inertia of the motor and load. All motor shaft torques and the moment of inertia are slip dependent. The rotational inertia (H) of the induction motor is directly proportional to the motor's moment of inertia, and is expressed in MegaWatt-seconds of stored energy at rated speed per MVA of motor rating [29]. The calculated RTDS electrical and mechanical parameters for motors P1, P2 and P3, are shown in Table 3.1. The details of how the parameters in Table 3.1 were calculated are shown in Appendixes B, C and D.

Table 3.1: 440 V System induction motor parameters.

Parameters	RTDS	Equivalent Circuit Symbol (Figure 2.6)	Pump 1	Pump 2	Pump 3
Rated phase voltage (kV)	vbase	V_Φ	0.2540	0.2540	0.2540
Rated phase current (kA)	ibase	I_1	0.2093	0.2546	0.6906
Rated frequency (Hz)			60	60	60
Stator resistance (p.u.)	r_a	R_1	0.0109	0.0777	0.0050
Stator leakage reactance (p.u.)	x_a	X_1	0.0965	0.0907	0.0827
Unsaturated magnetising reactance (p.u.)	xmd0	X_m	4.4311	4.2952	3.9457
First cage rotor resistance (p.u.)	rfd	R_2	0.0453	0.0424	0.0442
First cage rotor leakage reactance (p.u.)	xfd	X_2	0.0965	0.0907	0.0827
Inertia Constant (MWs/MVA)	H		0.4035	0.4106	0.5918

3.3.3 Drilling Drive System

As shown in Figure 3.1, the drilling drive system consists of a transformer (TR1) with two secondary windings (phase shifted by 30°), AC to DC converter (REC), DC link, DC to AC inverter (INV) and an induction machine. Figure 3.2 showed that these components of the drilling drive system are represented in a small time-step sub-system bridge box in the RSCAD DRAFT model. The function of the bridge box is to interface the small time-step sub-system with the main system network. Figure 3.8 now shows the detailed model of the drilling drive system developed within the small time-step bridge box in DRAFT, which comprises three single-phase interface transformers (IFTR1, IFTR2 and IFTR3), a drilling drive system transformer (TR1) with two secondary windings, AC to DC converter, DC link, DC to AC inverter, drilling motor (DRILLMT), and inverter controls.

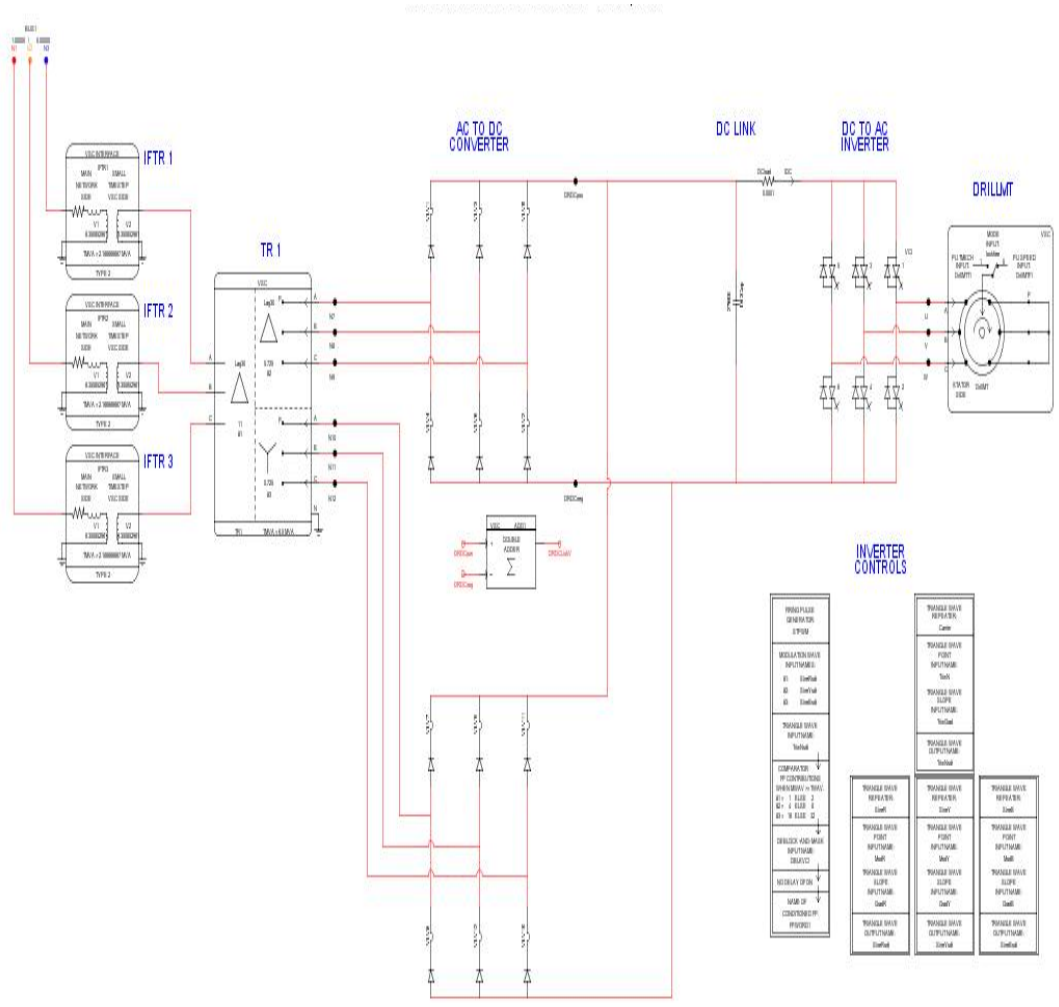

Figure 3.8 Drilling drive system.

The sub-sections below outline each of the components of the small-time step simulation model of the drilling drive system.

a) Interface transformers

In the simulation model created in DRAFT, the three single-phase transformers (IFTR1, IFTR2 and IFTR3) are the components that connect the small time-step subsystem to the main system network (BUS1). Each single-phase interface transformer is rated at 2.17 MVA, which is one-third of 6.5 MVA (the rating of the three-phase drilling drive system transformer) at a 1:1 transformation ratio. The single-phase RMS voltage applied to the primary side of each interface transformer was 6.35 kV, and the voltage at the secondary winding was 6.35 kV. The primary side of the interface transformer (large DT) was connected to the main system network (BUS1) and the secondary side (small DT) was connected to the primary side of the drilling drive transformer (TR1).

b) Drilling drive transformer (TR1)

The small time-step three-phase three-winding transformer provides for the requirements of a 12-pulse rectifier (AC to DC converter), and the windings are phase-shifted by 30°. One of the secondary windings is delta connected and supplies one six-pulse rectifier, while the other secondary winding is star connected and supplies the second parallel six-pulse rectifier. The drilling drive transformer power rating is 6.5 MVA, the primary winding is rated at 11 kV, and the secondary windings are each rated at 725 V.

c) AC to DC converter (REC)

The drilling drive transformer (TR1) supplies two parallel-connected six-pulse rectifiers (AC to DC converters). Each rectifier consists of six diodes that are configured for three-phase supply. The RSCAD rectifier model is parameterised so that it represents the actual rectifier on the drillship electrical network. The diode switching voltage magnitude was set at 4 kV and the switching current magnitude was set at 4 kA, which is also the current rating on the actual rectifier. The diode base frequency setting was set at 60 Hz, which is the drillship electrical network frequency.

The average output voltage of each simulation rectifier is:

$$Vdc = \frac{2}{2\pi f \ 6} \int_{0}^{\pi/6} \sqrt{3} Vm \cos\omega t \, d(\omega t) = \frac{3\sqrt{3}}{\pi} Vm \qquad (3.3)$$

Where, V_{dc} = six-pulse rectifier output DC voltage and V_m = line voltage.

Therefore, $Vdc = 1.654\,Vm$ = 1.654 (725 V) = 1199.15 V, and this is the expected average output voltage of the rectifier section in the simulation model.

The DC link section consists of a bank of capacitors (DCCap) connected across the DC output of the diode rectifier with a capacitance of 27 600 micro Farads (μF). The capacitance value was taken from the nameplate data of the actual DC link on the drillship electrical network. The DC link capacitance of 27 600 μF is made up of a series of connected capacitors and the voltage balancing of capacitors is critical for the operation of inverters. If the capacitor voltage is not regulated properly, it causes a large amount of current flow from the inner capacitors as compared to the outer capacitors, and that will result in inverters not operating efficiently.

d) DC to AC inverter

The two-level three-leg voltage source converter (VSC) bridge model in DRAFT was parameterised to represent the actual VDS inverter on the drillship electrical network. Each individual device switching voltage magnitude and current magnitude was set to 2 kV and 14 kA, respectively in the converter model with a base frequency of 60 Hz. The output signals of the large time-step controls (linear v/f drive STPWM) shown in Figure 3.9 are the inputs supplied to the small time-step controls (INVERTER CONTROLS) of Figure 3.8. These small time-step controls in Figure 3.8 comprise a high-precision triangle wave repeater and a PWM comparator to generate the firing pulses for each switching device in the DC to AC inverter that supplies the drilling motor.

The actual drillship electrical network drive inverter uses direct torque control which is a sophisticated, but proprietary variable speed drive control technique of ABB, the company that manufactured the drive, whereas the RSCAD VSD model uses a slightly simpler form of variable speed drive control known as

voltage to frequency (v/f) control, so that the ratio of the voltage to frequency (and hence the motor flux) is kept constant over the speed range. Figure 3.9 shows the linear voltage and frequency controls of the v/f drive implemented using sinusoidal PWM. Developing the actual models of the variable speed drive system described here was beyond the scope of work of this dissertation. As such, a working small time-step model of a v/f VSD system was provided to the author arising out of previously-completed research work in [26] by another student.

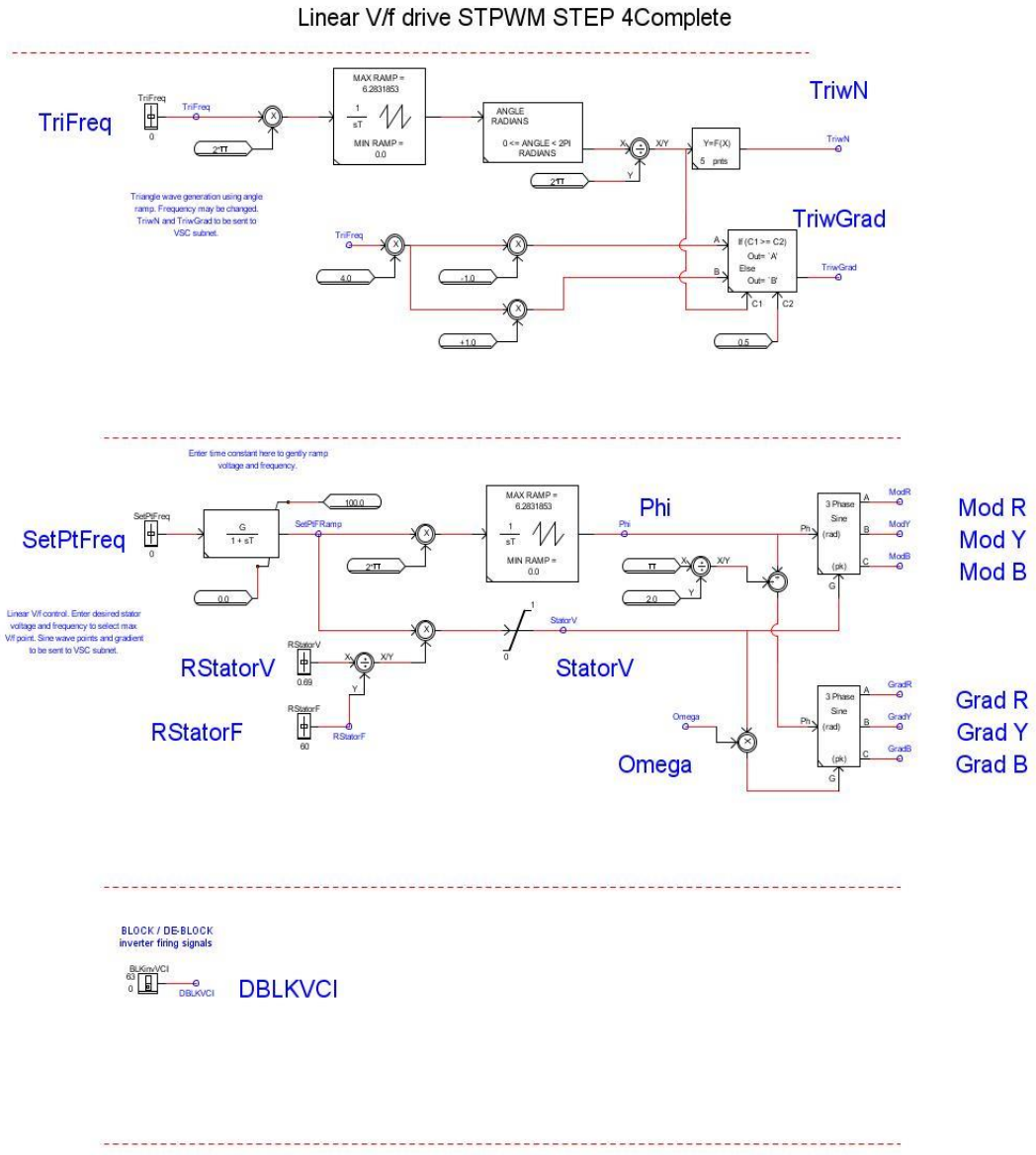

Figure 3.9 Linear V/f drive SPWM.

e) Drilling drive system motor (DRILLMT)

The parameterisation of the induction machine model in the small time-step sub-system is the same as the normal motor parameterisation discussed in section 3.3.2.1 (above). Table 3.2 presents the calculated electrical and mechanical parameters for the induction machine model in the small time-step sub-system used to represent the drilling drive system motor:

Table 3.2: Drilling drive system induction motor parameters.

Parameters	**RTDS**	**DrillMT**
Rated stator voltage-L-L RMS	vbsll	0.690 kV
Rated MVA	pbase	1.410 MVA
Rated frequency	hertz	60 Hz
Stator resistance	r_a	0.0174 p.u.
Stator leakage reactance	x_a	0.0414 p.u.
Unsaturated magnetising reactance	xmd0	4.7909 p.u.
First cage rotor resistance	rfd	0.1537 p.u.
First cage rotor leakage reactance	xfd	0.0414 p.u.
Inertia Constant (MWs/MVA)	H	0.1959 MWs/MVA

The induction machine model used within the small time-step sub-system in Figure 3.8 has a control signal input to select the mechanical operating mode of the machine, i.e. whether the machine's rotor is locked or free. When the machine is operated in "lock" mode, it reacts to the speed (in p.u) from an external model of the load dynamics and when it is operated in "free" mode, the machine reacts to the applied mechanical torque (p.u). Figure 3.10 shows the mathematical representation of the drilling motor mechanical system in the DRAFT model of the drilling drive system.

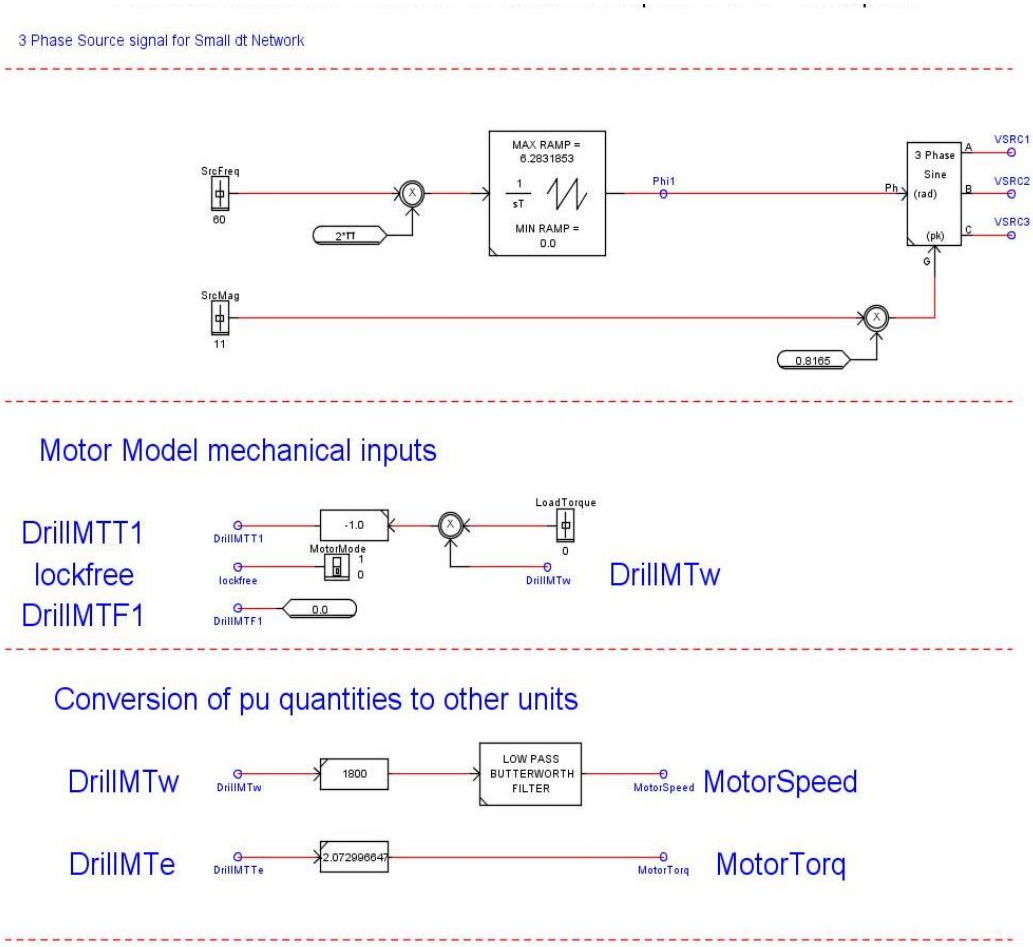

Figure 3.10 Small time-step drilling motor mechanical inputs.

3.3.4 Thruster Drive System

As shown in the system overview diagram of Figure 3.1, the thruster drive system is a medium voltage system that comprises a 6.5 MVA transformer (TR3) with two secondary windings (phase shifted by 30°), an AC to DC converter (REC), a DC link, and a series connected resistor to represent the load on the DC side. Figure 3.2 showed that in DRAFT this thruster drive system is represented within the small time-step bridge box labelled as 'THRUSTER DRIVE SYSTEM'. The function of the bridge box is to interface the small time-step sub-system with the main system network. Figure 3.11 now shows the detailed model of the thruster drive system developed within the small time-step bridge box in DRAFT, which comprises three single-phase interface transformers (THTR1, THTR2 and THTR3), a thruster drive system

transformer (TR1) with two secondary windings, an AC to DC converter (REC), a DC link, and a 4.2 Ohm (Ω) resistor.

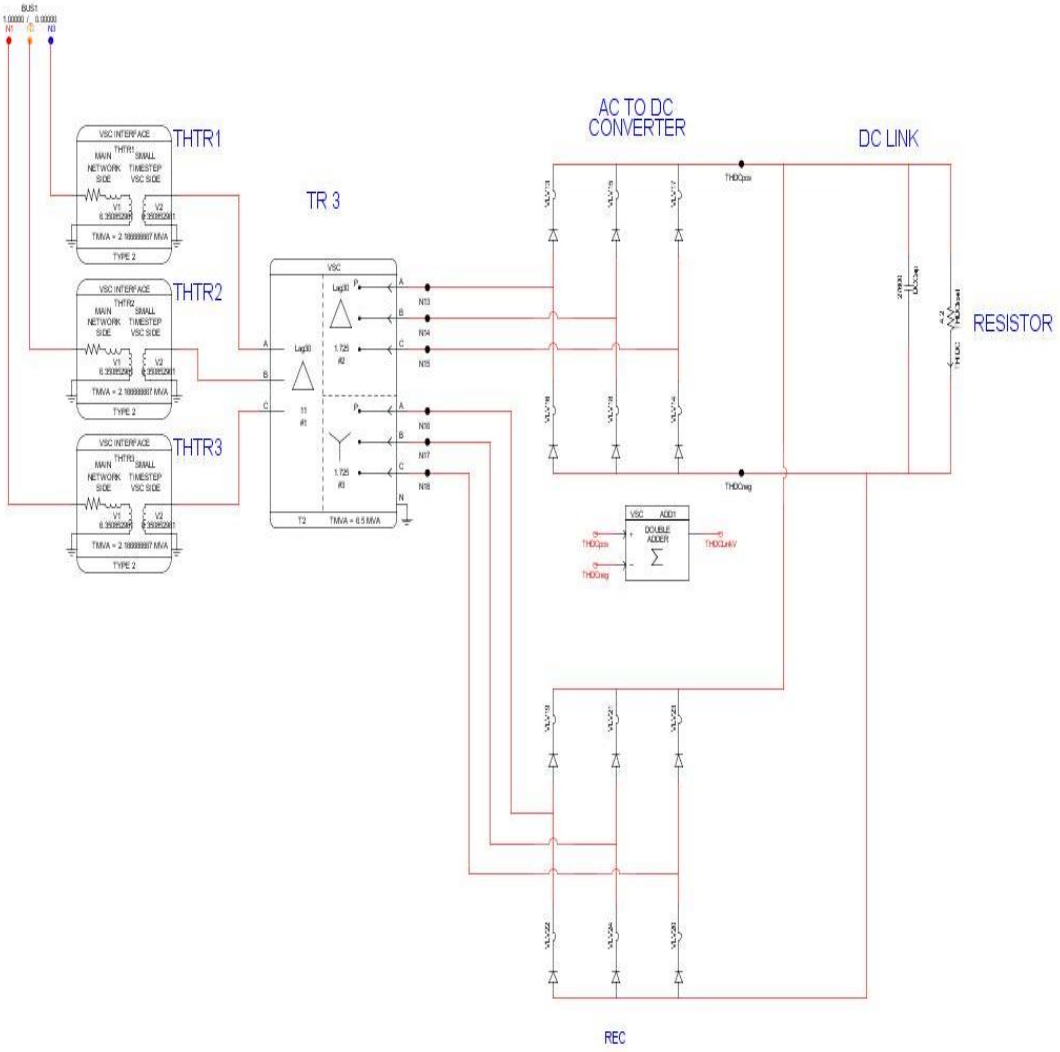

Figure 3.11 Thruster Drive System.

The sub-sections below outline each of the components of the small time-step simulation model of the thruster drive system.

a) Interface transformers

In the simulation model created in DRAFT, the three single-phase transformers (THTR1, THTR2 and THTR3) are the components that connect the small time-step subsystem to the main system network (BUS1). Each single-phase interface transformer is rated at 2.17 MVA, which is one-third of 6.5 MVA (the rating of the three-phase thruster system transformer) at a 1:1 transformation

ratio. The single-phase RMS voltage applied to the primary side of each interface transformer was 6.35 kV, and the voltage at the secondary winding was 6.35 kV. The primary side of the interface transformer (large DT) was connected to the main system network (BUS1), and the secondary side (small DT) was connected to the primary side of the thruster drive transformer (TR3).

b) Thruster drive transformer (TR3)

The small time-step three-phase three-winding transformer provides for the requirements of a 12-pulse rectifier (AC to DC converter), and the windings are phase-shifted by 30°. One of the secondary windings is delta connected and supplies one six-pulse rectifier, while the other secondary winding is star connected and supplies the second parallel six-pulse rectifier. The thruster transformer power rating is 6.5 MVA, the primary winding is rated at 11 kV, and the secondary windings are each rated at 1725 V.

c) AC to DC converter (REC)

The thruster drive transformer (TR3) supplies two parallel-connected six-pulse rectifiers (AC to DC converters). Each rectifier consists of six diodes that are configured for three-phase supply. The RSCAD rectifier model is parameterised so that it represents the actual rectifier on the drillship electrical network. The diode switching voltage magnitude was set at 4 kV and the switching current magnitude was set at 4 kA, which is also the current rating on the actual rectifier. The diode base frequency setting was set at 60 Hz, which is the drilling ship electrical network frequency.

The average output voltage of the each rectifier is $Vdc = 1.654\,Vm$ = 1.654 (1725 V) = 2853.15 V, and this is the expected average output voltage of the rectifier section in the simulation model.

The DC link section consists of a bank of capacitors (DCCap) connected across the DC output of the diode rectifier, with a capacitance of 27 600 micro Farads (μF).

d) Resistor

A shunt resistor was connected across the DC output terminals of the rectifier to provide a constant load for the thruster drive system. The resistor was selected to represent a load of 27.38% of the rectifier section full load current.

3.4 Development of Measurements Model

The naming convention of the RSCAD models is very important, and it requires that each model have a unique name. Each measured variable must also have a unique name. Figure 3.12 indicates the two-input summing blocks that are configured to measure the line-to-line voltages at Bus1 and Bus 2 of the drilling ship electrical network in Figure 3.2 from the respective phase to neutral voltages output by the simulation model. Figure 3.13 indicates the two-input summing junctions that are configured to measure currents at various locations on the drillship simulation electrical network.

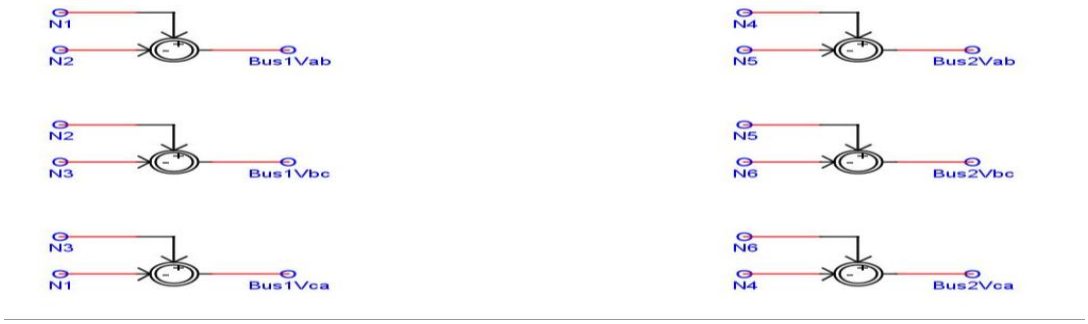

Figure 3.12 Bus1 and Bus 2 voltage measurements in DRAFT.

Figure 3.13 Current measurements in DRAFT.

Figures 3.14 and 3.15 show the components added to the simulation model to calculate current and voltage harmonics up to the seventh harmonic content.

In the phase-locked loop (PLL), the input is selected as either voltage or current. In Figures 3.12 and 3.13, the three inputs to the PLL block are the transformer (TR2) primary side-line currents or voltages, and the output (Phi) represents the phase angle of the A-phase input. The output of the PLL block is an input to the Discrete Fourier Transform (DFT) block, with reference to the signal input (IN) that can be either of the three line currents or voltages, and the output (Cn) from the DFT block is the harmonic content of the respective current or voltage harmonic parameter number selected. The harmonic number can be selected as a parameter input within the DFT block, and can be set as 1, 3, 5 or 7. The output current or voltage harmonic content can be plotted as a graph.

This combination of a phase locked loop (PLL) block and Discrete Fourier Transform (DFT) block was used to measure the voltage and current harmonic content of several different plant variables. The inputs to the PLL are either the line currents or voltages of interest, and the output selected was the phase angle (PHI). The output from the PLL is supplied as an input to the DFT block. The information extracted through this block is given out as the magnitude (C_n) and phase (phi) of the selected harmonic.

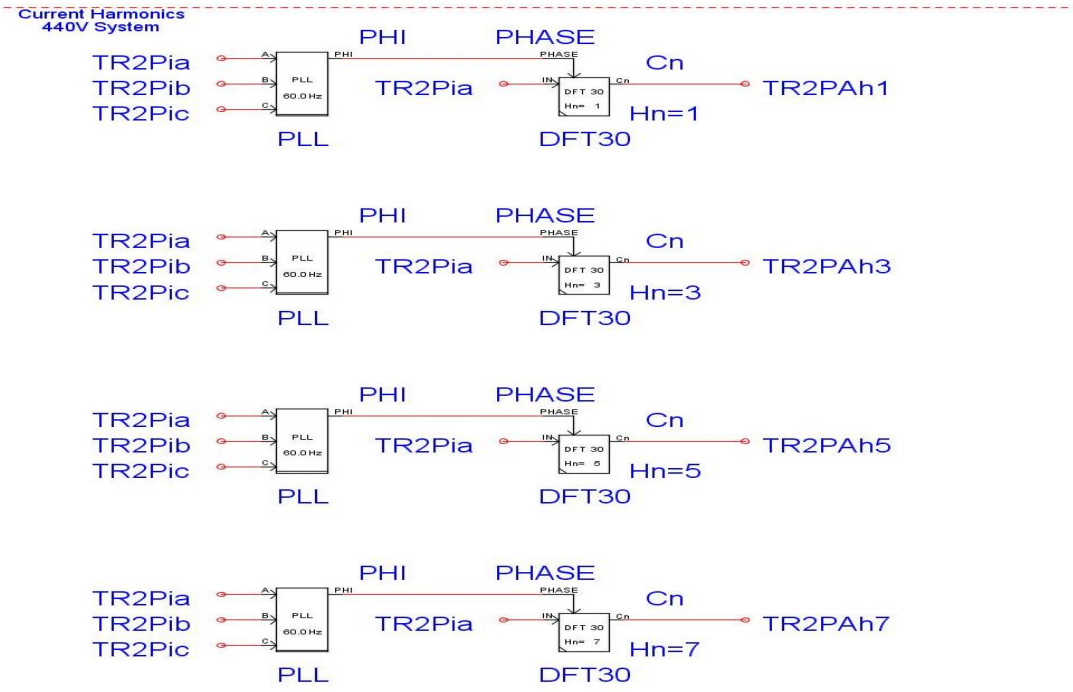

Figure 3.14 RSCAD harmonic current measurement model.

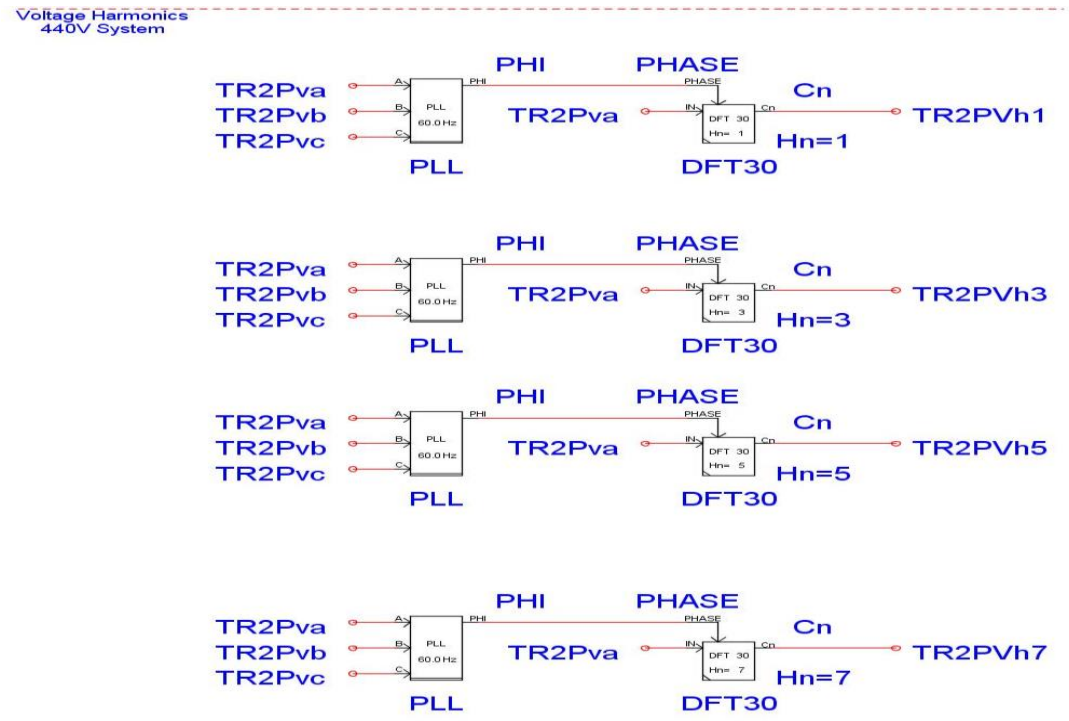

Figure 3.15 RSCAD harmonic voltage measurement model.

3.5 Power Quality Meter

Measurements of voltage and current harmonics are essential for the reliability of the drillship electrical network, in order to prevent major breakdowns and malfunctioning of equipment that could lead to catastrophic failures [2, 4, 8]. The measurements on a drillship electrical network are important, as they can be used to monitor existing harmonic contents against recommended or admissible levels. The reason for this field study measurement was to verify the study simulation results. The power analyser used for field measurements was the Fluke 435-II Power Quality and Energy Analyser, which has been designed and tested in accordance with the standard EN61010-1-2nd edition (2001) [2].

The meter measures and records up to the fiftieth harmonic. It also measures the DC components, THD and K-factor data. The K-factor is a number that quantifies potential overload in transformers due to harmonic currents [4]. The meter consists of four voltage probes and four current probes that are used for measurement purposes, and are rated for low voltages (up to 1000 V). The IEEE 519 standard states that the requirements for the meter are:

- Accuracy – the meter must measure a steady-state harmonic component with an error compatible with permissible limits.
- Selectivity – the meter must be able to separate harmonic components of different frequencies.

The measured data over a period of time, as per the IEEE standard requirements, are presented in a tabulated or graphical form. The field measurements were taken at various locations within the drillship electrical network. Due to safety considerations, measurements were taken on the 690 V drilling drive systems and the 440 V systems.

3.6 Conclusion

This chapter has presented an overview of a simplified representation of the drillship electrical network that is to be used for the study of harmonics in a real-time simulation. The developed real-time simulation model of this simplified electrical network was based on pre-developed generic models of induction motors, generators, rectifiers, and inverters, each configured to closely represent the characteristics and ratings of the actual equipment in the drillship system.

The RSCAD software models of induction motors and variable speed drives were reviewed and discussed in detail, since they are the core components of the study system being tested. A simplified drillship electrical system, set up for this study, illustrated how the real-time simulation model was conducted for determining the behaviour and performance of induction motors and variable speed drives to measure the level of harmonics. Furthermore, this chapter also presented the power quality analyser used for field measurements.

The next chapter focuses on the presentation and analysis of simulation results in comparison with field measurement results.

CHAPTER FOUR

Presentation of Results

4.1 Introduction

The previous chapter discussed the real-time simulation modelling of the simplified drilling ship electrical network that was developed within the real-time digital simulator interface, RSCAD electromagnetic transients software platform, in order to study the basic fundamentals of harmonics in electrical power systems. The detailed description of the power quality meter used for field harmonic measurements on the actual drilling ship electrical network was laid out in the preceding chapters. Models for the induction motor, variable speed drive, transformer and generator were configured using the calculated parameters found in Chapter Three in order to validate the actual equipment of the drilling ship electrical network model to be analysed.

This chapter presents the simulation results obtained from the simplified drilling ship electrical network model. The field measurement results taken using the power quality meter are also presented in this chapter. In addition, a comparison is drawn between the numerical simulated and field measured results. The comparison is not direct since the exact operating conditions during field measurements were unknown. As a result, the modelling assumptions used in the simulation studies, although representative and reasonable, were not based on any specific drilling ship operating conditions. The following section presents an overview of the drilling ship operating sequence adopted for the simplified drilling ship electrical network simulation studies in the chapter.

4.2 Overview of the drilling ship operating sequence

In order to gain insights into the validation of the simulation results and practical measurements that are to be contrasted in the latter part of this chapter, it is necessary to first understand the way in which the plant on the drilling ship is used in practice during typical operating conditions. This section, therefore, provides a brief overview of a typical operating sequence of the

drilling ship plant which is then followed by an explanation of how this operating sequence is replicated using the RUNTIME controls of the real-time simulation model of the plant that was introduced in Chapter Three.

Referring to Figure 3.1 of Chapter Three, which showed a reduced-scale representation of the actual drilling ship electrical network, an overview of a typical operating sequence of the plant is as follows. In order to closely replicate the practical operating sequence, in the simulation model of the drilling ship in Figure 3.1 the thruster system is permanently connected to the 11 kV busbar BUS1 which therefore begins to supply the rectifier REC and its constant load resistance R via transformer TR3 as soon as the simulation starts. This initial condition in the real-time simulation model replicates the steady-state operation of the thruster system on board the practical drilling ship when it is running at constant speed while holding the drilling ship in position over the well-head.

The RUNTIME Generator controls sliders shown in Figure 4.1 illustrate the generator model's user-adjustable settings for the supply voltage and frequency. The generator output voltage was fixed at 11 000 V at 60 Hz, and represented the actual drilling ship generator. These parameters were maintained for the entire duration of the simulation study.

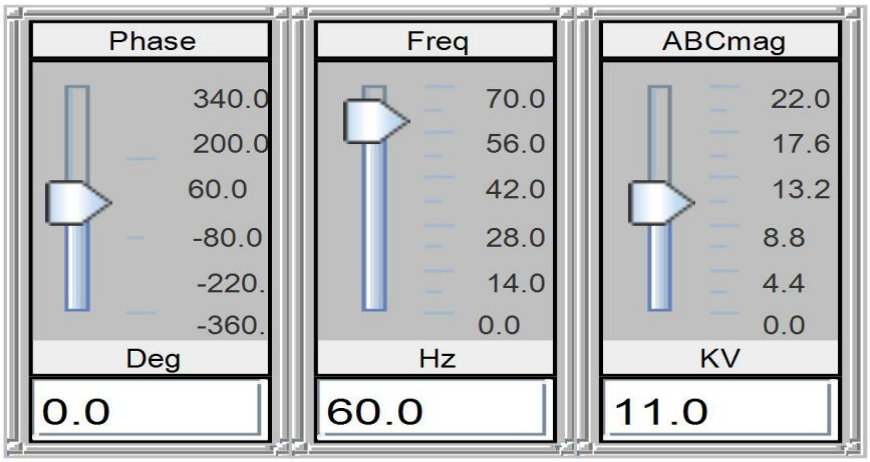

Figure 4.1 RUNTIME GENERATOR Sliders.

In the simplified representation of the drilling ship shown in Figure 3.1, the drilling auxiliary system is labelled 440V SYSTEM. In the simulation model the transformer TR2 that supplies this auxiliary drilling system is permanently

connected to the 11kV busbar BUS1 which therefore energises the 440V busbar BUS2 as soon as the simulation starts. The 440V system consists of a hydraulic pump, a drilling water pump and a fire system pump that are represented within the real-time simulation model by the three pump motors P1, P2 and P3 respectively. In the detailed diagram of the simulation model shown in Figure 3.2, the three pump motors are fed by transformer TR2 and each pump motor has its own circuit breaker. The first two pump motors (P1 and P2) are started simultaneously by closing their respective circuit breakers once the thruster drive system has reached its steady-state, in order to provide lubrication for the drilling drive system equipment and to supply process water used during the drilling process. The third pump (P3) supplies fire system water depending on the required pressures within the fire system; in the simulation model the pump motor P3 is manually started and stopped during the study by opening and closing its circuit breaker.

In the simplified representation of the plant in Figure 3.1, the drilling drive system is labelled as DRILLING and its front-end rectifier REC is permanently connected, via the transformer TR1, to the 11kV busbar BUS1 so that the DC link capacitor of the drive is charged up as soon as the simulation is started. However, the drive inverter is only started after each of the three pumps P1 to P3 described previously have started and reached their respective steady-state conditions. In the simulation model shown in Figure 3.2, the DRILLING DRIVE SYSTEM inverter was started at zero speed (0Hz). The speed was then increased to full speed (60Hz) at rated load torque (0.74 p.u.)

The starting, stopping and control of the equipment within the simplified drilling ship electrical network model shown in Figure 3.2 was done from within the RUNTIME interface using the switches and sliders shown in Figure 4.2. The two sliders in Figure 4.2 represent the operator-adjustable settings inputs of the drilling drive system used to vary the speed and torque of the inverter-motor DRILLMT. The sliders are used to set the speed and torque for the initial starting condition (both speed and torque set at zero) and then to increase the drilling drive system's settings to full speed and rated load at the appropriate time in the simulation of the operating cycle. Figure 4.3 shows the positions of

the switches and sliders during the final steady-state operation of the model, with the sliders indicating the load settings of the inverter motor at steady-state.

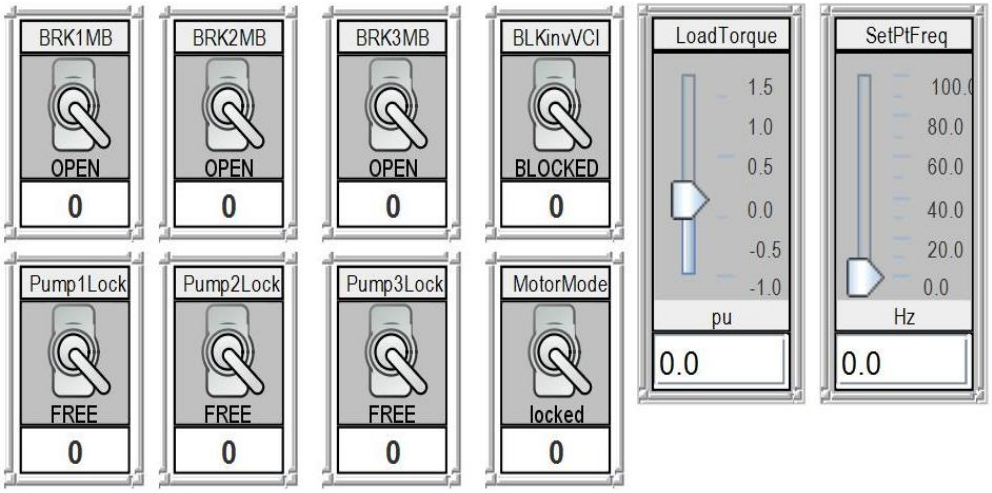

Figure 4.2 RUNTIME simulation model switches and sliders in their initial states.

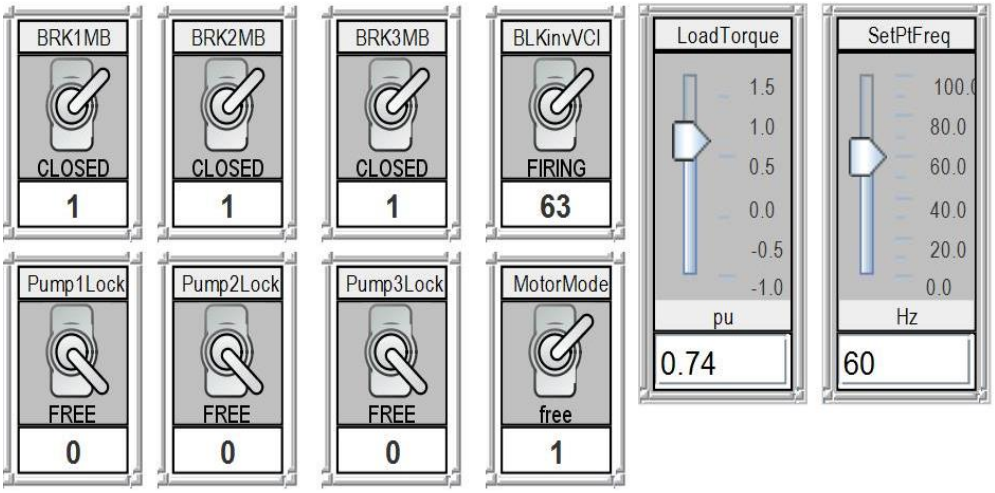

Figure 4.3 RUNTIME simulation model switches and sliders in their final states, with all motors running.

The following section presents some of the simulation results taken during different stages of the aforementioned operating sequence summarised in Appendix J.

4.3 Simplified drilling ship electrical network simulation results

The results presented in this section were taken from the simplified drilling ship electrical network simulation model shown in Figure 3.2. The primary objectives of the studies presented in this section were mainly:

- To illustrate the impact of direct on line starting of large induction motors on the network variables such as voltage and current;
- To evaluate the impact of starting and running the variable speed drive on the network variables (current and voltage).

As discussed in Chapter 3, the studies of poor power quality on a drilling ship electrical network were carried out using the real-time simulation model shown in Figure 3.2. With the exception of recording the initial ENGINE 1 open-circuit voltage output characteristics for reference purposes, all of the simulation results were taken at different stages during the normal drilling ship operating sequence described in Section 4.2. Therefore, the results to come (Figure 4.5 to Figure 4.16) present the responses of selected variables (current, voltage, speed and torque) of the simplified drilling ship electrical network simulation model during normal drilling operations.

4.3.1 ENGINE 1 open-circuit voltage waveform

The generator output voltage is a critical variable for the simplified drilling ship electrical network simulation model shown in Figure 3.2. Therefore for reference purposes, it was important to record the nature of this voltage waveform with no other equipment connected to the 11kV busbar BUS1, even though this open-circuit generator condition is not part of the normal operating sequence of the plant. Figure 4.4 shows the generator open-circuit output voltage waveforms. These pure sinusoidal voltage waveforms under open-circuit conditions are presented to demonstrate that the generator itself does not contribute harmonics into the simulation network, in the studies that are to be presented hereafter.

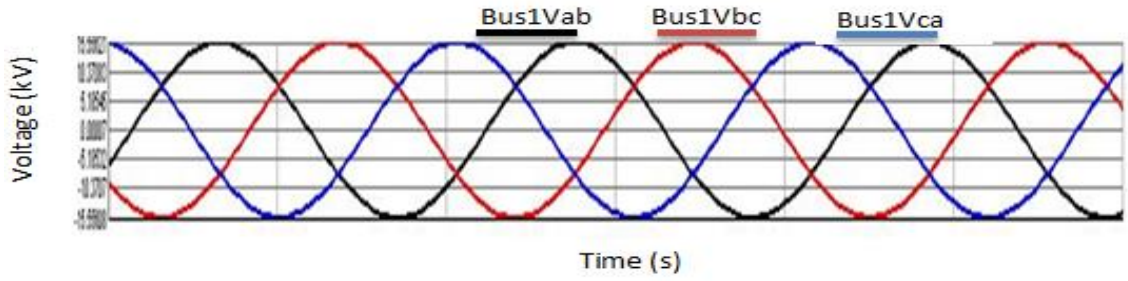

Figure 4.4 Generator output voltage waveform under open-circuit conditions.

4.3.2 Simplified drilling ship electrical network simulation model initial condition

Section 4.2 indicated that the simulation study starts with the steady-state load of the thruster drive system already connected. The graphical results in Figure 4.5 now show the voltage waveforms at selected locations within the simplified drilling ship electrical network under these initial steady-state conditions. The voltage waveforms in Figure 4.5 show the peak voltages at the busbars in the respective systems (BUS1, BUS2 and on each of the two secondary-side windings of transformers TR1 and TR3) as follows:

- Graph 1 – BUS1 voltage waveforms;
- Graph 2 – BUS2 voltage waveforms;
- Graph 3 – transformer TR1 *delta*-connected secondary winding voltage waveforms of the drilling drive system;
- Graph 4 – transformer TR1 *star*-connected secondary winding voltage waveforms of the drilling drive system;
- Graph 5 – transformer TR3 *delta*-connected secondary winding voltage waveforms of the thruster drive system;
- Graph 6 – transformer TR3 *star*-connected secondary winding voltage waveforms of the thruster drive system.

The peak voltage (V_p) at BUS1, taken from Graph 1, was found to be 15.55 kV for which the calculated RMS value is as follows:

Vp = 1.02 k

$$V_{RMS} = \frac{V_p}{\sqrt{2}}$$ Vp = 2.3 k V

$$= \frac{15.55\,\text{kV}}{\sqrt{2}} = 11.0\ \text{kV}$$ Vp = 2.3 k V

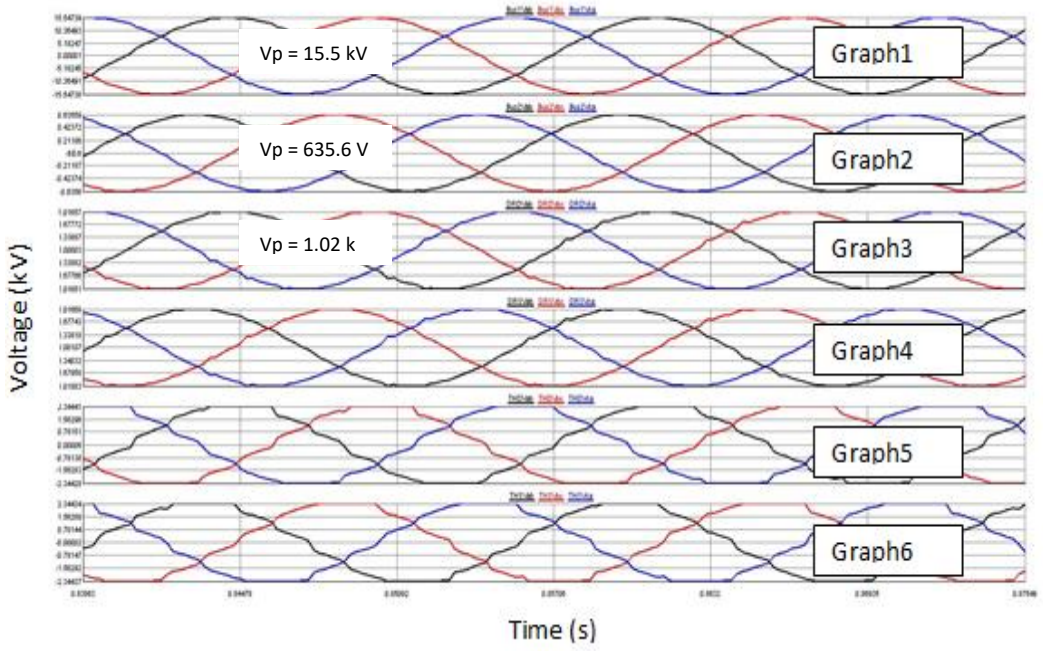

Figure 4.5 Voltages within the simplified electrical network recorded during the initial steady-state conditions in the simulation study (thruster drive system running at steady-state, motors P1 to P3 and DRILLMT not yet in service).

The peak voltage at BUS2, taken from Graph 2 was 635.6 V and its calculated RMS value is 449.4 V. The drilling drive system transformer TR1 secondary winding (delta and star) peak voltages (Graphs 3 and 4) were 1.02 kV (calculated RMS values 718.8 V). The thruster drive system transformer TR3 secondary winding (delta and star) peak values were both found to be 2.3 kV (calculated RMS values 1.7 kV). The rectifiers of the thruster drive system draw non-sinusoidal currents from BUS1, resulting in distorted waveforms in the secondary-side voltages of transformer TR3 under these steady-state initial load conditions as shown in Graphs 5 and 6.

4.3.3 Direct On Line starting of induction motors and its impact on the network variables

Figures 4.6 to 4.8 show the responses, during direct on line sequential starting of the three pump motors P1, P2 and P3, of each motor's own variables as it starts and runs up to speed. The motor variables selected for plotting are the speed, current and torque. Figure 4.6 shows the transient envelope of the instantaneous current, the fluctuating torque and increasing speed during the starting period of the P1 pump motor. The duration of the starting transient of the P1 pump motor was 0.7 seconds, during which time the speed increased from zero to 377 radians per second and the current decayed from the maximum starting current drawn of 1 315 A to 209.3 A at steady-state. The starting current was approximately 6.3 times the P1 pump motor's full load current of 209.3 A.

Figure 4.7 shows the transient envelope of the instantaneous current, the fluctuating torque and increasing speed during the starting period of the P2 pump motor. The duration of the starting transient of the P2 pump motor was 1.1 seconds, during which time the speed increased from zero to 377 radians per second and the current decayed from the maximum starting current drawn of 1 550 A to 254.6 A at steady-state. The starting current was approximately 6.1 times the P2 pump motor's full load current of 254.6 A.

Figure 4.8 shows the transient envelope of the instantaneous current, the fluctuating torque and increasing speed during the starting period of the P3 pump motor. The duration of the starting transient of the P3 pump motor was 1.35 seconds, during which time the speed increased from zero to 377 radians per second and the current decayed from the maximum starting current drawn of 4 602.5 A to 690.6 A at steady-state. The starting current was approximately 6.7 times the P3 pump motor's full load current of 690.6 A.

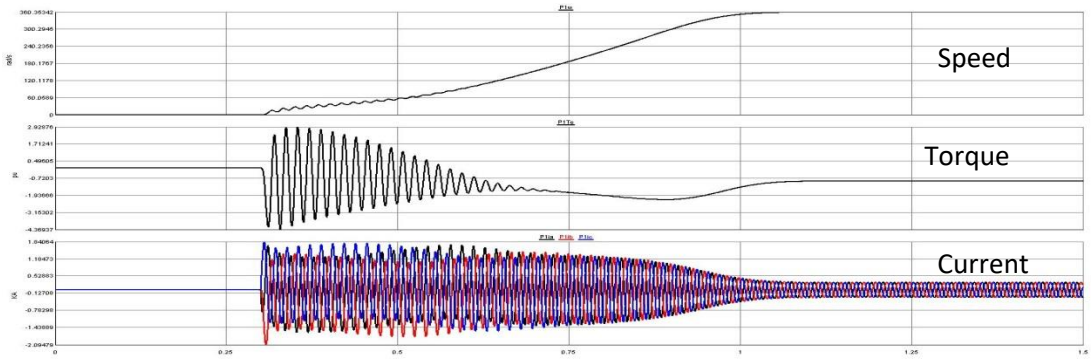

Figure 4.6 The characteristic behavior of P1 pump motor variables during its own direct on line start.

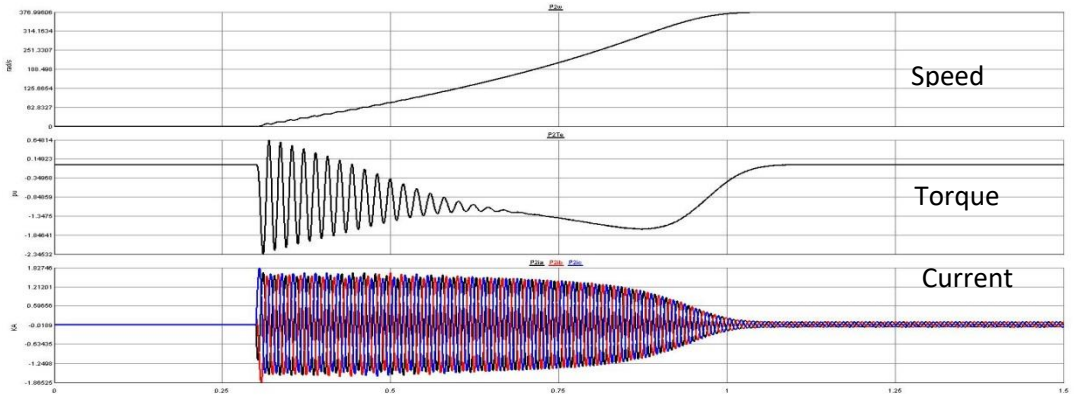

Figure 4.7 The characteristic behavior of P2 pump motor variables during its own direct on line start.

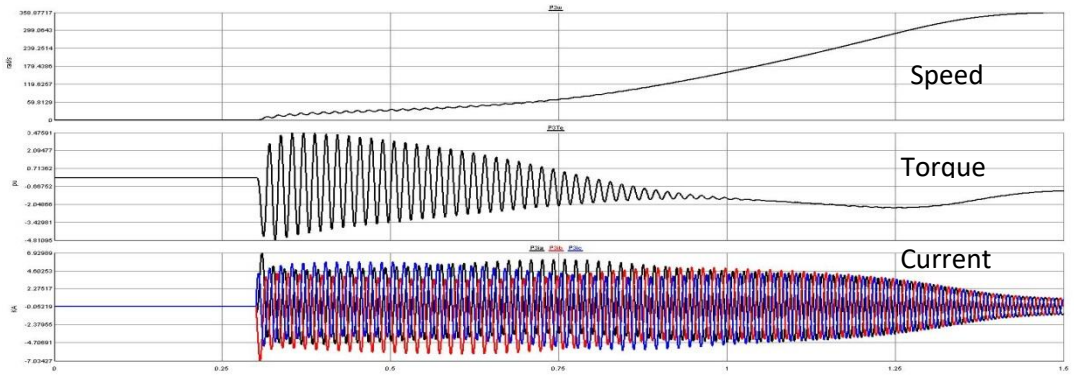

Figure 4.8 The characteristic behavior of P3 pump motor variables during its own direct on line start.

The differences between the amplitudes and durations of the transients during the direct on line starting of the three pump motors seen in the simulation results of Figures 4.6 to 4.8 are as a result of the different sizes (ratings) of these mechanical pumps, and the induction motors that drive them, in the actual drillship plant. The nameplate ratings and detailed parameters of the induction motors driving pumps P1, P2 and P3 are given in Table 3.1 of Chapter Three and in Appendices B to D, but the parameters of the motors with the most significant impact on their starting transients (motor ratings and inertia constants) are summarized here as follows: pump motor P1 is rated at 132 kW and has an inertia constant H of 0.4035 seconds; pump motor P2 is rated at 160 kW with an inertia constant of 0.4106 seconds; pump motor P3 is rated at 450kW with an inertia constant of 0.5918 seconds.

As seen in the above comparison of the motor parameters, machines with larger power ratings typically have larger inertias because they have physically larger motor frame sizes. The larger the inertia of the motor, the longer it takes to run up from standstill to rated speed during a direct on line start. Figure 4.8 confirms that the largest rated pump motor, P3, takes the longest time (1.35 seconds) to run up from zero to rated speed when started direct on line. Figure 4.7 shows that the next largest pump motor, P2, takes 1.1 seconds to run up to rated speed whilst Figure 4.6 shows that the smallest pump motor, P1, takes only 0.7 seconds to reach rated speed.

Furthermore, comparison of Figures 4.6 to 4.8 shows that the larger the size of the pump motor, the bigger the amplitude of the currents it draws during its starting transients and hence the greater the likely impact on the power quality of surrounding network variables during that starting transient. Therefore, pump motors P1 and P2 would be expected to have a smaller impact on the surrounding network variables during starting, and this impact would be expected to last for a shorter duration, than would be the case for the much-larger rated pump motor P3, based on the results of Figures 4.6 to 4.8.

Figures 4.9 to 4.12 now show the impact of direct on line starting of two of the pump motors (P2 and P3) on the rest of the drillship electrical network variables during the above simulation studies, specifically: the current

waveforms of the pump motors that are already running; the voltages of the upstream busbars (BUS1 and BUS2); the voltages of each of the two secondary-side windings of transformers TR1 and TR3.

Figure 4.9 consists of two graphs that show the impact of direct on line starting of the the pump motor P2 on the current drawn by the pump motor P1 that is already running. Graph 1 shows the current waveforms of the pump motor P1 that is already running when P2 pump motor is started. Graph 2 shows the transient envelope of the instantaneous currents of the pump motor P2 during its run up to full speed as seen earlier in Figure 4.7. Figure 4.9 shows that the pump motor P1 was initially at steady-state, drawing full load current, until the time T1 at which the pump motor P2 was started directly on line. Figure 4.9 then shows that immediately after the starting of motor P2 at time T1, the current drawn by the motor P1 briefly decreases (for approximately two cycles) but then increases again until at time T2, its amplitude is larger than its steady-state value prior to the starting of motor P2. During the time period T2 to T3 in Figure 4.9, while the pump motor P2 draws large transient starting currents, the current drawn by the motor P1 increases to 309 A, a value that exceeds its full load current of 254.6 A. Only after time T3, when the transient current drawn during the starting of motor P2 begins to decrease, does the current drawn by motor P1 return to a value below its nameplate rating.

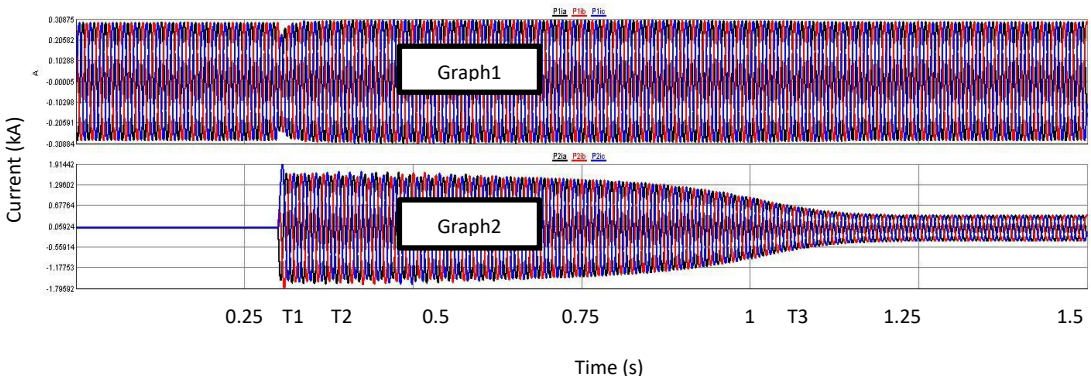

Figure 4.9 The impact of direct on line starting of pump motor P2 on the current drawn by pump motor P1 that is already running.

The results of Figure 4.9 show clearly how the transient currents caused by direct on line starting of one motor can impact the currents drawn by another motor already started and running in the same plant. The reason that the

starting transient of one motor can impact on the currents drawn by a neighboring motor is the impact of such starting currents on their shared voltage at the point of common coupling in the electrical network. Hence the next two figures (Figures 4.10 (a) and (b)) consider the voltages in the drillship electrical network at different times during the simulation study shown in Figure 4.9.

Figure 4.10 (a) shows the voltage waveforms within the electrical network, during the time when the thruster drive system and the P1 pump motor are running at steady-state, prior to the direct on line starting of the P2 pump motor. Figure 4.10 (b) shows the depressed voltage waveforms during the run up of the P2 pump motor; the recorded voltages are shown for a period of approximately two cycles corresponding to the time period between 0.84 and 0.88 seconds in Figure 4.9. Figures 4.10 (a) and (b) consist of six graphs, showing the peak voltages at the busbars in the respective systems (BUS1, BUS2 and on each of the two secondary-side windings of transformers TR1 and TR3 as follows:

- Graph 1 – BUS1 voltage waveforms;
- Graph 2 – BUS2 voltage waveforms;
- Graph 3 – transformer TR1 *delta*-connected secondary winding voltage waveforms of the drilling drive system;
- Graph 4 – transformer TR1 *star*-connected secondary winding voltage waveforms of the drilling drive system;
- Graph 5 – transformer TR3 *delta*-connected secondary winding voltage waveforms of the thruster drive system;
- Graph 6 – transformer TR3 *star*-connected secondary winding voltage waveforms of the thruster drive system.

The peak value V_p of the voltage at BUS2, taken from Graph2 of Figure 4.10 (a) was 633.37 V whilst the peak value V_p of the voltage at BUS2 from Graph2 of Figure 4.10 (b) was 614.75 V; this difference between the peak voltages at BUS2 prior to the starting of the P2 pump motor and during the run up of the P2 pump motor is 18.62 V, corresponding to a 3.03 percent voltage sag. Even though the recorded peak voltage at BUS2 in Figure 4.10 (b) corresponds to a

two-cycle period of the entire duration of the starting transient of the P2 pump motor that lasted 1.1 seconds, it can be used to show the impact on the power quality of the electrical network variables.

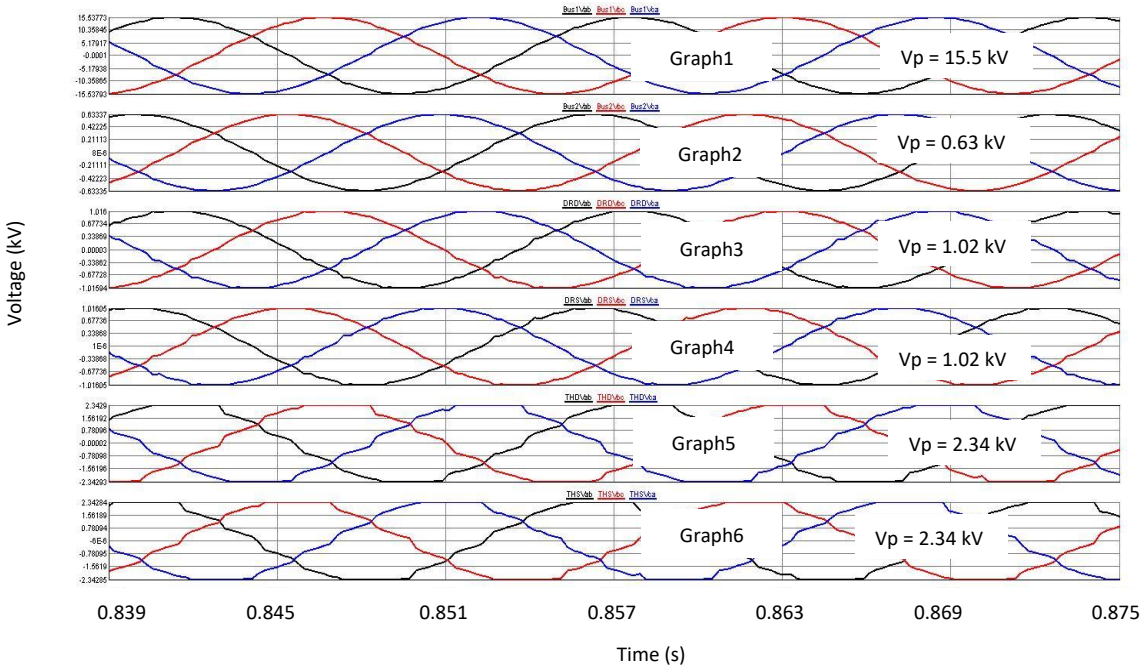

Figure 4.10 (a) Voltages within the electrical network during the P1 pump motor steady-state conditions (thruster drive system and P1 motor running at steady-state, motors P2 to P3 and DRILLMT not yet in service).

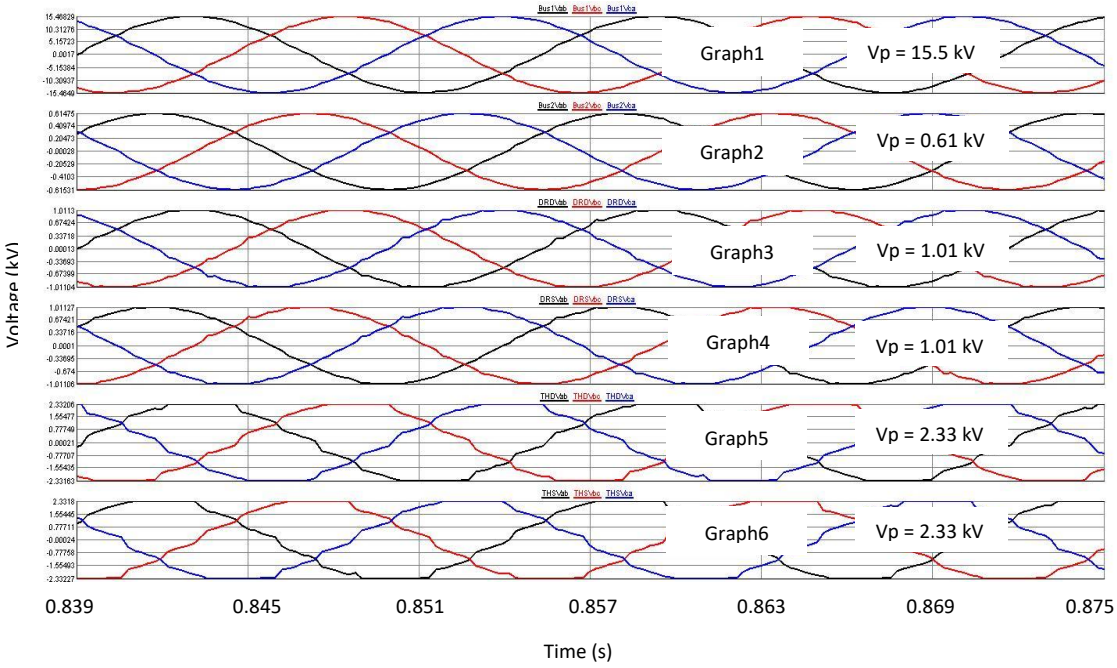

Figure 4.10 (b) The impact of direct on line starting of pump motor P2 on the electrical network voltage waveforms.

Figures 4.10 (a) and (b) show that the peak values of the voltages at BUS1 and on each of the two secondary-side windings of transformers TR1 and TR3 during the starting and run up of the P2 pump motor remain unchanged. The above analysis has shown how the transients caused by starting the pump motor P2 affect the pump motor P1 by causing a measurable sag in the voltage at the point of common coupling of these pump motors in the drillship electrical plant (the 440 V busbar BUS2 in Figure 3.1). The topology of the electrical network in Figure 3.1 shows that there is also a busbar further upstream in the network (the 11 kV busbar BUS1) that is a point of common coupling between the pump motors P1 to P3 and the drilling and thruster drive systems. If the transient currents drawn by direct on line starting of motors P1 to P3 were also to cause a significant sag in the 11 kV BUS1 voltage, these starting transients could also affect the performance of these drive systems. However, analysis of the voltages at BUS1, and on the secondary-sides of transformers TR1 and TR3 during the transients in Figure 4.9 showed that there is no measurable impact at these locations in the neighboring plant during direct on line starting of pump P2.

Figure 4.11 now shows the impact of direct on line starting of the pump motor P3 on the currents drawn by the pump motors P1 and P2 when both of these motors are already in service. Graphs 1 and 2 show the current waveforms of the P1 and P2 pump motors that are already running when the P3 pump motor is started. Graph 3 shows the transient envelope of the instantaneous current of the P3 pump motor during its run up to full speed as seen earlier in Figure 4.8. In Figure 4.11, the P1 and P2 pump motors are initially running at steady-state, drawing full load current until time T1 prior to the starting of the P3 pump motor. At time T1, the P3 pump motor is started directly on line resulting in a significant but brief decrease in the currents drawn by the P1 and P2 pump motors as shown in Graphs 1 and 2.

These initial transient decreases in the P1 and P2 motors' currents lasted for half a cycle on the red and black phases. Thereafter, the current of the P1 pump motor increased in amplitude to 358.05 A (calculated RMS value 253.18 A), corresponding to 1.21 times the rated full load current (209.3 A) of the motor; the current of the P2 pump motor likewise then increased in amplitude to 450.41 A (calculated RMS value 318.49 A), corresponding to 1.25 times the motor rated current of 254.6 A. Graphs 1 and 2 show that both the P1 and P2 pump motors remained in this temporary overload condition until time 1.25 seconds, whereafter the transient envelope of the P3 motor's starting current starts to decrease in amplitude and reaches steady-state condition at time T2. At time T2, the P3 pump motor reaches its steady-state load condition as shown in Graph3, and the motors P1 and P2 return to normal full-load current.

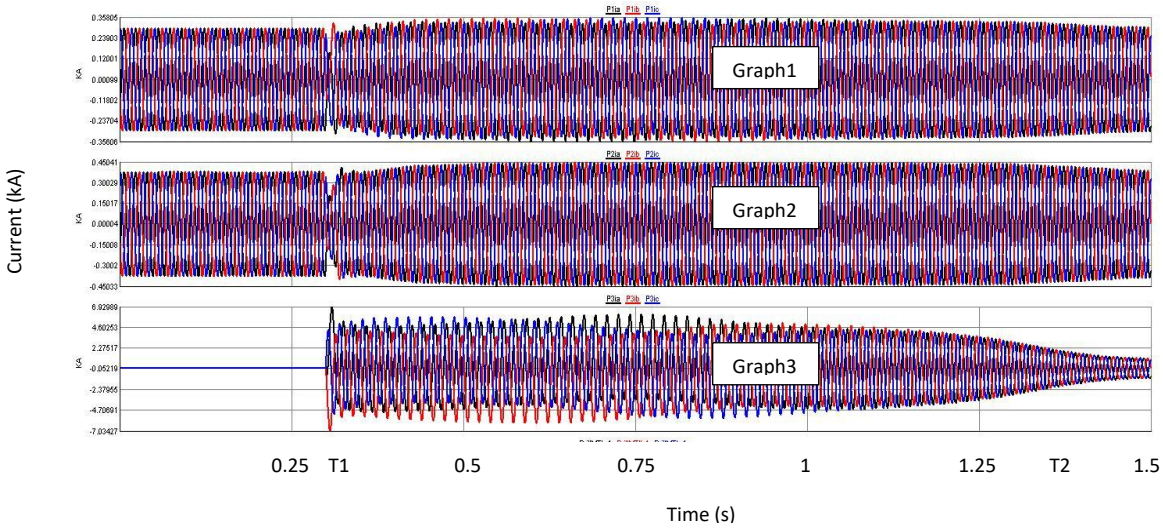

Figure 4.11 The impact of direct on line starting of pump motor P3 on the currents drawn by the pump motors P1and P2 that are already running.

Figure 4.12 (a) shows the voltage waveforms within the electrical network, during the time when the thruster drive system, and the P1 and P2 pump motors are running at steady-state, prior to the direct on line starting of the P3 pump motor. Figure 4.12 (b) shows the depressed voltage waveforms during the run up of the P3 pump motor; the recorded voltages are shown for a period of approximately two cycles corresponding to the time between 0.84 and 0.88 seconds in Figure 4.11. Figures 4.12 (a) and (b) consist of six graphs, showing the peak voltages at the busbars in the respective systems (BUS1, BUS2 and on each of the two secondary-side windings of transformers TR1 and TR3 as follows:

- Graph 1 – BUS1 voltage waveforms;
- Graph 2 – BUS2 voltage waveforms;
- Graph 3 – transformer TR1 *delta*-connected secondary winding voltage waveforms of the drilling drive system;
- Graph 4 – transformer TR1 *star*-connected secondary winding voltage waveforms of the drilling drive system;
- Graph 5 – transformer TR3 *delta*-connected secondary winding voltage waveforms of the thruster drive system;
- Graph 6 – transformer TR3 *star*-connected secondary winding voltage waveforms of the thruster drive system.

The values of the peak voltage V_p at BUS2, taken from Graph2 of Figures 4.12 (a) and (b) were 630.55 V and 537.28 V, respectively. The difference between these two values of the BUS2 voltage prior to, and during direct on line start of the P2 pump motor is 93.27 V, corresponding to a 14.8 percent voltage sag. Even though the recorded voltage at BUS2 in Figure 4.12 (b) corresponds to a two-cycle period of the entire duration of the starting transient of the P3 pump motor that lasted 1.35 seconds, it can be used to show the impact on the power quality of the electrical network variables. The results show that, as expected, the starting of the largest pump motor, P3, direct on line has a much more significant impact (14.8% voltage sag) on the 440 V BUS2 voltage than is the case for the direct on line starting of the smaller pump motor P2 (3% voltage sag).

The impact on the electrical network caused by the starting of the bigger pump motor P3 (450 kW) can also be seen in the sags it causes in the voltages of the busbars further upstream (11 kV BUS1) and in the voltages of the two secondary-side windings of transformers TR1 and TR3. As seen previously in Figure 4.10 (a) and (b), the starting of the smaller pump P2 had no measurable impact on the BUS1 voltage or on the transformer TR1 and TR3 secondary voltages. By contrast, Figure 4.12 (a) and (b) shows that direct on line starting of the P3 pump motor causes a sag in the BUS1 voltage of 340 V (2.2%), a sag in the TR1 secondary-side voltage of 40 V (3.9%) and a sag in the TR3 secondary-side voltage of 50 V (4.9%).

Thus, direct on line starting of the P3 pump motor draws sufficiently large transient currents to influence not only the performance of the other pumps P1 and P2 fed off the common 440 V busbar, but also to influence the drilling and thruster drive systems fed off the upstream 11 kV busbar.

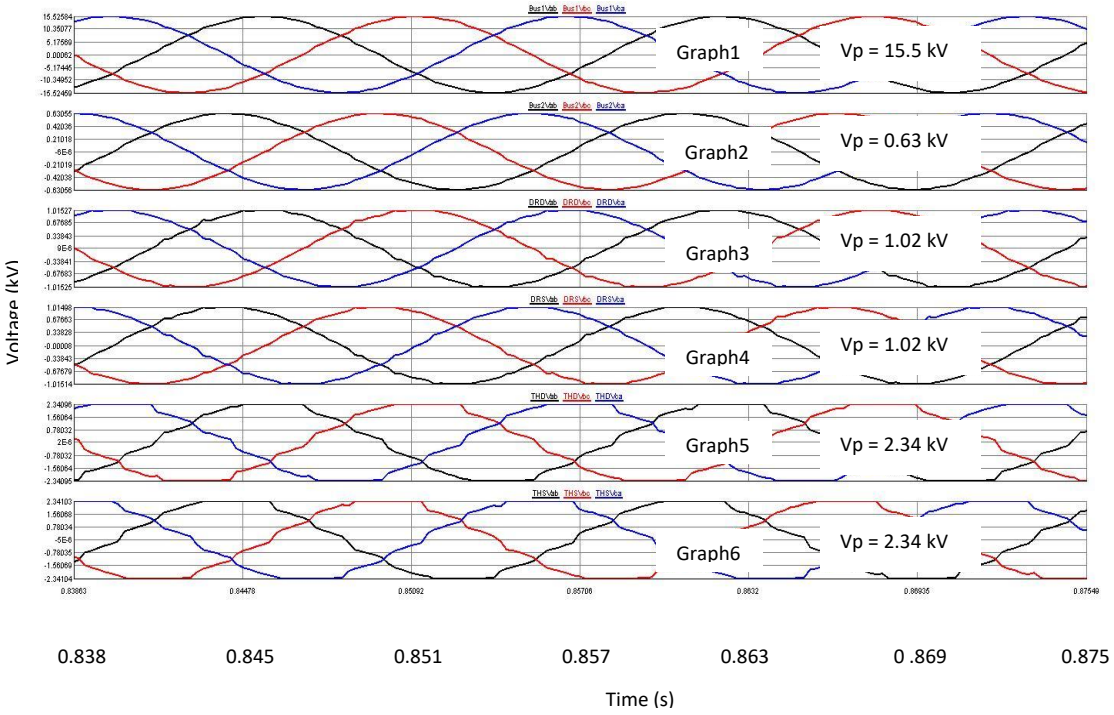

Figure 4.12 (a) Voltages within the simplified electrical network with the P1 and P2 pump motors in service (thruster drive system, P1 and P2 motors running at steady-state, motors P3 and DRILLMT not yet in service).

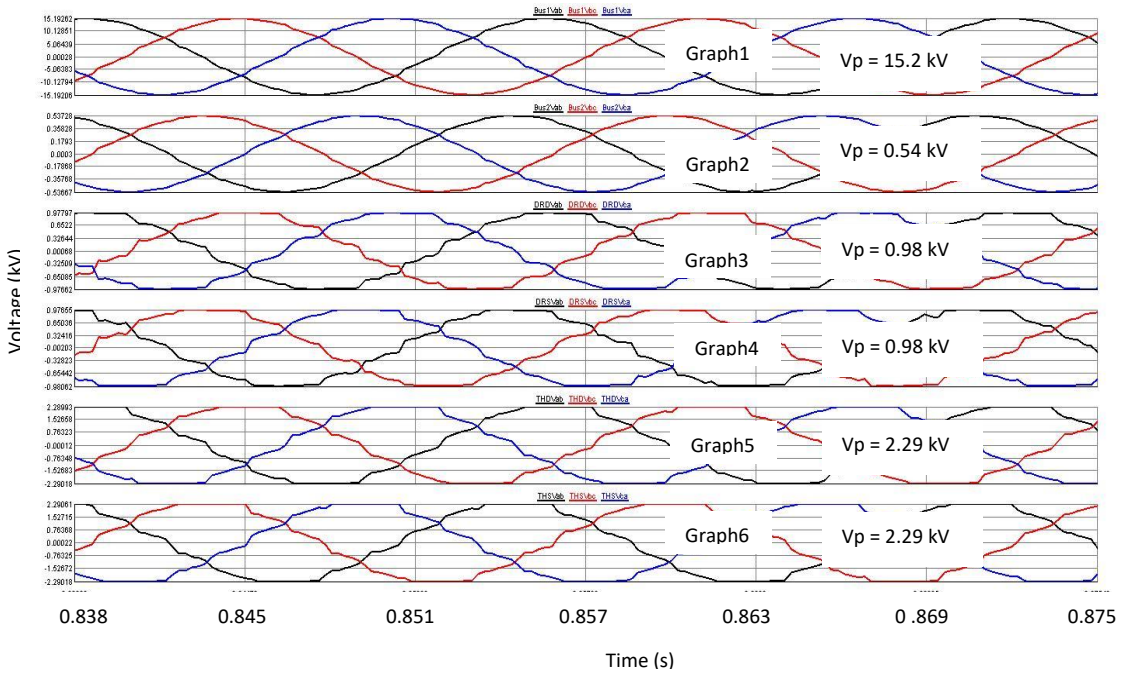

Figure 4.12 (b) The impacts of direct on line start of pump motor P3 on the electrical network voltage waveforms.

4.3.4 The impact of operating a VSD inverter motor on electrical network variables

The previous section presented the impact of direct on line starting of the three pump motors on the drillship electrical network variables. The previous section also showed that when the largest pump motor P3 was started, a measurable impact was noticed in the voltages of both busbars BUS1 and BUS2, and in the secondary-side voltages of transformers TR1 and TR3, even though the pump motor P3 is connected to BUS2. This is caused by fact that the 11kV busbar BUS1 is the drillship electrical network point of common coupling, and all other systems are fed from it. Therefore, this section presents the impact on the drill ship electrical network caused by running the variable speed drive operated drilling motor that is fed from this 11kV busbar BUS1.

Figures 4.13 to 4.18 show the impact of running the variable speed drive operated drilling motor on the drillship electrical network variables; these recordings of current and voltage in the electrical network were taken under steady-state conditions during the simulation study (motors P1, P2, P3 and DRILLMT in service).

Figure 4.13 shows the currents and voltages on the delta-connected secondary winding of the transformer TR1 that feeds the drilling drive system. Figure 4.13 shows the distorted nature of the current and voltage waveforms when the motor DRILLMT is running at steady-state; the recorded currents and voltages are shown for a period of approximately two cycles (between 0.56 and 0.6 seconds) of a longer study. The voltage waveforms, although very distorted, are quasi-sinusoidal, while the currents are seen to be non-sinusoidal, as expected, since each secondary-side winding of the transformer TR1 feeds a six-pulse diode rectifier at the front end of the drilling drive system (see Figure 3.8 in Chapter Three).

Figure 4.14 now shows the amplitudes of the main harmonic components of the voltage on the delta-connected secondary winding of transformer TR1 during the time when the motor DRILLMT is running at steady-state and on load; the frequency components shown are the fundamental, third, fifth and seventh harmonics calculated over a period of 1.5 seconds during steady-state conditions. The average RMS amplitudes of the fundamental, third, fifth and

seventh harmonic components in Figure 4.14 are respectively, 1.014 kV, 0 kV, 0.013 kV and 0.012 kV. The absence of any third harmonic component in this secondary-side transformer voltage (0 kV) is expected since the triplen harmonic currents circulate within a delta-connected winding of a transformer.

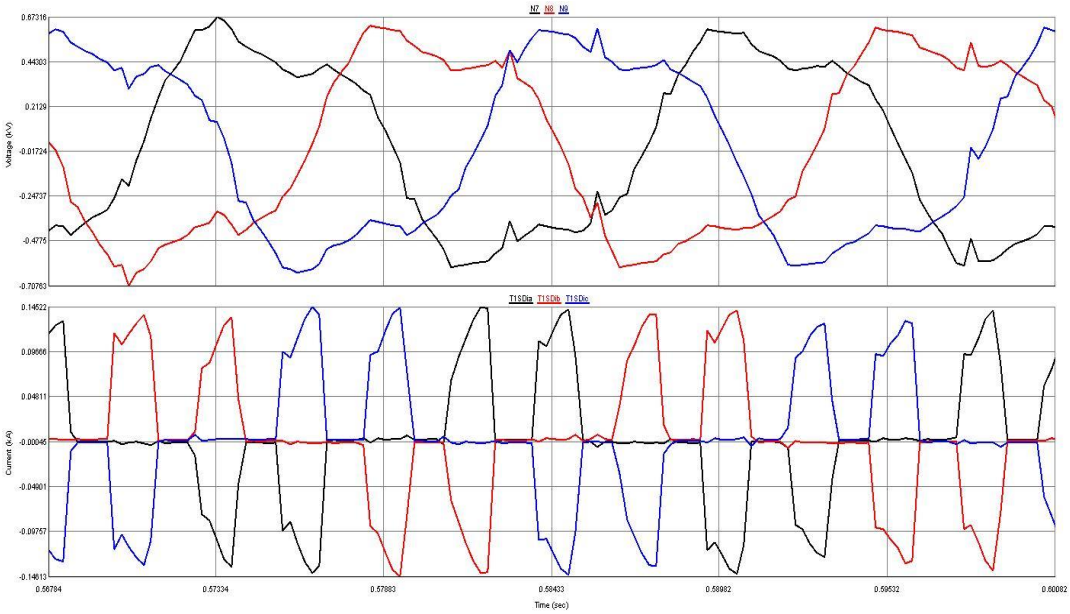

Figure 4.13 Current and voltage waveforms recorded on the delta-connected secondary winding of transformer TR1 with the motor DRILLMT in service (thruster drive system and motors P1, P2, P3 and DRILLMT all running at steady-state).

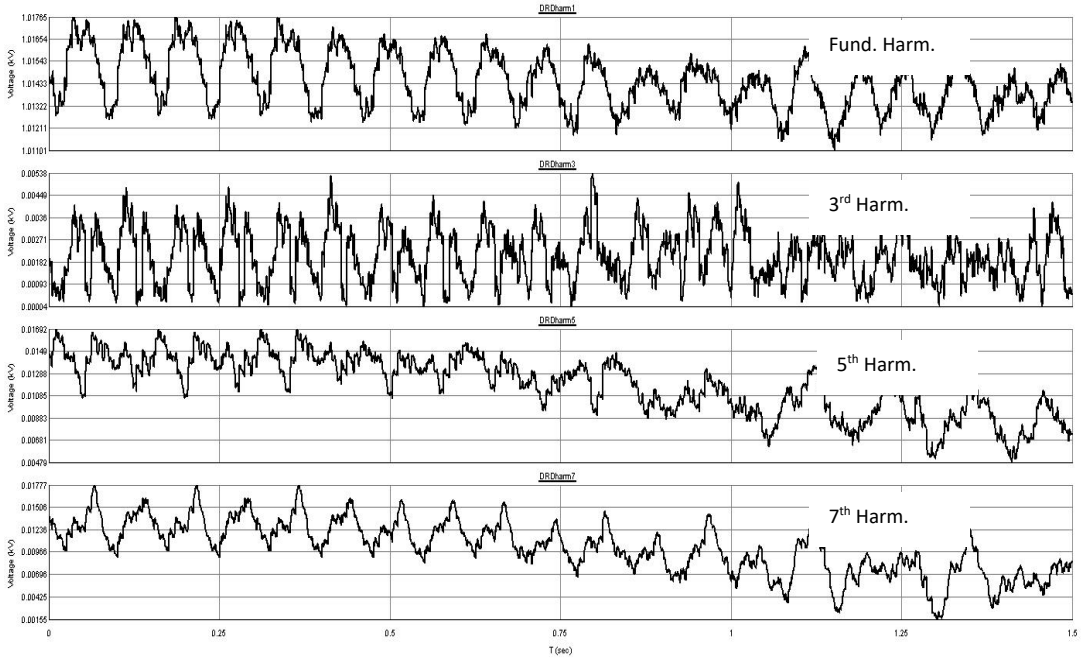

Figure 4.14: Harmonic amplitudes in the voltage on the delta-connected secondary winding of transformer TR1 with the motor DRILLMT in service (thruster drive system and motors P1, P2, P3 and DRILLMT all running at steady-state).

Figure 4.15 shows the currents and voltages on the star-connected secondary winding of the transformer TR1 that feeds the drilling drive system. The recorded currents and voltages are shown for a period of approximately five cycles (between 0.41 and 0.48 seconds) of a longer study. Figure 4.15 also shows the distorted nature of the current waveforms during the time when the motor DRILLMT is running at steady-state and on load. The voltage waveforms of Figure 4.15 do show some distortion but they are much closer to the ideal sinusoidal characteristics when compared to the voltage distortions of the delta-connected secondary winding of the same transformer TR1 as seen previously in Figure 4.13. However the currents in Figure 4.15 are again seen to be non-sinusoidal and have the same distorted characteristics as the currents on the delta-connected secondary side of the same transformer TR1 (see Figure 4.13). The non-sinusoidal shape of the currents is expected, since the star-connected secondary side winding of the transformer TR1 feeds a six-pulse diode rectifier at the front end of the drilling drive system (see Figure 3.8 in Chapter Three).

Figure 4.16 now shows the amplitudes of the main harmonic components of the voltage on the star-connected secondary winding of transformer TR1 during the time when the motor DRILLMT is running at steady-state and on load; the frequency components shown are the fundamental, third, fifth and seventh harmonics calculated over a period of 1.5 seconds during steady-state conditions. The average RMS amplitudes of the fundamental, third, fifth and seventh harmonic components in Figure 4.16 are respectively, 1.001 kV, 0.01 kV, 0.027 kV and 0.017 kV.

The time-domain plots of the voltages on the delta-connected side of TR1 shown in Figure 4.13, and on the star-connected side of TR1 shown in Figure 4.15, show different distortion levels. The voltage distortion on the star winding is much lower with the resultant waveform peak value of 0.61 kV, as compared to the delta winding resultant waveform peak value of 0.67 kV. The amplitude of the fundamental component of the voltage on the delta winding is 1.014 kV, whilst the amplitude of the fundamental component of the voltage on the star winding is 1.001 kV. Table 4.1 presents a comparison of the magnitudes of the frequency components (fundamental, third, fifth and seventh harmonics) present in the voltages on the delta and star windings of the transformer TR1. The amplitudes of the third, fifth and seventh harmonics on the star winding are higher than those of the corresponding harmonics in the voltages on the delta winding.

Table 4.1 Comparison of voltage harmonics recorded on the delta and star windings of transformer TR1, during the steady-state on-load operation of the DRILLMT motor.

Harmonics	**Delta Winding**	**Star Winding**
Fundamental	1.014kV = 100%	1.001kV = 100%
3rd	0kV = 0%	0.01kV = 0.99%
5th	0.013kV = 1.27%	0.027kV = 2.68%
7th	0.012kV = 1.22%	0.017kV = 1.72%

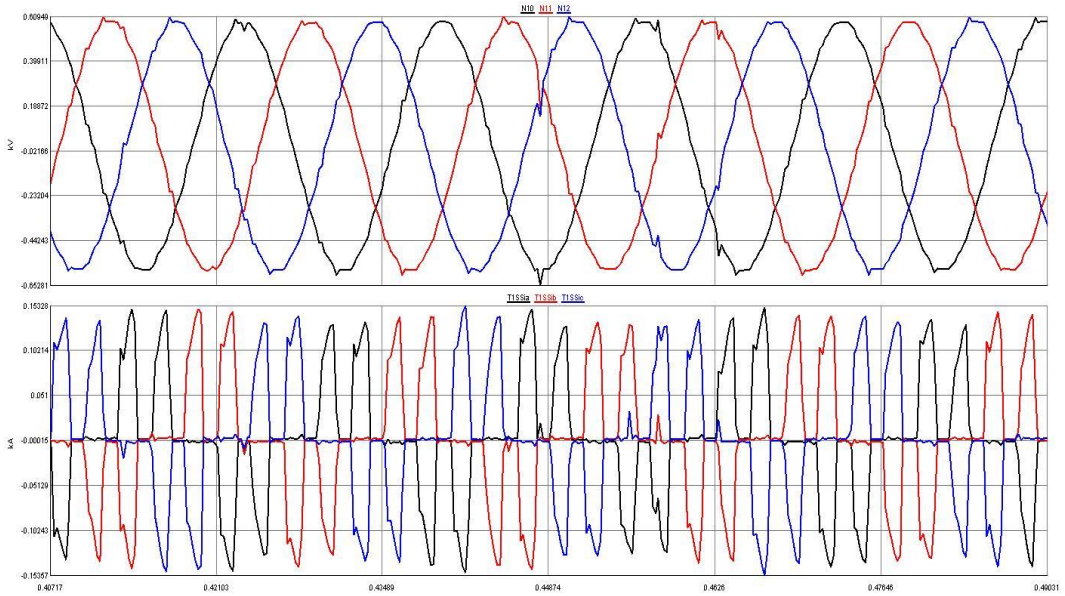

Figure 4.15 Current and voltage waveforms recorded on the star-connected secondary winding of transformer TR1 with the motor DRILLMT in service (thruster drive system and motors P1, P2, P3 and DRILLMT all running at steady-state).

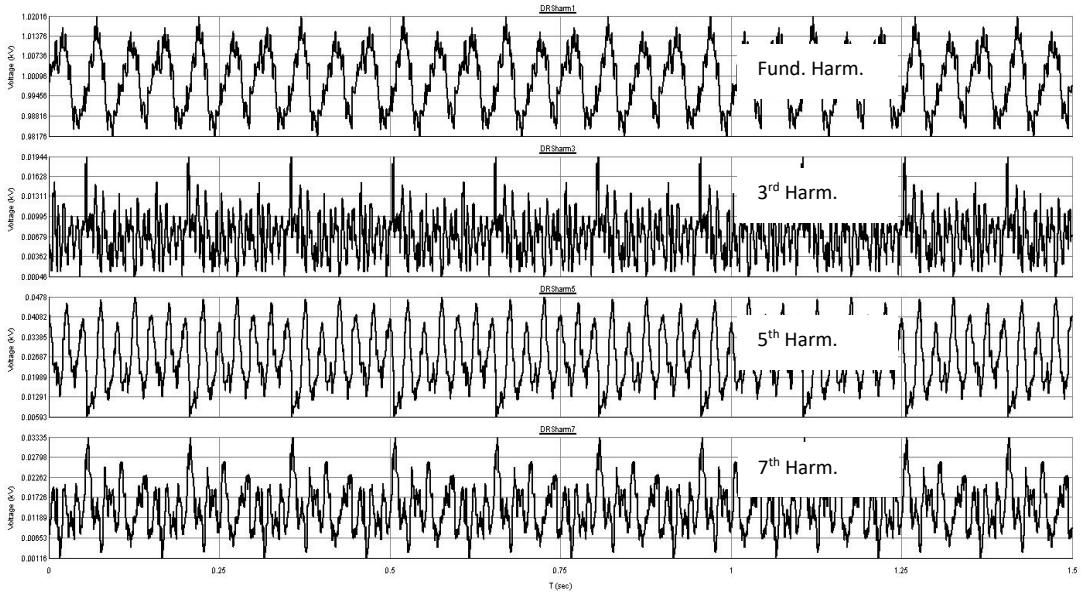

Figure 4.16 Harmonic amplitudes in the voltage on the star-connected secondary winding of transformer TR1 with the motor DRILLMT in service (thruster drive system and motors P1, P2, P3 and DRILLMT all running at steady-state).

The results presented so far in this section have shown the impact of running the variable speed drive operated drilling system motor on the secondary-side variables of the star and delta windings of the drilling drive's own transformer

TR1. The results and figures have thus so far focussed on the harmonic distortion within the drilling drive system itself. The remainder of the section now focuses on the harmonic characteristics of selected electrical variables elsewhere in the drillship electrical network that arise as a result of running the variable speed drive operated drilling motor.

Figures 4.17 to 4.18 show the current and voltage waveforms within the drillship electrical network as a whole under steady-state conditions, during the time when the thruster drive system and motors P1, P2, P3 and DRILLMT are all in service.

Firstly, Figure 4.17 shows the final steady-state condition of the voltage waveforms within the electrical network when all plant is in-service and operating on load. The recorded voltages are shown for a period of approximately two cycles corresponding to the time between 0.84 and 0.88 seconds. Figure 4.17 consists of six graphs, showing the peak voltages at the various busbars in the system (BUS1, BUS2 and on each of the two secondary-side windings of transformers TR1 and TR3) as follows:

- Graph 1 – BUS1 voltage waveforms;
- Graph 2 – BUS2 voltage waveforms;
- Graph 3 – transformer TR1 *delta*-connected secondary winding voltage waveforms of the drilling drive system;
- Graph 4 – transformer TR1 *star*-connected secondary winding voltage waveforms of the drilling drive system;
- Graph 5 – transformer TR3 *delta*-connected secondary winding voltage waveforms of the thruster drive system;
- Graph 6 – transformer TR3 *star*-connected secondary winding voltage waveforms of the thruster drive system.

The values of the peak voltages at BUS1 and 2, taken from Graphs 1 and 2 in Figure 4.17 were 15.5 kV (calculated RMS value 11kV) and 622 V (calculated RMS value 440 V), respectively. The drilling drive system transformer TR1 secondary winding (delta and star) peak voltages (Graphs 3 and 4) were 1 kV (calculated RMS values 707.1 V). The thruster drive system transformer TR3 secondary winding (delta and star) peak values were both found to be 2.3 kV

(calculated RMS values 1.7 kV). The rectifiers of the thruster and drilling drive systems were found to draw non-sinusoidal currents from BUS1, resulting in distorted waveforms in the secondary-side voltages of transformers TR1 and TR3 under the final steady-state operating conditions considered in the simulation study as shown in Figure 4.17 Graphs 3 to 6.

Figure 4.18 now shows the currents supplied by ENGINE1 to the plant as a whole under the final steady-state operating conditions considered in the simulation study, with the thruster drive system and motors P1, P2, P3 and DRILLMT all operating under their rated load conditions and the system at steady-state. The value of the peak currents recorded at the output of the generator ENGINE1 was 116.4 A (calculated RMS value 82.3 A). Figure 4.18 also shows that the current waveforms drawn from the ENGINE1 supply are distorted, even though the internal voltages of this supply are sinusoidal, as shown earlier in the reference study in Figure 4.4.

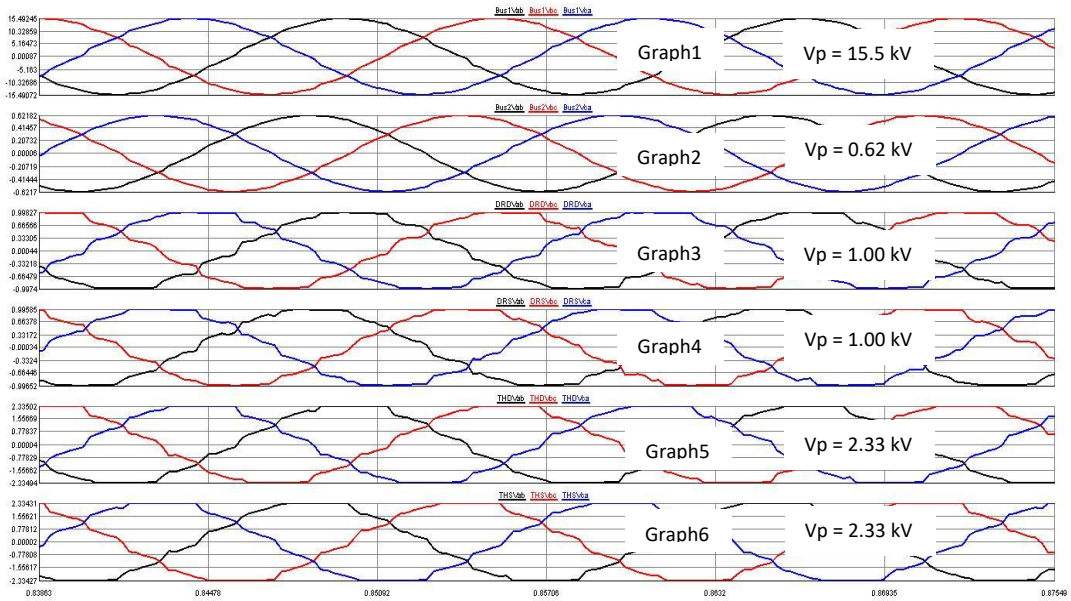

Figure 4.17 Voltages within the drillship electrical network with the motor DRILLMT in service (thruster drive system and motors P1, P2, P3 and DRILLMT all running at steady-state).

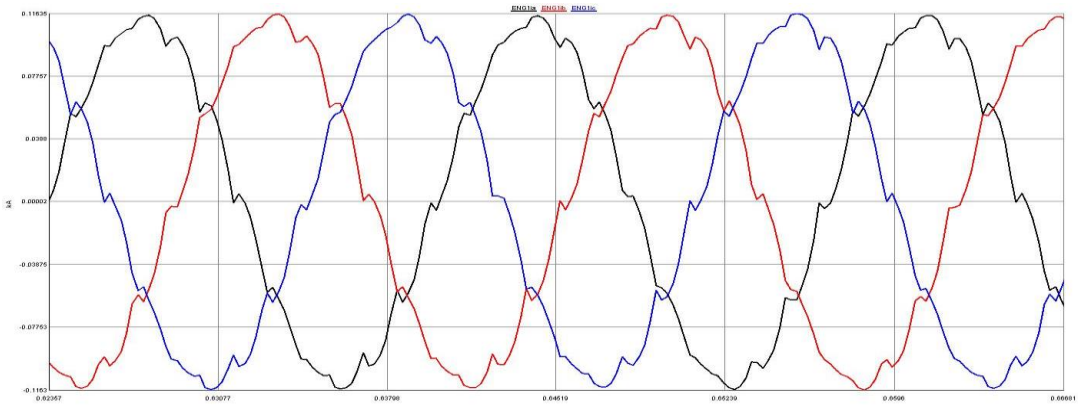

Figure 4.18: ENGINE1 currents when all plant is in service and operating on load (thruster drive system and motors P1, P2, P3 and DRILLMT all in service and running under steady-state conditions).

Figures 4.17 and 4.18 show that both the current and voltage waveforms in the electrical network are distorted, indicating that there are harmonics present in the drillship electrical network when all plant is in service and at steady-state operation on load. Such harmonics are harmful to the generator ENGINE1 and the three pump motors; therefore, it is important to determine the level of the individual current and voltage harmonics, and the total harmonic distortion, at busbars BUS1 and BUS2. Therefore, it is necessary to measure the level of the harmonics that are now present when the thruster and drilling drive systems are in service. Tables 4.2 (a) and (b) now present the amplitudes of the main current and voltage harmonics at busbars BUS1 and BUS2, as recorded during the simulation study, for the final steady-state operation condition of the plant (thruster drive system and motors P1, P2, P3 and DRILLMT all in service).

Table 4.2 (a) shows the levels of the third, fifth and seventh current and voltage harmonics at BUS1 relative to their fundamental-frequency components. The results show the high values of the frequency components of the fifth and seventh voltage harmonics, 2.79% and 2.93%, respectively. The results also show the high value (1.53%) of the frequency component of the seventh current harmonic, while both the third and fifth current harmonics are below one percent. The calculated values for the total harmonic distortions in the voltages and currents at BUS1 are 4.05% and 1.81%, respectively.

Table 4.2 (a) Amplitudes of the main harmonic components in the currents and voltages recorded at BUS1 under steady-state conditions (thruster drive system and motors P1, P2, P3 and DRILLMT all in service).

BUS	**Vh1 (kV)**	**Vh3 (kV)**	**Vh5 (kV)**	**Vh7 (kV)**	**Ih1 (kA)**	**Ih3 (kA)**	**Ih5 (kA)**	**Ih7 (kA)**
1	8.74	9.6 E^{-3}	0.24	0.26	0.35	7.3 E^{-4}	3.4 E^{-3}	5.4 E^{-3}
%	100	0.08	2.79	2.93	100	0.21	0.96	1.53

The current and voltage total harmonic distortions at BUS1 are calculated as follows:

$$THDv = \frac{\sqrt{\sum_3^7 (Vh)^2}}{Vh1}$$

$$= \frac{\sqrt{(0.0095^2 + 0.2436^2 + 0.2564^2}}{8.7365}$$

= 0.0405 x 100%

= 4.05%.

$$THDi = \frac{\sqrt{\sum_3^7 (Ih)^2}}{Ih1}$$

$$= \frac{\sqrt{(0.00073^2 + 0.00337^2 + 0.00535^2}}{0.35105}$$

= 0.01813 x 100%

= 1.81%.

Table 4.2 (b) now shows the levels of the third, fifth and seventh current and voltage harmonics at BUS2 relative to their fundamental-frequency components. Section 4.3.3 indicated that when the largest of the three pump motors (P3) was started, the impact of its starting transients was measured on parts of the plant that are not directly connected to P3 at BUS2 but that share

the same point of common coupling at the upstream busbar BUS1. Therefore, it is important to measure harmonics also at BUS2, to determine if both the thruster and drilling drive systems inject harmonics into the entire drillship electrical network via their impact on the harmonic distortion at BUS1.

The results in Table 4.2 (b) show that the levels of the fifth and seventh voltage harmonics at BUS2 are 1.3% and 1.93%, of the fundamental respectively, while the level of the third harmonic voltage is below one percent. The results also show the low levels of the third, fifth and seventh current harmonics, each of which is below one percent of the fundamental. The values of the total harmonic distortion in the voltage and current at BUS2 are calculated as 2.35% and 0.75% respectively.

Table 4.2 (b) Amplitudes of the main harmonic components in the currents and voltages recorded at BUS2 under steady-state conditions (thruster drive system and motors P1, P2, P3 and DRILLMT all in service).

BUS	**Vh1 (kV)**	**Vh3 (kV)**	**Vh5 (kV)**	**Vh7 (kV)**	**Ih1 (kA)**	**Ih3 (kA)**	**Ih5 (kA)**	**Ih7 (kA)**
2	0.35	9.8 E^{-3}	4.5 E^{-3}	6.7 E^{-3}	1.67	1.3 E^{-3}	7.3 E^{-3}	0.01
%	100	0.28	1.3	1.93	100	0.08	0.43	0.6

The total harmonic distortion in the voltages and currents at BUS2 are calculated as follows:

$$THDv = \frac{\sqrt{\sum_3^7 (Vh)^2}}{Vh1}$$

$$= \frac{\sqrt{(0.00098^2 + 0.00455^2 + 0.00675^2}}{0.34906}$$

= 0.02349 x 100%

= 2.35%.

$$THDi = \frac{\sqrt{\sum_3^7 (Ih)^2}}{Ih1}$$

$$= \frac{\sqrt{(0.00129^2 + 0.00726^2 + 0.01006^2}}{1.67299}$$

$$= 7.46\ E^{-3} \times 100\%$$

$$= \underline{0.75\%.}$$

Even though all the recordings of individual harmonics at both BUS1 and BUS2 are limited to the seventh harmonic and lower in the simulation studies presented here, the results can be used to indicate the approximate level of harmonic distortion expected in the drillship electrical network as a result of running the thruster and drilling drive systems. The calculated value of the total harmonic voltage distortion at BUS1 was 4.05 percent in these simulation studies; taking into consideration that power quality meters take measurements up to the fiftieth harmonic, it is expected that the total voltage harmonic distortion at BUS1 could well be above five percent (IEEE 519 standard voltage distortion limit) if the simulation model allowed for the recording of individual-harmonics up to the fiftieth harmonic. The calculated value of the total voltage harmonic distortion at BUS2 was 2.35 percent and it is expected that if the model allowed for the measurement of the harmonics up to the fiftieth level, this value might also approach, or exceed five percent. Therefore, the simulation results prove the presence of harmonics, and suggest the strong possibility that the drillship electrical network may not meet the five percent (IEEE 519 standard) permissible limit for total harmonic distortion at the point of common coupling under practical operating conditions.

4.4 DRILLSHIP ELECTRICAL NETWORK FIELD MEASUREMENTS

The previous section presented the results from the reduced-scale simulation model of the drillship electrical network shown in Figure 3.2 of Chapter Three. To validate the simulation model, field measurements were required to be

taken onboard the actual drillship electrical network, so that they could be compared with the simulation results, ideally using the same operating conditions. Therefore, this section presents the field measurements taken onboard the actual, full-scale drillship electrical network, the details of which are shown in Appendices G and H. The field measurements were taken at various locations on the drillship electrical network: on the delta and star secondary windings of the drilling drive system, and on the 440V system busbars. However, the exact operating conditions were unknown during each of the specific times when the onboard drillship electrical network field measurements were taken, and hence, only qualitative comparisons will be presented here. Therefore, the measurements to come (Figure 4.19 to 4.31) present the harmonics onboard the drilling ship electrical network during various different practical drilling operations.

4.4.1 Drillship drilling drive system transformer delta-connected secondary-side winding measurements

Figure 4.19 shows the RMS average current and voltage profile on the drilling drive system transformers' (Transformer No.1 in Appendix H) delta-connected secondary-side winding for the whole duration of the field measurement which lasted seven hours, seven minutes and forty seconds. The top three graphs in Figure 4.19 represent the voltage profile for the whole duration of the measurement. The average RMS value of the voltage for the entire duration was approximately 717 V. All three phases of the measured voltage were balanced for the entire measurement, even though the load varied during the drilling process. The RMS value of 717 V shows a voltage difference of 1.1 percent when compared to the transformer output RMS voltage of 725 V. This voltage difference between the rated and measured of 1.1 percent is within the power quality standard limit as presented in Table 2.4.

The bottom three graphs in Figure 4.19 show the varying load profile on the delta-side rectifier for the duration of the measurement, as represented by the three line currents drawn by the rectifier. The measured current shows that all three phases were balanced for the entire duration of the measurement. The three phases were identical to each other. During the drilling operation, the

DrawWorks would hoist the Top Drive system (without any load) from the Drill-floor to the top of the Derrick, and the drill pipes were attached to the Top Drive and the drilling string. The DrawWorks then lowered the drilling string towards the well-head, until the Top Drive reached the floor. This cycle is repeated for a couple of weeks until the drilling bit reached the well-head, where drilling would eventually start. Therefore, the current graphs are a representation of the load during various stages of the drilling operation. The current and voltage profiles in Figure 4.19 were taken during one of those drilling stages explained above.

The current and voltage harmonic measurements presented below were taken during the duration presented by Figure 4.19.

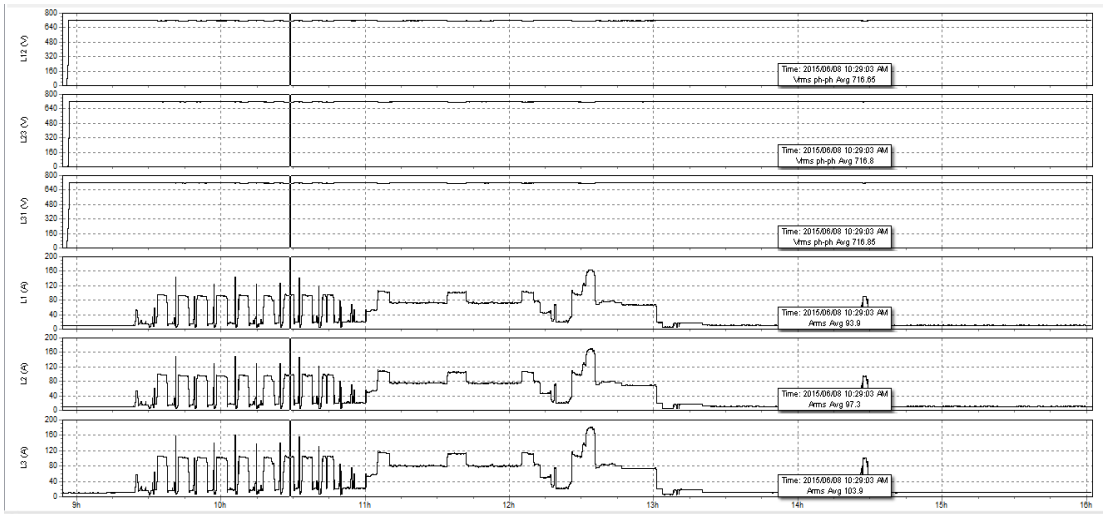

Figure 4.19 Drillship drilling drive transformer delta-connected, secondary-side winding operating load condition (current and voltage profile) for the duration of seven hours, seven minutes and forty seconds of the field measurement.

Figure 4.20 shows the voltage harmonic spectrum taken from the drilling drive system transformer (Transformer No.1 in Appendix H) delta-connected secondary-side winding for the whole duration of the measurement. The bar charts of Figure 4.20 show the amplitudes of the main harmonic components of the voltage on the delta-connected secondary-side winding of the drilling drive system transformer, from the fundamental up to the fiftieth harmonic.

The amplitudes of the triplen harmonics in the voltages on the delta winding are almost zero (all below one percent) as seen from the harmonic spectrum

of Figure 4.20, and such results are expected since triplen harmonic currents circulate within a delta-connected winding of a transformer. For the purposes of comparison with the simulation results of Table 4.1: the amplitudes of the third, fifth and seventh voltage harmonics in the field measurements are shown in Table 4.3 below.

Table 4.3 Field Measurements of the third, fifth and seventh harmonics in the voltages on the delta-connected winding explaining the usage of the largest value instead of the average value for the fifth voltage harmonic.

Voltage Harmonics	Description of the measurement taken	Measured Value
3^{rd}	Average of the 3^{rd} Voltage Harmonic	0.65
5^{th}	Largest Value measured on the 5^{th} Voltage Harmonic as shown in Figure 4.20	1.25
7^{th}	Average of the 7^{th} Voltage Harmonic	0.96

As indicated in Table 4.3, the average value of the measured harmonic amplitude in each phase in the results of Figure 4.20 was used for the third and the seventh harmonics when calculating the total harmonic voltage distortion. However, due to the imbalance between the amplitudes of the fifth harmonic voltage in each phase in the measurements of Figure 4.20 the largest value of the fifth harmonic voltage from Figure 4.20 was used as it represents the worst-case harmonic impact when calculating the total harmonic voltage distortion.

The amplitudes of all remaining harmonics, up to the fiftieth harmonic are small and each below 1%. The total harmonic distortion in the voltages on the delta-connected secondary-side winding was 2.89 percent for the whole duration of the measurement, as seen from the left-most bar in the charts in Figure 4.20. The calculated total harmonic distortion in these measured voltages, up to the seventh harmonic, is 1.7 percent as seen in Table 4.4 below. The harmonic measurements were taken when the drillship was in operation during the load conditions shown previously in Figure 4.19.

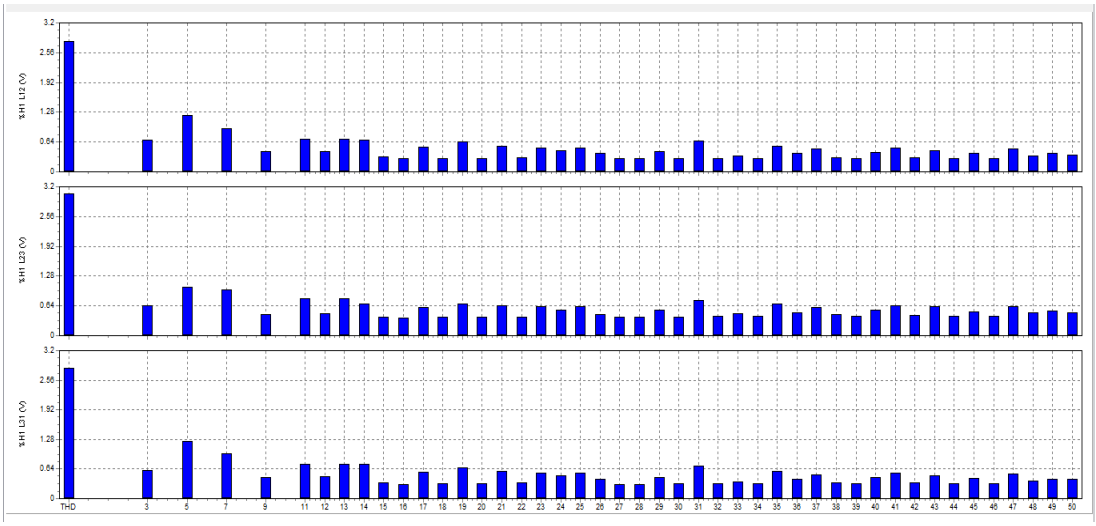

Figure 4.20 Drillship drilling drive transformer delta-connected secondary-side winding measured voltage harmonic spectrum during the field measurement.

Figure 4.21 now shows voltage waveforms of the drilling drive system transformers' delta-connected secondary-side winding taken during a certain period in time during the onboard measurement of Figure 4.19. The recorded voltages are shown for a period of approximately four cycles of the full measurement. The average peak value V_p of the voltage on the delta-connected secondary-side winding in Figure 4.21 was 717 V. The voltage waveforms of Figure 4.21 do show some distortions especially almost flattening on the top of the waveform, but they are much closer to sinusoidal characteristics than was the case in the simulation results shown in Figure 4.13.

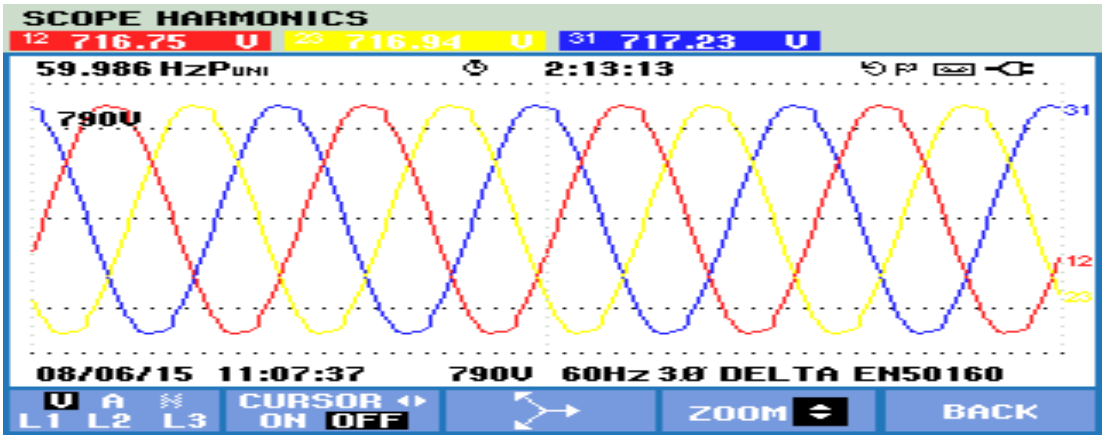

Figure 4.21 Drillship drilling drive system transformer delta-connected, secondary-side winding measured voltage waveforms from one four-cycle period in time during the full field measurement.

Table 4.4 presents a comparison between the voltage harmonics on the delta-connected secondary-side winding of the drilling drive system transformer, as calculated from the earlier simulation results and from the field measurements just presented. The simulation results show very small values (almost zero) of the third harmonic voltage as seen from Figure 4.14, while there are small values of the triplen harmonics present in the field measurements as shown in Figure 4.20. Therefore, it can be concluded that the findings about triplen harmonics for both the simulation results and measurements are consistent with one another, and the findings are expected in a delta-connected windings as the currents circulate within the delta winding; the small values of third harmonic voltage in the field measurements are caused by voltage unbalances between phases which were not present in the simulation studies.

Table 4.4 also shows that the amplitude of the fifth harmonic voltage from the simulation results (1.27%) is slightly greater than the fifth harmonic amplitude of 1.25 percent in the field measurements. The amplitudes of the seventh harmonic voltages from the simulation results and field measurements are 1.22 and 0.96 percent respectively. Even though both the simulation results and field measurements were taken at different load conditions, the readings are broadly consistent with one another and are below the individual harmonic limit of 5 percent from the IEEE 519 STD in Table 2.2 of Chapter Two. Finally, Table 4.4 presents the voltage total harmonic distortion for both the simulation results and field measurements, and are both 1.7 percent, well below the IEEE 519 STD limit of 8 percent. The voltage waveform from the simulation study of Figure 4.13 is more distorted as compared with the voltage waveform from the field measurement of Figure 4.21, and both represent the voltages on the delta-connected secondary side of the drilling drive system.

The results presented in Table 4.4 compare the voltage harmonics generated on the lower-voltage side of the drilling drive system transformer by an individual six-pulse rectifier as predicted by the simulation model and from direct measurements on the actual drillship electrical network. Unfortunately, similar direct measurements were not possible on the 11 kV parts of the drillship electrical network during the author's time working onboard the ship, and hence the voltage harmonics on the high-voltage side of the drilling drive

system transformer (11 kV busbar) are shown only as predictions from simulation results (Table 4.2 (a)) in this work.

Harmonic filters are not present on the onboard drillship electrical network, either on the supply side of the drilling drive system or on the 11 kV distribution network because theoretically the twelve-pulse rectifiers eliminate some of the harmful harmonics at the point of common coupling: the third, fifth and seventh harmonics. The current and voltage harmonics predicted from the simulation study results shown in Figure 4.2 (a) were taken on the 11 kV busbar and indicate the presence of the third, fifth and seventh voltage harmonics which theoretically should not be present when a twelve-pulse rectifier is used. As there is consistency between the findings from the field measurements and simulation results on the delta-connected secondary-side winding of the drilling drive system, therefore, the conclusion is that these predicted third, fifth and seventh voltage harmonics on the 11 kV side are expected to be present on the actual drillship electrical network at the 11 kV switchboard.

Table 4.4: Comparison between the voltage harmonics on the delta winding of the drilling drive system transformer calculated from the simulation results and from the field measurements.

Harmonics	**Simulation results**	**Field Measurements**	**IEEE 519 STD Voltage distortion limits**
3rd	0%	0.65%	5%
5th	1.27%	1.25%	5%
7th	1.22%	0.96%	5%
THD	1.7%	1.7%	8%

The line currents shown in the bottom three graphs in Figure 4.19 indicate the drilling drive system delta-side six-pulse rectifier load profile for the entire duration of the field measurement. Figure 4.22 now shows the current harmonic spectrum taken from the drilling drive system transformer (Transformer No.1 in Appendix H) delta-connected secondary-side winding for the whole duration of the field measurement in Figure 4.19. The bar charts of Figure 4.22 show the amplitudes of the main harmonic components of the

current on the delta-connected secondary-side winding of the drilling drive transformer, from the fundamental up to the fiftieth harmonic. Figure 4.22 shows that there is a presence of the triplen harmonic currents in the spectrum, even though theoretically the six-pulse rectifier (harmonic order 6k $\pm$ 1) only creates the fifth, seventh, seventeenth, nineteenth, etc., harmonics at the source side. The presence of these triplen harmonics in the field measurements are caused by voltage unbalance. However it can be noticed on the bar chart that the amplitudes of the triplen currents decreases from the third towards the fiftieth harmonics.

Table 4.5 now shows the amplitudes of the main harmonic components of the currents taken from the bar charts of Figure 4.22. Table 4.5 also shows the selected IEEE 519 STD current limits taken from Table 2.1 in Chapter Two showing the current distortion limits. The fault current level at the delta-connected secondary-side winding of the drilling drive system transformer was assumed to be 11.30 kA (this value of short-circuit fault level was taken from the actual ABB electrical network short circuit calculations provided for this system).

The average value of the line current during the onboard field measurement was taken to be 170.6 A as it provides a stringent harmonic limit. The ratio between the short circuit current and the measured average line current at the delta-connected secondary-side winding of the drilling drive system transformer is therefore 66.2 ($\frac{\mathrm{Isc}}{\mathrm{Il}} = \frac{11300}{170.6}$).

This calculated value of the ratio I_{SC} / I_L for the system of 66.2 falls within the 50 < SCR < 100 range shown in Table 2.1. This means that the amplitudes of the current harmonics in Table 4.5 need to be analysed in relation to the current distortion limits related to the provided short-circuit ratio, 50 < SCR < 100 as seen in Table 2.1. Of the triplen harmonics highlighted in yellow in Table 4.5, only the amplitude of the third current harmonic (10.7%) is slightly above the IEEE 519 STD current limit of 10 percent and the rest are below each related current distortion limit. Table 4.5 also shows that the amplitudes of the fifth and seventh current harmonics are 79.1 and 68.8 percent and are well above the IEEE 519 STD current limit of 10 percent. The table also shows that

the amplitudes of the eleventh (46.2%) and thirteenth (37.4%) current harmonics are above the limit of 4.5 percent.

Table 4.5 also shows that the seventeenth (27.8%) and the nineteenth (23.4%) current harmonics are above the limit of 4 percent. The twenty-third (14.4%), twenty-fifth (11.7%), twenty-ninth (8.7%) and thirty-first (7.6%) average amplitudes for the entire duration were above the IEEE 519 STD current distortion limit of 1.5 percent. Finally, Table 4.5 shows the amplitudes of the thirty-fifth (5.9%), thirty-seventh (5.4%), forty-first (4.8%), forty-third (4.4%), forty-seventh (3.5%) and forty-ninth (3.1%) current harmonics are above the current limit of 0.7 percent. In conclusion, Table 4.5 presents the total harmonic current distortion for the entire duration of the measurement to be 135.2 percent which is well above the IEEE 519 STD limit of 12 percent. Of all the measurements, all the triplen harmonics are below five percent and below the IEEE 519 STD current limits with the exception of the third harmonic.

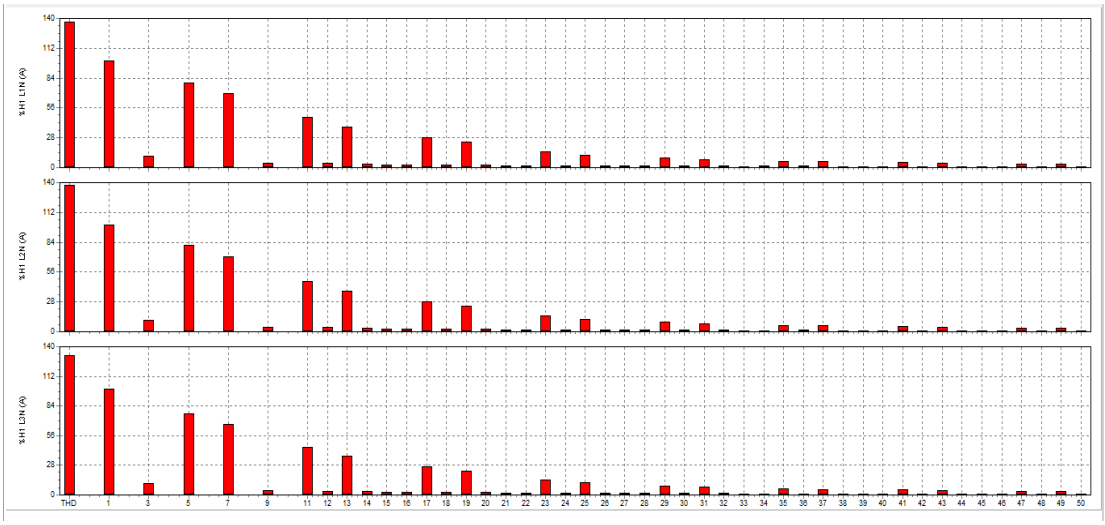

Figure 4.22 Drillship drilling drive transformer delta-connected secondary-side winding measured current harmonic spectrum during the field measurement.

Figure 4.23 shows the current waveforms of the drilling drive system transformers' delta-connected secondary-side winding taken during a certain period in time during the onboard measurement of Figure 4.19. Figure 4.23 also shows the distorted nature of the current waveforms and the currents are seen to be non-sinusoidal and to have very similar shapes to the currents seen in the simulation results of Figure 4.13.

The bottom three graphs of Figure 4.19 show the average RMS value of the peak current at the delta-connected secondary-side winding of the drilling drive system transformer to be approximately 170.6 A. The simulation results presented earlier in Figure 4.13 showed that the value of the peak current at the delta-connected secondary-side winding of the drilling drive system transformer was approximately 145.22 A (RMS value of 102.7 A). The findings show that the current drawn by the delta-side rectifier during the simulation results and the field measurement are not too different, and therefore it can be concluded that if simulation results were able to show harmonics up to the fiftieth harmonic, these higher-frequency would have followed the same pattern as the field measurements.

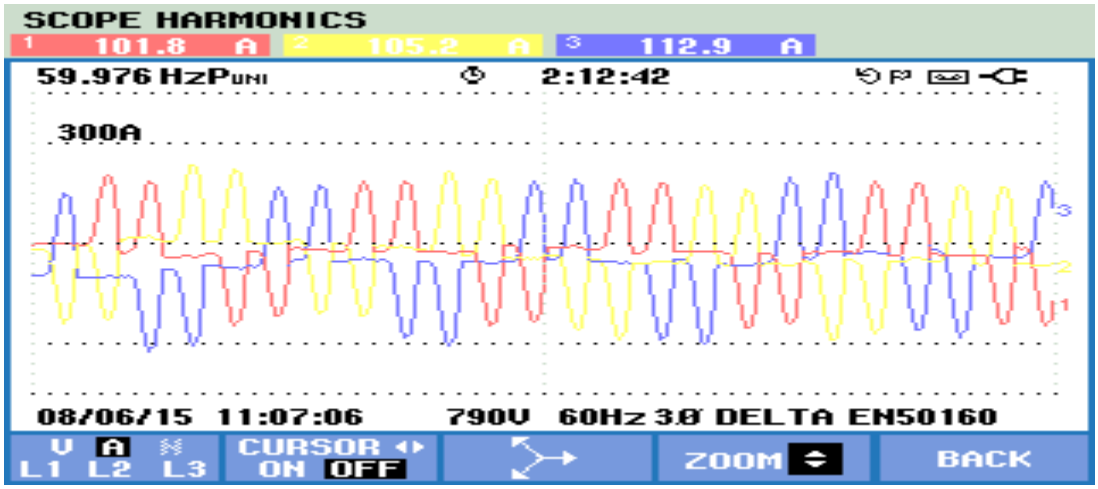

Figure 4.23: Drillship drilling drive system transformer delta-connected secondary-side winding measured current waveforms from a short period in time during the full field measurement.

Table 4.5 Amplitudes of specific harmonics taken from the current harmonic spectrum of the delta winding of the drilling drive system transformer compared to the IEEE 519 STD current distortions limits.

HARMONICS	DELTA SIDE - MEASUREMENTS	IEEE 519 STD CURRENT DISTORTION LIMIT (50> SCR <100)	I_{SC} / I_L (SCR)
3rd	10.7%	10%	Calculated short-circuit ratio (SCR) = 11300 / 170.6 = 66.2
5th	79.1%		
7th	68.8%		
9th	4.1%		
11th	46.2%	4.5%	
13th	37.4%		
15th	2.5%		
17th	27.8%	4%	
19th	23.4%		
21st	1.8%		
23rd	14.4%	1.5%	
25th	11.7%		
27th	1.4%		
29th	8.7%		
31st	7.6%		
33rd	1.1%		
35th	5.9%	0.7%	
37th	5.4%		
39th	1%		
41st	4.8%		
43rd	4.4%		
45th	0.91%		
47th	3.5%		
49th	3.1%		
THD	135.2%	12%	

4.4.2 Drillship drilling drive system star-connected secondary-side winding transformer measurements

Figure 4.24 shows the RMS average current and voltage profile on the drilling drive system transformers' (Transformer No.1 in Appendix H) star-connected secondary-side winding for the whole duration of the field measurement, which lasted ten hours and forty-six minutes. The top three graphs in Figure 4.24 represent the voltage profile for the whole duration of the measurement. The average RMS value of the phase voltages for the entire duration was approximately 419.8 V (line voltage value, 727 V). All three phases of the measured voltage were balanced for the entire measurement, even though the load varied during the drilling process. The measured RMS value of 727 V on the voltage profile is 0.3 percent above the transformer output RMS voltage of

725 V. The voltage swell of 0.3 percent is caused by low power drawn by the rectifier, and the difference is within the power quality standard limit as presented in Table 2.4. The bottom three graphs in Figure 4.24 show the varying load profile on the star-side rectifier for the duration of the measurement, as represented by the three line currents drawn by the rectifier. The measured current shows that all three phases were balanced for the entire duration of the measurement. The three phases were identical to each other. During the drilling operation, the DrawWorks would hoist the Top Drive system (without any load) from the Drill-floor to the top of the Derrick, and the drill pipes were attached to the Top Drive and the drilling string. The DrawWorks then lowered the drilling string towards the well-head, until the Top Drive reached the floor. This cycle is repeated for a couple of weeks until the drilling bit reached the well-head, where drilling would eventually start. Therefore, the current graphs are a representation of the load during various stages of the drilling operation. The current and voltage profiles in Figure 4.24 were taken during one of those drilling stages discussed above.

The current and voltage harmonic measurements presented below were taken during the duration presented by Figure 4.24.

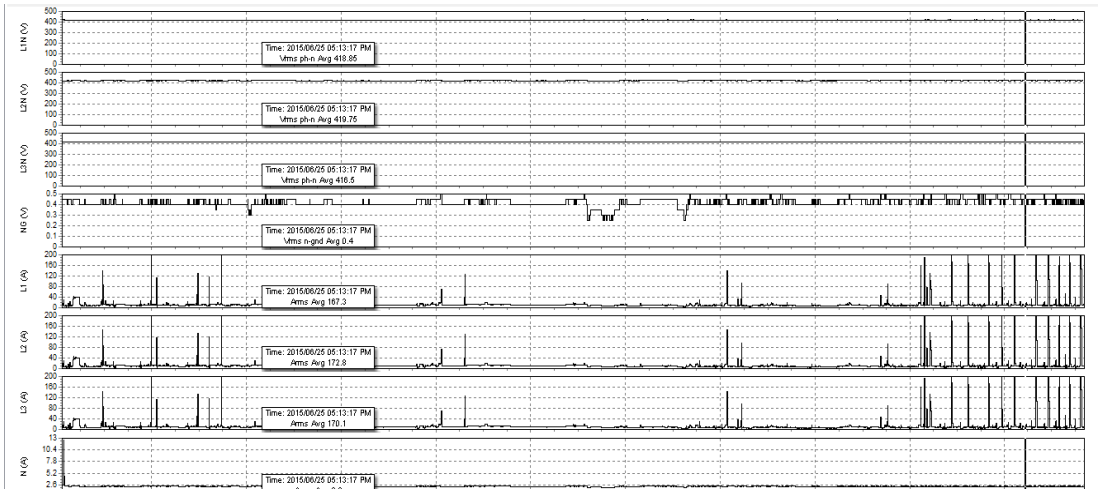

Figure 4.24 Drillship drilling drive transformer star-connected, secondary-side winding operating load condition (current and voltage profile) for the duration of ten hours and forty-six minutes of the field measurement.

Figure 4.25 now shows the voltage harmonic spectrum taken from the drilling drive system transformer (Transformer No.1 in Appendix H) star-connected

secondary-side winding for the whole duration of the measurement. The bar charts of Figure 4.25 show the amplitudes of the main harmonic components of the voltage on the star-connected secondary-side winding of the drilling drive system transformer, from the fundamental up to the fiftieth harmonic.

There is a presence of the triplen voltage harmonics in the measurement as expected, because the star-point of the transformer winding is grounded, and these are shown in the bar charts of Figure 4.25. For comparison with the simulation results of Table 4.1: the amplitudes of the third, fifth and seventh voltage harmonics in the field measurements are approximately 6.5, 5.6 and 2.2 percent respectively, as seen from the bar chart of Figure 4.25. The amplitudes of all remaining harmonics, up to the fiftieth harmonic are small and each below 5 percent. The total harmonic distortion in the voltages on the star-connected secondary-side winding was 13.4 percent for the whole duration of the measurement, as seen from the left-most bar in the charts in Figure 4.25. The calculated total harmonic distortion in these measured voltages, up to the seventh harmonic, is 3.3 percent as seen in Table 4.6 below. The harmonic measurements were taken when the drillship was in operation during the load conditions shown previously in Figure 4.24.

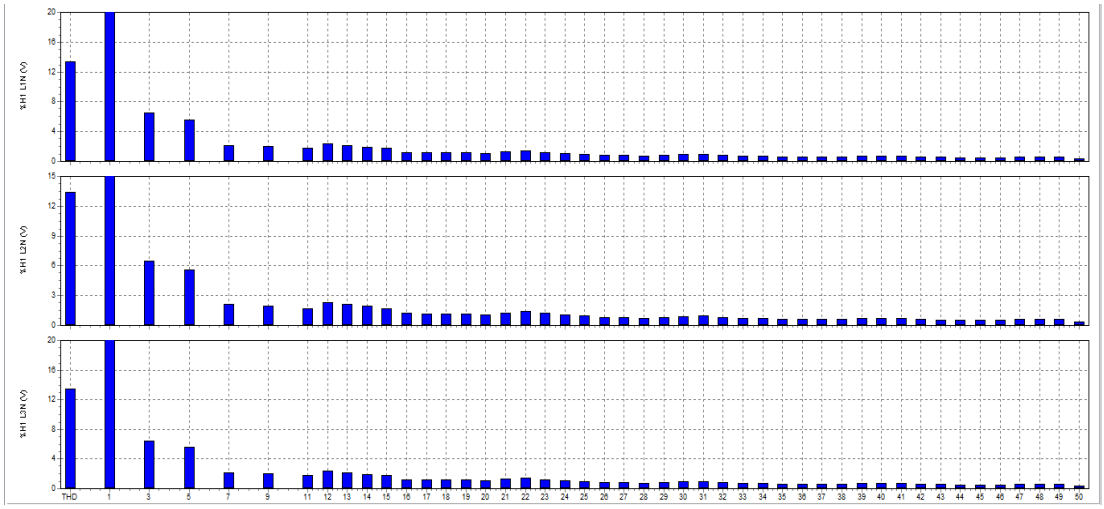

Figure 4.25 Drillship drilling drive transformer star-connected secondary-side winding measured voltage harmonic spectrum for the duration of ten hours and forty-six minutes.

Table 4.6 presents a comparison between the voltage harmonics on the star-connected secondary-side winding of the drilling drive system transformer, as calculated from the earlier simulation results and from the field measurements

just presented. The amplitudes of the third voltage harmonic from the simulation results and field measurements are approximately 0.99 and 6.5 percent respectively, and the significant difference is because of the different load conditions for each study. Therefore, it can be concluded that both the simulation results and the field measurements show the presence of third harmonic, as expected because the star-point of the transformer winding is grounded. In conclusion the presence of triplen harmonics are expected also from the simulation results if they were measured up to the fiftieth harmonic as per the findings of the field measurements in a wye-connected secondary winding with a grounded star-point. The amplitude of the third voltage harmonic (6.5%) from the field measurement is above the IEEE 519 STD voltage distortion limits of 5 percent.

Table 4.6 also shows that the amplitude of the fifth voltage harmonic from the simulation results (2.68%) is smaller than the fifth harmonic amplitude of 5.6 percent in the field measurements. The amplitudes of the seventh harmonic from the simulation results and field measurements are 1.72 and 2.2 percent respectively. Even though both the simulation results and field measurements were taken at different load conditions, the readings are broadly consistent with one another and only the amplitude of the fifth harmonic from the field measurement is above the IEEE 519 STD individual voltage harmonic limit of 5 percent in Table 2.2 of Chapter Two. The total harmonic voltage distortion figures for both the simulation results and field measurements are 3.3 and 8.9 percent respectively as shown in Table 4.6 and the difference is because of the different load conditions. The total harmonic voltage distortion of the field measurement is above the IEEE 519 STD voltage limit of 8 percent.

Table 4.6 Comparison between the voltage harmonics on the star winding of the drilling drive system transformer calculated from the simulation results and from the field measurements.

Harmonics	Simulation results	Measurements	IEEE 519 STD Voltage distortion limits
3rd	0.99%	6.5%	5%
5th	2.68%	5.6%	5%
7th	1.72%	2.2%	5%
THD	3.3%	8.9%	8%

Figure 4.26 now shows voltage waveforms of the drilling drive system transformers' star-connected secondary-side winding taken during a certain period in time during the onboard measurement of Figure 4.24. The recorded voltages are shown for a period of approximately four cycles of the full measurement. The average peak value V_p of the phase voltage on the star-connected secondary-side winding in Figure 4.26 was 418.8 V. The voltage waveform of Figure 4.26 during the field measurement is more distorted as compared with the voltage waveform obtained in the simulation results of Figure 4.15, and both represent the voltages on the star-connected secondary side of the drilling drive system. As indicated above, the average currents drawn by the star side six-pulse rectifier happened to be low for most of the time during the field measurement as shown in Figure 4.24; therefore, large voltage distortions are expected at low loads. The findings from the simulation results and the field measurement are consistent with one another, and therefore it can be concluded that if simulation results were taken up to the fiftieth harmonic, they would have followed the same pattern as the field measurements.

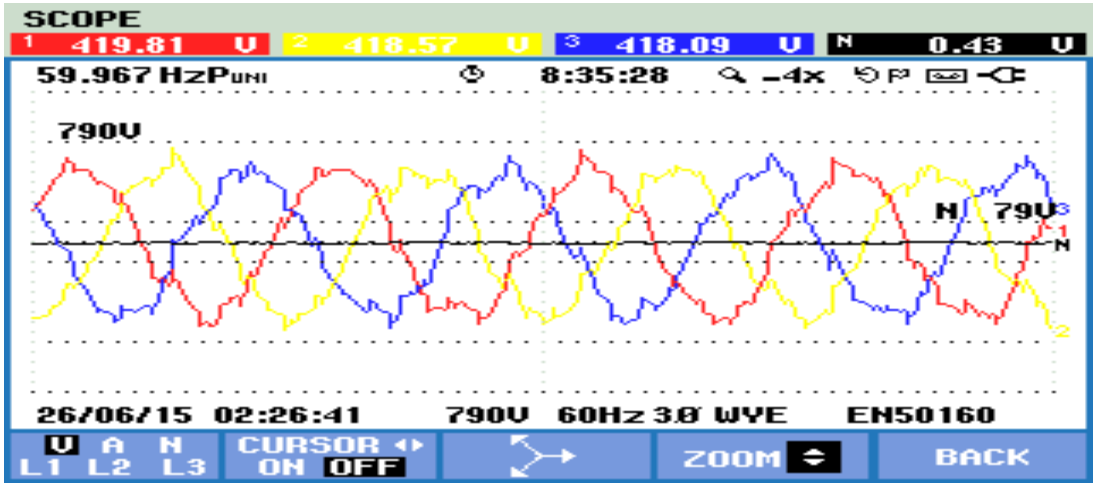

Figure 4.26 Drillship drilling drive system transformer star-connected, secondary-side winding measured voltage waveforms from one four-cycle period in time during the full field measurement.

The line currents shown in the bottom three graphs in Figure 4.24 indicate the drilling drive system star-side six-pulse rectifier load profile for the entire duration of the field measurements. Figure 4.27 now shows the current harmonic spectrum taken from the drilling drive system transformer (Transformer No.1 in Appendix H) star-connected secondary-side winding for the whole duration of the field measurement in Figure 4.24. The bar charts of Figure 4.27 show the amplitudes of the main harmonic components of the current on the star-connected secondary-side winding of the drilling drive transformer, from the fundamental up to the fiftieth harmonic. Figure 4.27 shows that there is a high presence of the triplen harmonic currents in the spectrum, even though theoretically the six-pulse rectifier (harmonic order 6k $\pm$ 1) only creates the fifth, seventh, seventeenth, nineteenth, etc., harmonics at the source side. The presence of these triplen harmonics in the field measurements are caused by the fact that the star-point of the transformer is grounded. However it can be noticed on the bar chart that the amplitudes of the triplen currents decreases from the third towards the fiftieth harmonic.

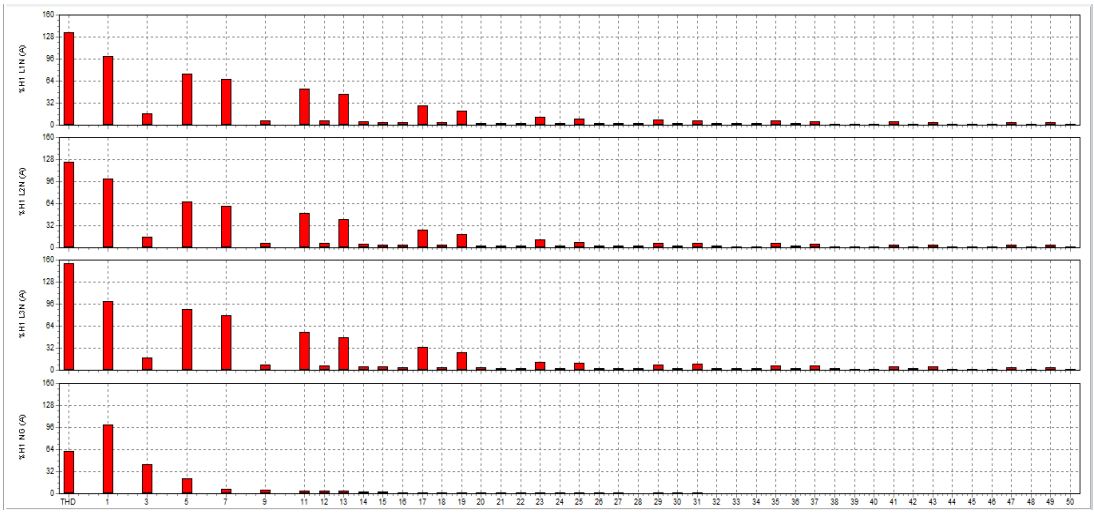

Figure 4.27 Drillship drilling drive transformer star-connected secondary-side winding measured current harmonic spectrum during the field measurement.

Table 4.7 now shows the amplitudes of the main harmonic components of the currents taken from the bar charts of Figure 4.27. Table 4.7 also shows the selected IEEE 519 STD current limits taken from Table 2.1 in Chapter Two. The fault current level at the delta-connected secondary-side winding of the drilling drive system transformer was assumed to be 11.17 kA (this value of short-circuit fault level was taken from the actual ABB electrical network short circuit calculations provided for this system.

The average value of the line current during the onboard field measurement was taken to be 170.1 A as it provides a stringent harmonic limit. The ratio between the short circuit current and the measured average line current at the star-connected secondary-side winding of the drilling drive system transformer is therefore 65.7 ($\frac{\text{Isc}}{\text{Il}} = \frac{11170}{170.1}$). This calculated value of the ratio I_{SC} / I_L for the system of 65.7 falls within the 50 < SCR < 100 range shown in Table 2.1. This means that the amplitudes of the current harmonics in Table 4.5 need to be analysed in relation to the current distortion limits related to the provided short-circuit ratio, 50 < SCR < 100 as seen in Table 2.1.

Of the triplen harmonics highlighted in yellow in Table 4.7, the amplitudes of the third (16.3%), twenty-seventh (2.3%), thirty-third (2%), thirty-ninth (1.7%) and the forty-fifth (1.5%) current harmonics are above the IEEE 519 STD current distortion limits of 10, 1.5 and 0.7 percent respectively, and the rest are

below each related current distortion limit. Table 4.7 also shows that the amplitudes of the fifth and seventh current harmonics are 76.5 and 68.8 percent and are above the IEEE 519 STD current distortion limit of 10 percent. The table also shows that the amplitudes of the eleventh (52.6%) and thirteenth (44.6%) current harmonics are above the current distortion limit of 4.5 percent.

Table 4.7 also shows that the seventeenth (28.9%) and the nineteenth (21.8%) current harmonics are above the IEEE 519 STD current distortion limit of 4 percent. The twenty-third (11.5%), twenty-fifth (9%), twenty-ninth (7.4%) and thirty-first (7.2%) average harmonic amplitudes for the entire field measurement were above the IEEE 519 STD current distortion limit of 1.5 percent. Finally, Table 4.6 shows the amplitudes of the thirty-fifth (6.3%), thirty-seventh (5.8%), forty-first (4.6%), forty-third (4.2%), forty-seventh (3.6%) and forty-ninth (3.7%) current harmonics are above the IEEE 519 STD current distortion limit of 0.7 percent. In conclusion, Table 4.7 presents the total harmonic current distortion for the entire duration of the measurement to be 137.8 percent, well above the IEEE 519 STD limit of 12 percent.

Figure 4.28 shows the current waveforms of the drilling drive system transformers' star-connected secondary-side winding taken during a certain period in time during the onboard measurement of Figure 4.24. Figure 4.28 also shows the distorted nature of the current waveforms and the currents are seen to be non-sinusoidal and to have very similar shapes to the currents seen in the simulation results of Figure 4.15. Even with the difference in load conditions between the simulation results and the field measurement, the shapes of the currents are similar and therefore it can be concluded that if simulation results were taken up to the fiftieth harmonic, they would have followed the same pattern as the field measurements.

Table 4.7 Amplitudes of specific harmonics taken from the current harmonic spectrum of the star winding of the drilling drive system transformer compared to the IEEE 519 STD current distortions limits.

HARMONICS	STAR SIDE - MEASUREMENTS	IEEE 519 STD CURRENT DISTORTION LIMIT (50> SCR <100)	I_{SC} / I_L (SCR)
3rd	16.3%	10%	Calculated short-circuit ratio (SCR) = 11170 / 170.1 = 65.7
5th	76.5%		
7th	68.8%		
9th	7.1%		
11th	52.6%	4.5%	
13th	44.6%		
15th	4.1%		
17th	28.9%	4%	
19th	21.8%		
21st	2.8%		
23rd	11.5%	1.5%	
25th	9%		
27th	2.3%		
29th	7.4%		
31st	7.2%		
33rd	2%		
35th	6.3%	0.7%	
37th	5.8%		
39th	1.7%		
41st	4.6%		
43rd	4.2%		
45th	1.5%		
47th	3.6%		
49th	3.7%		
THD	137.8%	12%	

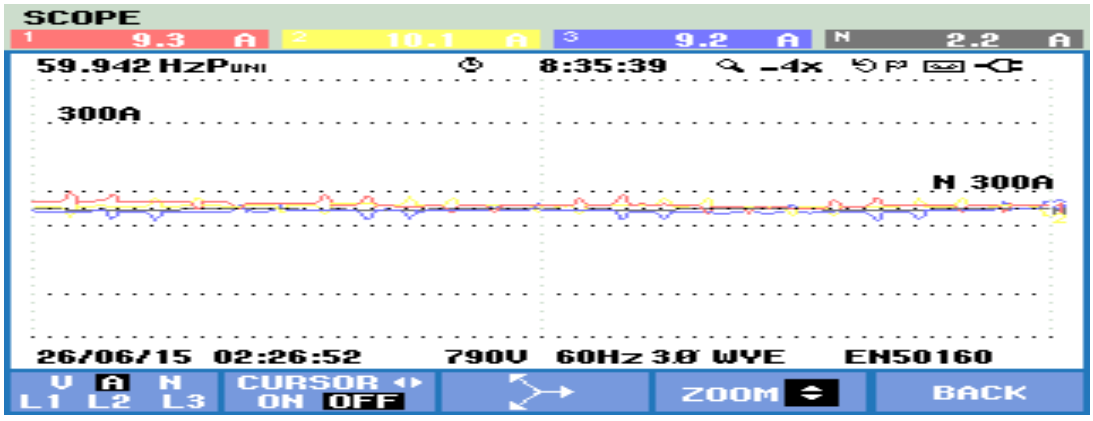

Figure 4.28 Drillship drilling drive transformer star-connected secondary-side winding measured current waveforms from a short period in time during the full field measurement.

4.4.3 Drillship 440V system measurements

The measurements have thus far focused on the harmonic distortion within the drillship drilling drive system, especially on the transformer secondary-side windings' current and voltage. Recall from Section 3.3 that there are three main 11 kV switchboards on the full drillship electrical network that are inter-linked to one another by two bus-couplers and supply various plants with similar loads as seen in Appendices G and H. The 440 V systems share the same point of common coupling (11 kV switchboards) with the harmonic generating systems, which are the thruster and drilling drive systems via 11 kV to 440 V transformers shown in Appendix H. Therefore, it is expected that the harmonics fed back into the electrical network will also have an impact on the 440 V systems as seen in the simulation results presented in Table 4.2 (b) in Section 4.3.4. The remainder of this section therefore now presents the amplitudes of the main harmonic components of the currents and voltages obtained from field measurements on the 440 V systems onboard the drillship.

Figure 4.29 shows the RMS average current and voltage profile on the secondary winding of FWD No.2 AC440V transformer (Appendix H) for the whole duration of the field measurement, which lasted seven hours, thirty-four minutes and ten seconds; the details of the drilling drive system load during the measurement was unknown. The top three graphs in Figure 4.29 represent the voltage profile for the whole duration of the measurement. The average RMS value of the line voltage for the entire duration was approximately 443.8 V. The bottom three graphs in Figure 4.29 show the varying load profile on the secondary winding of the FWD No.2 AC440V transformer for the duration of the measurement, represented by three line currents. The average RMS values of the current during field measurement shown in Figure 4.29, and the maximum line currents are approximately 15.3, 16.2 and 8.4 A. Based on the findings of high current unbalance in the line currents, it can be concluded that the FWD No.2 transformer supplies a lot of single-phase loads.

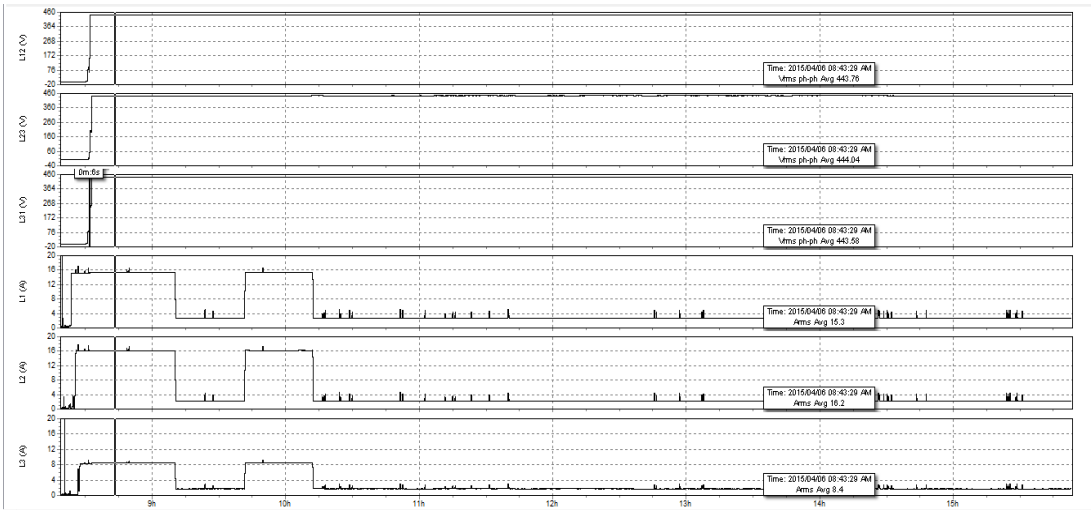

Figure 4.29 FWD No.2 AC440V transformer operating load condition (current and voltage profile) for the duration of seven hours, thirty-four minutes and ten seconds of the field measurement.

Figure 4.30 now shows the current and voltage harmonic spectrum taken from the FWD No.2 AC440V transformer (Transformer No.1 in Appendix H) secondary-side winding for the whole duration of the measurement. The bar charts of Figure 4.30 show the amplitudes of the main harmonic components of the current and voltage on FWD No.2 AC440V transformer secondary winding, from the fundamental up to the fiftieth harmonic. The blue coloured bar charts on top of Figure 4.30 show the amplitudes of the main harmonic components of the voltage, and the red coloured bar charts on the bottom of Figure 4.30 show the amplitudes of the main harmonic components of the current.

There is a presence of triplen harmonics in the voltages as seen on the three graphs on the top of Figure 4.30, as expected because the dominant loads on 440V system are single-phase loads, for example uninterruptible power supply and AC to DC power supplies. The amplitudes of all individual voltage harmonics shown in Figure 4.30 (blue colour bar charts) from the fundamental to the fiftieth are below the IEEE 519 STD voltage distortion limit of 5 percent in Table 2.2 of Chapter Two. In conclusion, Figure 4.30 presents the total harmonic voltage distortion for the entire duration of the measurement to be 9.4 percent and above the IEEE 519 STD voltage distortion limit of 8 percent.

There is also presence of triplen harmonics in the currents as seen on the three graphs on the bottom of Figure 4.30, as expected because the dominant loads on 440V system are single-phase loads, for example uninterruptible power supply and AC to DC power supplies. The third and fifth harmonics show high amplitudes on the white-phase (L2) as compared to the other phases, and a high unbalance in the currents as shown in Figure 4.30. The unbalances are seen on the third (11.3, 28.7 and 11%), the fifth (1.8, 8.4 and 4.2%) and also on the seventh (1.2, 0.6 and 1.1%) harmonics. The remainders of the harmonics are below 1 percent and after the twenty-first harmonic, their amplitudes are almost zero.

Figure 4.30 also presents the total harmonic current distortion in the three phases for the duration of the field measurement to be approximately 14.5, 32 and 14.3 percent. The white-phase (L2) current total harmonic distortion is higher than the red-phase (L1) and blue-phase (L3).

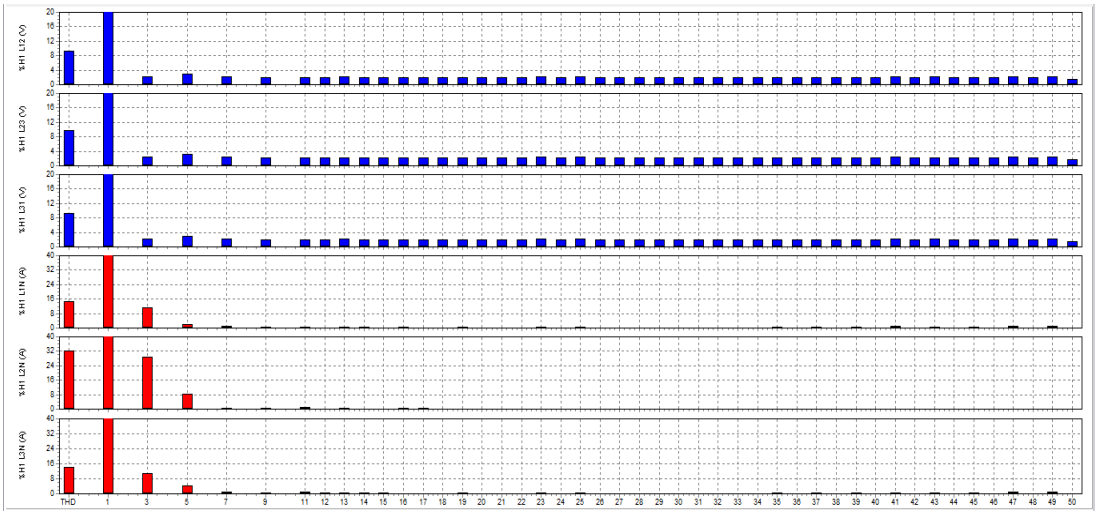

Figure 4.30 FWD No.2 AC440V transformer measured current and voltage harmonic spectrum during the field measurement.

Figure 4.31 now shows voltage waveforms of the FWD No.2 AC440V transformer secondary winding taken during a certain period in time during the onboard measurement of Figure 4.29. The recorded voltages are shown for a period of approximately four cycles of the full measurement. The average RMS value of the voltage at the secondary-side winding in Figure 4.31 was 443.81 V. The field measurement voltage waveforms of Figure 4.31 are similar to the

voltage waveforms of Graph 2 in the earlier simulation results shown in Figure 4.17.

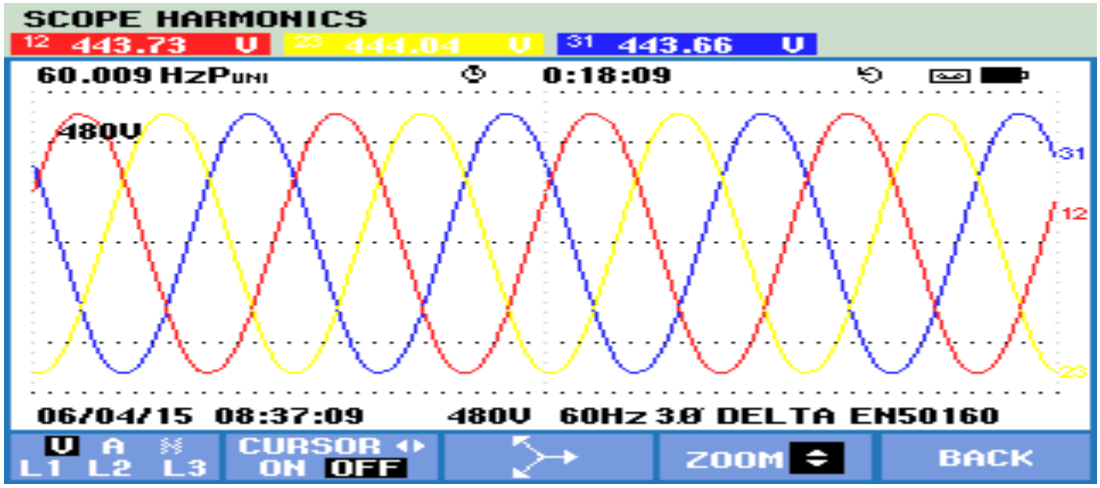

Figure 4.31 FWD No.2 AC440V transformer measured voltage waveforms from one four-cycle period during the full field measurement.

4.5 Conclusion

This chapter presented qualitative comparisons between simulation results obtained from the simplified drill ship electrical network model, and field measurements taken onboard the actual full drill ship electrical network, with both being assessed against the IEEE 519 STD voltage and current distortion limits. The comparison between the numerical simulated and field measured results was not direct, as the exact operating conditions during field measurements were unknown.

The original aim in this research project was to conduct a far more extensive measurement on board the drillship using the power quality meter and then develop a simulation model using the collected data on the actual drillship electrical network. Such further measurements would have firstly allowed the author to gain more extensive data on the actual operating conditions in the plant of the drill ship during typical load cycles, thereby allowing more direct comparison between field measurements and simulation studies. In addition, the availability of additional measurements would have allowed a greater number of operating conditions to be considered in such comparisons. However at a critical stage in the project work, the company that owned and

operated the drillship was forced to cease operations and hence, due to circumstances beyond the author's control, the full field measurement aspects of the study could not be completed as originally envisaged. Nevertheless, sufficient measurements were possible to establish the principle of using RTDS simulator as a tool for studying power quality issues and to determine the content of harmonics on an actual drillship electrical network.

The next chapter discusses the overall findings from the literature review, simulation results and field measurements of this study, and then presents the recommendations and conclusions of the study.

CHAPTER FIVE

Recommendations and Conclusion

5.1 Introduction

This dissertation has evaluated the impact of poor power quality on selected variables of a drillship electrical network. The results from the simulation model have shown that the largest pump motor caused power quality issues, during direct on line starts, at the busbar where it is connected as well as at the upstream 11 kV busbar, affecting other systems that share the same point of common coupling, which is the 11 kV busbar. The simulation results also showed the presence of harmonics caused by the front-end, six-pulse rectifiers of both the thruster and drilling drive systems. Even though the harmonics were measured up to the seventh harmonic, the simulation results confirmed the impact on the electrical network caused by running the variable speed drive. Subsequent field measurements presented in the dissertation then confirmed the level of harmonics on the actual drillship electrical network, even though the exact operating conditions were unknown during the recording of the data onboard the ship.

Therefore, the simulation results and field measurements provided the author with adequate information to validate the objectives of the study, which was to determine the impact of poor power quality on an island electrical network. The validity of using the RTDS real-time simulator to study poor power quality, especially harmonics and voltage sags, on a drillship electrical network was confirmed in this dissertation and therefore similar testing approaches can be followed for power quality issues on a bigger scale drillship or an island electrical network in the future.

This chapter now summarises the findings of the study and the conclusions of each chapter in the dissertation, and then presents some suggestions for further research studies in the area of power quality in the future.

5.2 Conclusions

5.2.1 Literature Review

Chapter One briefly discussed power quality and the impact of poor power quality on an offshore drillship electrical network. The chapter further introduced power electronics equipment as one of the main sources of voltage distortions, as such equipment draws non-sinusoidal currents from the supply. Poor power quality is not healthy for an electrical network, as it can cause electrical equipment to malfunction with disastrous consequences, especially on an offshore drilling ship. Finally, the chapter introduced the RTDS real-time simulator which was used to develop a detailed model of a reduced-scale representation of the drillship electrical network in order to determine the level of harmonics and voltage sags during the direct on line starting of large induction motors. The chapter also introduced the power quality meter which was used to take harmonic measurements on-board the actual drillship electrical network.

Chapter Two provided the theoretical background to the research topic by presenting a general view of power quality and harmonics in a complex electrical network that consists of linear and nonlinear loads. The chapter further discussed harmonic producing loads that are part of a drilling ship electrical network. The harmful effects of harmonics and their impact on electrical equipment were presented in this chapter. The chapter briefly discussed the properties of an induction motor and the characteristics of variable speed drives, as they are the major loads in a drilling ship electrical network. In conclusion, the chapter discussed the motivation behind the focus on the current and voltage harmonics in studying power quality on an electrical network.

Finally, the chapter presented the harmonic performance standards that are used to monitor and police utilities and end-users, by dictating the allowable harmonic current and voltage limits at the point of common coupling, which need to be adhered to. The IEEE 519 STD is the reference standard used in this dissertation, and the acceptable current and voltage harmonic limits associated with this standard were shown in Tables 2.1 and 2.2, respectively.

5.2.2 Research Methodology

Chapter Three presented an overview of the actual drilling ship electrical network that was simplified so that it could be modelled on the RTDS real-time simulator in order to study poor power quality issues, as voltage sag and harmonics are of interest in this dissertation. The chapter further discussed individual component models of plant that are simulated within the main RTDS simulator network solution (50µs solution time step) such as generators, transformers and induction motors, and plant that is simulated within the small time step RTDS simulator network solution (4µs solution time step) such as rectifiers, inverters and induction motor drive systems. The entire simulation model was parameterised so that the model represented the real drilling ship electrical network as closely as possible, and hence allowed it to be used to study voltage sags caused by direct on line starting of induction motors, and harmonics caused by the thruster and drilling drive system rectifiers. In conclusion, the chapter discussed the power quality meter used to take field measurements onboard the actual drilling ship electrical network.

Chapter Four presented the results of simulation studies using the reduced-scale drillship electrical network simulation model and field measurements taken onboard the actual drillship electrical network using a power quality meter. The results have shown the poor power quality issues, voltage sags on the electrical network, caused by direct on line starting of large induction motor pumps. The findings showed the impact of direct on line starts on the 440 V busbar where the pump motors are connected, and also on the upstream busbar 11 kV busbar. These voltage sags were shown to affect other induction motors on the 440V bus as well as other plant connected to the 11 kV busbar.

The results were also able to demonstrate the harmonic content on an island electrical network, generated by six-pulse rectifiers. The findings show that harmonics were recorded at both the 440 V and 11 kV busbars, because the six-pulse rectifiers are connected to the 11 kV busbars via transformers TR1 and TR3. The harmonic standards set the recommended allowable current and voltage distortions at the point of common coupling, and each component of plant needs to adhere to them, so that harmful harmonics do not have an impact on other pieces of plant.

Chapter Four also demonstrated the harmonic content on an actual drillship electrical network obtained by onboard measurements using the power quality meter. The measurements taken were to validate the simulation results, even though the actual drillship electrical network loads and operating conditions were unknown. Therefore, the author was not able to replicate the exact operating condition on the simulation model. Nevertheless, the findings of both sets of data (simulation studies and field measurements) are broadly consistent with one another, and therefore, the developed model can be used to study poor power quality on an offshore installation. Both the simulation results and field measurements were compared with current and voltage distortion limits set by harmonic standards (IEEE 519 STD) to see if the collected data do adhere to the limits. In the field measurements on the full drillship network, the point of common coupling was the secondary side of transformers and in the simulation results the point of common coupling was BUS1 (11 kV busbar).

The reduced-scale simulation model representing the drillship electrical system in these studies has the following limitations:

- The model was limited to one variable speed drive, due to capacity restrictions on the RTDS simulator, while the actual drillship drilling drive system consists of a minimum five DrawWorks, eight Mud Pumps and two Top Drive variable speed drives. Even though the single variable speed drive represented in the simulation model was able to demonstrate the harmonics generated by six-pulse rectifiers, and how a twelve-pulse system eliminates certain harmonics on the main supply side (11 kV), the reduced-scale model was unable to show the content of harmonics for the entire drilling drive system.
- There are six medium-voltage thruster drive system variable speed drives on an actual drillship electrical network, while only a single front-end rectifier section supplying a resistive load was included in the reduced-scale model to represent the steady-state operation of the thruster drives once the ship is in position. In normal operation, a minimum of three thruster drive systems operate to maintain the drillship in position.

- There are ten 440 V systems on an actual drillship electrical network, supplying induction motors (DOL starting), variable speed drives, three-phase UPSs and also single-phase (230 V) system loads. The reduced-scale simulation model only included three pump motors, each started using the direct on line starting technique.

Based on the limitations of the reduced-scale network model assumed in this study, there is a need of future research as an extension of this work. In conclusion, the last two sections provide some recommendations and future research in this field of power quality within an island network.

5.3 Recommendations

The study has developed a small-scale, proof of concept simulation model to study poor power quality on a drillship electrical network, especially voltage sag and harmonics. Both the simulation results and the field measurements have shown the presence of harmonics on the drillship electrical network. The literature review has presented information about accidents that have happened on offshore installations, resulting in the loss of lives, environmental and equipment damage where the cause of failures were unknown but pointed to malfunctioning of measuring instruments. Therefore it is recommended that the power quality standards that are in force for industries that operate plant connected to the national electrical grid should also be enforced, and adhered to with the same level of importance, on island networks such as drillships.

5.4 Future Research Work

The research in this study has confirmed the validity of using real-time simulation models to determine the content of harmonics on a drillship electrical network using generator, induction motor, transformer, rectifier and variable speed drive models.

The current and voltage harmonics calculated from the simulation results were limited to the seventh harmonic, and with the connection of external hardware to the model, a power quality meter can be used to measure harmonics up to

the fiftieth harmonic. Therefore, the simulation model of Figure 3.2 can be developed further by adding the analogue output channels (GTAO cards), and these components could be used to write signals to a twelve channel GTAO card via an optical port. The power quality meter could then be connected to measure voltage sag and harmonics up to the fiftieth harmonics. Therefore, the harmonic analysis from the simulation results would be more detailed and would allow for a truer comparison with the field measurements up to the fiftieth harmonic.

The simulation model developed in this study could only be used to identify if there are harmonics present in a drillship electrical network due to running a single variable speed drive. However, for an improved and more detailed representation of the drillship electrical network in the simulation model to study the harmonic content, the model should include the minimum number of variable speed drives on the drilling drive systems that are actually used for a normal operation, that is three thruster drive systems, and the 440 V system should include the minimum detail of the actual loads that are required during normal drilling operation. The limitation on the amount of equipment that can be added to the simulation model will depend on the capacity of the RTDS real-time simulator. However, significant advances in simulator technology have been made since the simulator hardware available to the author for this study was purchased, so such studies using more detailed representations of the system plant are now quite feasible with newer simulators.

REFERENCES

[1] M. Salam, “Power Quality Disturbances in a Test Distribution System: An Overview,” *Journal of Applied Science Research,* vol. 9, no. 1, pp. 560 - 566, 2013.

[2] American Bureau of Shipping, Guidance Notes on Control of Harmonics in Electrical Power System, Houston: American Bureau of Shipping, 2006.

[3] M. McGranaghan, “Power Quality Standards,” Electrical Contractor Magazine (Power Quality for the Electrical Contractor Course), 1998.

[4] IEEE Standard Board, IEEE 519 - 1992, New York: IEEE, 1993.

[5] M. Ramaite, “Study of Effects of Harmonics in the Design of Transmission Network Shunt Compensators: Network Simulation and Analysis Methods,” MSc, University of KwaZulu-Natal, Durban, 2013.

[6] D. Alberto and S. Leva, “Power Quality and Harmonic Analysis of End User Devices,” *Energies,* pp. 5453 - 5466, 2012.

[7] P. Swart, Power System Harmonics, Johannesburg: Mechanaut Systems, 2011.

[8] IEEE Standard Board, IEEE STD 519 - 2014, New York: IEEE, 2014.

[9] A. Soliman and M. Ahmad, “Electric Power Systems Harmonics - Identification and Measurement,” *Power Quality Analysis and Real Measurements Data,* pp. 3 - 68, 2011.

[10] T. Nzimande, “Voltage Dip Performance Analysis,” MSc, University of KwaZulu-Natal, Durban.

[11] A. Nassif, “On the Reliability of Real Measurement Data for Assessing Power Quality Disturbances,” *Power Quality Analysis and Real Measurements Data,* pp. 69 - 88, 2011.

[12] M. Bollen, Understanding Power Quality Problems: Voltage Dips and Interruptions, New York: IEEE Press, 2000.

[13] J. Arrillanga and N. Watson, Power System Harmonics, Christchurch: John Wiley & Sons Ltd, 2003.

[14] SQUARE D, “Power System Harmonics: Causes and Effects of Variable Frequency Drives,” SQUARE D Product Data Bulletin, Bulletin No. 8803PD9402, Raleigh, 1994.

[15] A. Rash, “Power quality and harmonics in the supply network: a look at common practices and standards,” in *Electrotechnical Conference*, Tel-Aviv, 1998.

[16] A. Hernedi, Taufik and M. Anwari, “Modeling and Simulation of 6-Pulse and 12-Pulse Rectifiers under Balanced and Unbalanced Conditions with Impacts to Input Current Harmonics,” in *Second Asia International Conference on Modelling & Simulation (IEEE Computer Society)*, 2000.

[17] S. Pyakuryal and M. Matin, “Harmonic Analysis for a 6-pulse Rectifier,” *IOSR Journal of Engineering,* vol. 3, no. 3, pp. 57 - 60, 2013.

[18] M. Shwehdi, “Harmonics effect in Industrial and University Environments,” *Power Quality Harmonics and Real Measurements Data,* pp. 211 - 234, 2011.

[19] I. Angela, “Power Quality Problems Generated by Line Frequency Coreless Induction Furnaces,” *Power Quality Harmonics Analysis and Real Measurements Data,* pp. 235 - 260, 2011.

[20] R. Ellis, “Power System Harmonics: A Reference Guide to Causes, Effects and Corrective Measures,” Allen-Bradley.

[21] F. De La Rosa, Harmonics and Power Systems, Boca Raton: CRC Press, 2006.

[22] J. Bird, Electrical Circuit Theory and Technology, Oxford: Newnes, 2003.

[23] B. Theraja and A. Theraja, A Textbook of Electrical Technology, New Delhi: S.Chad & Company Ltd, 2002.

[24] W. Grady and R. Gilleskie, “Harmonics and how they relate to power factor,” in *In Process of the EPRI Power Quality Issues & Opportunities Conference*, San Diego, 1993.

[25] L. Eguiluz, P. Lavandero and Manana, “Performance Analysis of a Three-phase Induction Motor under Non-sinusoidal and Unbalanced Conditions,” 19 December 2017. [Online]. Available: researchgate.net/citeseerx.ist.psu.edu. [Accessed 27 December 2017].

[26] C. Palhad, “An Investigation Into The Use of Real-Time Simulation and Hardware-In-Loop Techniques For Studying The Dynamic Performance of Adjustable Speed Drives Under Fault Conditions,” MSc, University of KwaZulu-Natal, Durban, 2015.

[27] M. H. Rashid, Power Electronics: Circuits, Devices and Applications, Upper Saddle River: Pearson Prentice Hall, 2004.

[28] E. Acha, O. Anaya-Lara, J. Parle and M. Madrigal, “Real-Time Simulator for Power Quality Disturbances Applications,” in *IEEE Harmonics and Quality of Power (Ninth International Conference)*, Orlando, 2000.

[29] RTDS Technologies, Real-Time Digital Simulation for the Power Industry: Manual Set, Winnipeg, Manitoba: RTDS Technologies, 2006.

[30] I. Evans and M. Richards, “The Price of Poor Power Quality,” in *2011 AADE National Technical Conference and Exhibition*, Houston, 2011.

[31] T. Parveen, G. F. Ledwich and E. Palmer, “Induction Motor Parameter Identification from Operational Data,” in *2007 Australasian Universities Power Engineering Conference (AUPEC 2007)*, Perth, 2007.

[32] M. Garcia-Gracia, N. El Halabi, A. Alonso and P. M. Comech, “Harmonic Distortion in Renewable Energy Systems: Capacitive Couplings,” *Power Quality Harmonics Analysis and Real Measurements Data,* pp. 261 - 278, 2011.

[33] J. Luszcz, “Voltage Harmonics Measuring Issues in Medium Voltage Systems,” *Power Quality Analysis and Real Measurements Data,* pp. 89 - 108, 2011.

[34] S. Mansingh, “The Impact of Energy Efficient Lighting on Power Networks,” MSc, University of KwaZulu-Natal, Durban, 2013.

[35] J. Lupin and P. Ferracci, “Power Quality: Monitoring and Innovation in PFC and Harmonic Filtering,” in *CIRED2001*, 2001.

[36] R. El-Mahayni, T. Dionise and D. Shipp, “Power Quality Investigation, Field Measurements and Harmonic Analysis to Improve Production at a New Chemical Products Facility,” in *Petroleum and Chemical Industry Technical Conference, 2012 Records Conference Papers Industry Applications Society 59th Annual IEEE*, Chicago, 2012.

[37] N. Watson, V. Gosbell, S. Perera and S. Elphick, “Power Quality Management,” in *EEA Conference & Exhibition*, Auckland, 2014.

[38] Y.-T. Huang, “Investigation the Performance of Generator Protection Relays Using a Real-Time Simulator,” MSc, University of KwaZulu-Natal, Durban, 2013.

[39] I. Evans, “Statement of Capabilities to the Oil & Drilling Industry Worldwide,” Harmonics Solution (Oil & Gas), Ras Al Khaimah, 2014.

[40] N. Golovanov, M. Lazaroiu and D. Zaninelli, “Power Quality Assessment in Small Scale Renewable Energy,” *Ernegies,* pp. 634 - 645, 2013.

[41] S. Nam and S. Kang, “Real-Time Estimation of Power System Frequency Using a Three-Level Discrete Fourier Transform Method,” *Energies,* pp. 79 - 93, 2014.

[42] G. Ye, M. Nijhuis, V. Cuk and J. Cobben, “Stochastic Residential Harmonic Source Modeling for Grid Impact Studies,” *Energies,* p. 372, 2017.

[43] M. Hermoso-Orzaez, A. Gago-Calderon and J. Rojas-Sola, “Power Quality and Energy Efficiency in the Pre-Evaluation of an Outdoor Lighting Renewal with Light-Emitting Diode Technology: Experimental Study and Amortization Analysis,” *Energies,* p. 836, 2017.

APPENDIXES

Appendix A

Induction motor parameters and simulation behaviours

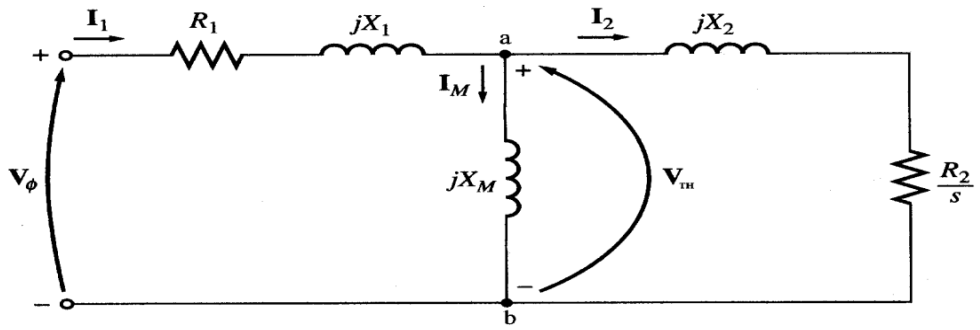

Figure A.1 Induction motor equivalent circuit

Drilling Drive motor parameters

Name plate data:

P = 1007kW

V = 690V

I = 1180A

pf = 0.81

N_R = 920RPM & N_S = 1200RPM

The values were calculated as follows:

$S = \sqrt{3}VI$

$S = \sqrt{3}$ x 690 x 1180A

$S = 1\,410\,235.768$ VA

$S = 1.410235768$ MVA

$P_m = P_w$

$$\omega_s = \frac{2\pi N}{60}$$

$$\text{Slip} = N_s - \frac{N_r}{N_s}$$

$$\text{Slip} = 1200 - \frac{920}{1200} = 0.23333333 = 23.3333333\%$$

$$\omega_s = \frac{2\pi \text{ x } 1200}{60} = 125.663706 \text{ rad/s}$$

Slip is 23.3333333%, so the motor is running at 76.6666667% of synchronous speed

$$\omega_r = 125.6637061 \text{ x } 0{,}766666667 = 96.34217468 \text{ rad/s}$$

$$Torque(\tau) = \frac{1\ 007\ 000}{96.34217468} = 10\ 452.3279 \text{ N.m}$$

No Load Test Calculations

No Load current = 420 A

$$P_{losses} = \sqrt{3}VIpf$$

$$P_{losses} = \sqrt{3} \text{ x } 690 \text{ x } 420 \text{ x} 0.81$$

$$P_{losses} = 406\ 578.1425 \text{ W}$$

$$P_{losses} = 406.5781425 \text{ kW}$$

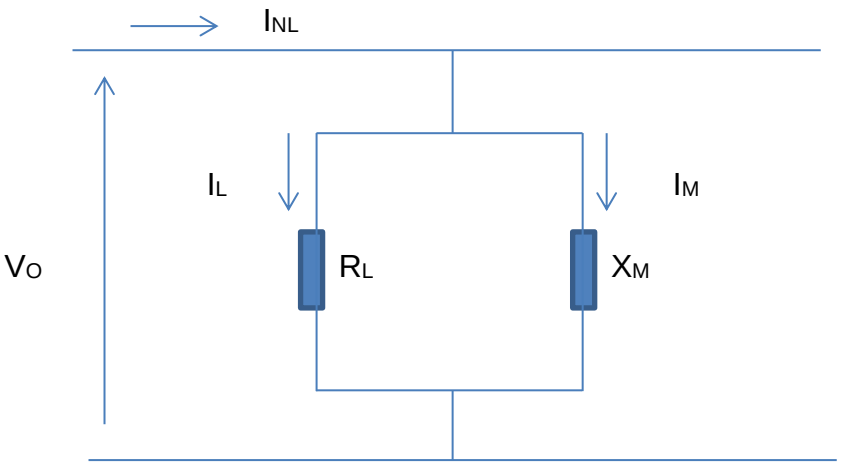

Figure A.2 Induction motor equivalent circuit – no load

$$P_O = \frac{3{V_o}^2}{R_L}$$

$$R_L = \frac{3{V_o}^2}{P_o}$$

$$R_L = \frac{3 \text{ x } (\frac{690}{\sqrt{3}})^2}{406\,578.1425}$$

$$R_L = 1.1709926 09\Omega$$

$$I_L = \frac{V_O}{R_L}$$

$$I_L = \frac{690/\sqrt{3}}{1.170992609}$$

$$I_L = 340.2\text{A}$$

$${I_O}^2 = {I_L}^2 + {I_M}^2$$

$$I_M = \sqrt{(420^2 - 340.2^2)}$$

$$I_M = 246.3005481 \text{ A}$$

$$X_M = \frac{V_O}{I_M}$$

$$X_M = \frac{690/\sqrt{3}}{246.3005481}$$

$$X_M = 1.617421028\ \Omega$$

Locked Rotor Test Calculations

$$I_{SC} = 1179.76 \text{ A}$$

$$V_{SC} = \frac{131.1\text{V}}{\sqrt{3}} = 75.69062029 \text{ V}$$

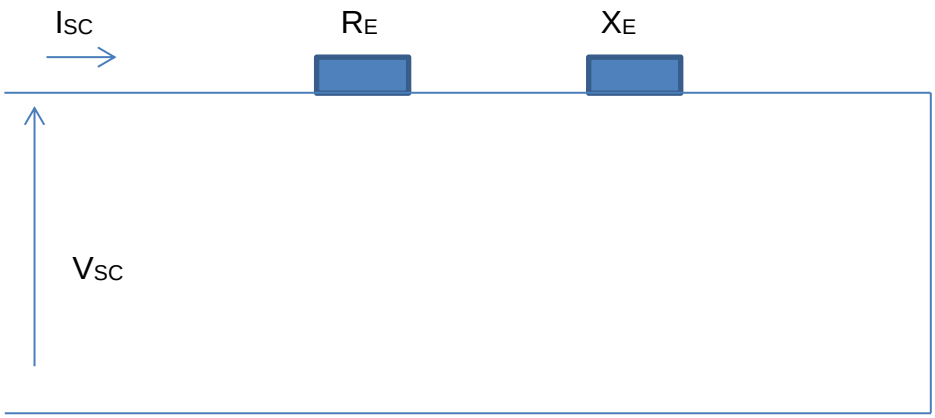

Figure A.3 Induction motor equivalent circuit – short circuit

$$P_{SC} = \sqrt{3}VIpf$$

$$P_{SC} = \sqrt{3}\text{ x } 131.1 \text{ x } 1179.76 \text{ x } 0.9$$

$$P_{SC} = 241\ 101.2687$$

$$P_{SC} = 241.1012687 \text{ Kw}$$

$$P_{SC} = 3{I_{SC}}^2 R_E$$

$$R_E = \frac{P_{SC}}{3{I_{SC}}^2}$$

$$R_E = \frac{241.1012687 \text{ x } 10^3}{3 \text{ x } 1179.76^2}$$

$$R_E = 0.05774187823\ \Omega$$

$$Z_E = \frac{V_{SC}}{I_{SC}}$$

$$Z_E = \frac{75.69062029}{1179.76}$$

$$Z_E = 0.06415764248\ \Omega$$

$$X_E = \sqrt{(0.06415764248^2 - 0.05774187823^2)}$$

$$X_E = 0.02796566801\ \Omega$$

DC Resistance Test Calculations

Assume Star Connection for the motor windings

$\mathrm{R_{DC}} = 0.01172\ \Omega$

$2r_1 = \mathrm{R_{DC}}$

$r_1 = \frac{\mathrm{R_{DC}}}{2}$

$r_1 = \frac{0.01172}{2}$

$r_1 = 0.00586\ \Omega$

$\mathrm{r_2} = \mathrm{R_E} - \mathrm{r_1}$

$\mathrm{r_2} = 0.05774187823 - 0.00586$

$\mathrm{r_2} = 0.05188187823\ \Omega$

Per Unit System

$V_{BASE} = \frac{690}{\sqrt{3}} = 398.3716857\ \mathrm{V}$

$I_{BASE} = 1180\ \mathrm{A}$

$Z_{BASE} = \frac{V_{BASE}}{I_{BASE}}$

$Z_{BASE} = \frac{398.3716857}{1180}$

$Z_{BASE} = 0.3376031235\ \Omega$

RTDS Electrical parameters

$\mathrm{r_a} = \mathrm{r_{1pu}} = \frac{\mathrm{r_1}}{\mathrm{Z_{BASE}}} = \frac{0.00586}{0.3376031235} = 0.01735765931\ \mathrm{pu}$

$\mathrm{jx_a} = \mathrm{X_{Epu}} = \frac{\mathrm{X_E}/2}{\mathrm{Z_{BASE}}} = \frac{0.02796566801/2}{0.3376031235} = 0.04141796397\ \mathrm{pu}$

$$jx_{mdO} = \frac{X_M}{Z_{BASE}} = \frac{1.617421028}{0.3376031235} = 4.790894738 \text{ pu}$$

$$r_{fd} = \frac{r_2}{Z_{BASE}} = \frac{0.05188187823}{0.3376031235} = 0.1536771274 \text{pu}$$

RTDS Mechanical parameters

$$H = \frac{5.48x10^{-9} \text{ x J x } {N_S}^2}{MVA_{rating}}$$

$$H = \frac{5.48x10^{-9} \text{ x } 36.252 \text{ x } 1200^2}{1.410235768}$$

$$H = 0.2028538695 \text{ s}$$

RTDS pu Torque

$$\text{RTDS Torque} = \frac{\text{Calculated MVA}}{N_S}$$

$$\text{RTDS Torque} = \frac{1\ 410\ 235.768}{125.6637061} = 11\ 222.29967 \text{ N. m}$$

$$1\text{pu} = 11\ 222.29967 \text{ N. m}$$

$$\text{Rated Torque} = 10\ 452.3279 \text{ N. m}$$

Rated pu RTDS Torque at full load current = 0.9313891273 pu

Appendix B

Pump 1 motor parameters

Name plate data:

P = 132kW

V = 440V

I = 209.3A

pf = 0.81

N_R = 1770RPM & N_S = 1800RPM

CALCULATIONS

S = √3 VI

S = √3 x 440 x 209.3

S = 155 508.023 VA

S = 0.159508023 MVA

$$P_m = T\omega_R$$

$$\omega_s = \frac{2\pi N}{60}$$

$$\text{Slip} = N_s - \frac{N_r}{N_s}$$

$$\text{Slip} = 1800 - \frac{1770}{1800} = 0.01666667 \ = 1.66666667\%$$

$$\omega_s = \frac{2\pi \text{ x } 1800}{60} = 188.4955592 \text{ rad/s}$$

Slip is 1.667%, so the motor is running at 98.333% of synchronous speed

$\omega_r = 188.4955592 \text{ x } 0.98333 = 185.3533383 \text{ rad/s}$

$Torque(\tau) = \frac{132\,000}{185.3533383} = 712.1533457 \text{ N.m}$

<u>No Load Test Calculations</u>

No Load current = 47.43 A

$P_{losses} = 3.280 \text{ kW}$

$P_O = \frac{3{V_o}^2}{R_L}$

$R_L = \frac{3{V_o}^2}{P_o}$

$R_L = \frac{3 \text{ x } (\frac{440}{\sqrt{3}})^2}{3280}$

$R_L = 59.02439024\ \Omega$

$I_L = \frac{V_O}{R_L}$

$I_L = \frac{440/\sqrt{3}}{59.02439024}$

$I_L = 4.303883825 \text{ A}$

${I_O}^2 = {I_L}^2 + {I_M}^2$

$I_M = \sqrt{(47.43^2 - 4.303883825^2)}$

$I_M = 47.23432527 \text{ A}$

$X_M = \frac{V_O}{I_M}$

$X_M = \frac{440/\sqrt{3}}{47.23432527}$

$$X_M = 5.378167614\ \Omega$$

Locked Rotor Test Calculations

$$I_{SC} = 209.40\ A$$

$$V_{SC} = \frac{88.47V}{\sqrt{3}} = 51.07817832\ V$$

$$P_{SC} = 8968\ W$$

$$P_{SC} = 3{I_{SC}}^2 R_E$$

$$R_E = \frac{P_{SC}}{3{I_{SC}}^2}$$

$$R_E = \frac{8968}{3\ x\ 209.40^2}$$

$$R_E = 0.06817434753\ \Omega$$

$$Z_E = \frac{V_{SC}}{I_{SC}}$$

$$Z_E = \frac{51.07817832}{209.40}$$

$$Z_E = 0.243926353\ \Omega$$

$$X_E = \sqrt{(0.243926353^2 - 0.06817434753^2)}$$

$$X_E = 0.2342057301\ \Omega$$

DC Resistance Test Calculations

Assume Star Connection for the motor windings

$$R_{DC} = 0.02637\ \Omega$$

$$2r_1 = R_{DC}$$

$$r_1 = \frac{R_{DC}}{2}$$

$$r_1 = \frac{0.02637}{2}$$

$$r_1 = 0.013185\ \Omega$$

$$r_2 = R_E - r_1$$

$$r_2 = 0.06817434753 - 0.013185$$

$$r_2 = 0.05498934753\ \Omega$$

Per Unit System

$$V_{BASE} = \frac{440}{\sqrt{3}} = 254.0341184\text{V}$$

$$I_{BASE} = 209.3\ \text{A}$$

$$Z_{BASE} = \frac{V_{BASE}}{I_{BASE}}$$

$$Z_{BASE} = \frac{254.031184}{209.3}$$

$$Z_{BASE} = 1.213732052\ \Omega$$

RTDS Electrical parameters

$$r_a = r_{1pu} = \frac{r_1}{Z_{BASE}} = \frac{0.013185}{1.213732052} = 0.01086318844\text{pu}$$

$$jx_a = X_{Epu} = \frac{X_E/2}{Z_{BASE}} = \frac{0.2342057301/2}{1.213732052} = 0.09648164507\text{pu}$$

$$jx_{mdO} = \frac{X_M}{Z_{BASE}} = \frac{5.378167614}{1.213732052} = 4.431099603\text{pu}$$

$$r_{fd} = \frac{r_2}{Z_{BASE}} = \frac{0.05498934753}{1.213732052} = 0.04530600262\text{pu}$$

RTDS Mechanical parameters

$$H = \frac{5.48x10^{-9} \text{ x J x } N_S{}^2}{MVA_{rating}}$$

$$H = \frac{5.48x10^{-9} \text{ x } 3 \text{ x } 1800^2}{0.159508023}$$

$$H = 0.3339368077 \text{ s}$$

RTDS pu Torque

$$\text{RTDS Torque} = \frac{\text{Calculated VA}}{N_S}$$

$$\text{RTDS Torque} = \frac{159\ 508.023}{188.4955592} = 846.2163442 \text{ N. m}$$

$$1\text{pu} = 846.2163442 \text{ N. m}$$

$$\text{Rated Torque} = 712.1533457 \text{ N. m}$$

Rated pu RTDS Torque at full load current = 0.8415736125 pu

Appendix C

Pump 2 motor parameters

Name plate data:

P = 160kW

V = 440V

I = 254.6 A

pf = 0.81

N_R = 1770RPM & N_S = 1800RPM

CALCULATIONS

S = √3 VI

S = √3 x 440 x 254.6

S = 194 031.2597 VA

S = 0.1940312597 MVA

$$P_m = T\omega_R$$

$$\omega_s = \frac{2\pi N}{60}$$

$$\text{Slip} = N_s - \frac{N_r}{N_s}$$

$$\text{Slip} = 1800 - \frac{1770}{1800} = 0.01666667 = 1.66666667\%$$

$$\omega_s = \frac{2\pi \text{ x } 1800}{60} = 188.4955592 \text{ rad/s}$$

Slip is 1.667%, so the motor is running at 98.333% of synchronous speed

$\omega_r = 188.4955592 \text{ x } 0.98333 = 185.3533383 \text{ rad/s}$

$Torque(\tau) = \frac{160\,000}{185.3533383} = 863.2161766 \text{ N.m}$

<u>No Load Test Calculations</u>

No Load current = 59.49 A

$P_{losses} = 3.760 \text{ kW}$

$P_O = \frac{3{V_o}^2}{R_L}$

$R_L = \frac{3{V_o}^2}{P_o}$

$R_L = \frac{3 \text{ x } (\frac{440}{\sqrt{3}})^2}{3760}$

$R_L = 51.4893617\Omega$

$I_L = \frac{V_O}{R_L}$

$I_L = \frac{440/\sqrt{3}}{51.4893617}$

$I_L = 4.933720482 \text{ A}$

${I_O}^2 = {I_L}^2 + {I_M}^2$

$I_M = \sqrt{(59.49^2 - 4.933720482^2)}$

$I_M = 59.28506137 \text{ A}$

$X_M = \frac{V_O}{I_M}$

$$X_M = \frac{440/\sqrt{3}}{59.28506137}$$

$$X_M = 4.284960031\Omega$$

Locked Rotor Test Calculations

$$I_{SC} = 254.64\ A$$

$$V_{SC} = \frac{82.78V}{\sqrt{3}} = 47.79305528\ V$$

$$P_{SC} = 9741\ W$$

$$P_{SC} = 3{I_{SC}}^2 R_E$$

$$R_E = \frac{P_{SC}}{3{I_{SC}}^2}$$

$$R_E = \frac{9741}{3\ x\ 254.64^2}$$

$$R_E = \ 0.05007593158\ \Omega$$

$$Z_E = \frac{V_{SC}}{I_{SC}}$$

$$Z_E = \frac{47.79305528}{254.64}$$

$$Z_E = 0.1876887185\ \Omega$$

$$X_E = \sqrt{(0.1876887185^2 - 0.05007593158^2)}$$

$$X_E = 0.1808852015\ \Omega$$

DC Resistance Test Calculations

Assume Star Connection for the motor windings

$$R_{DC} = 0.01551\ \Omega$$

$$2r_1 = R_{DC}$$

$$r_1 = \frac{R_{DC}}{2}$$

$$r_1 = \frac{0.01551}{2}$$

$$r_1 = 0.007755\ \Omega$$

$$r_2 = R_E - r_1$$

$$r_2 = 0.05007593158 - 0.007755$$

$$r_2 = 0.04232093158\ \Omega$$

Per Unit System

$$V_{BASE} = \frac{440}{\sqrt{3}} = 254.0341184\text{V}$$

$$I_{BASE} = 254.64\ \text{A}$$

$$Z_{BASE} = \frac{V_{BASE}}{I_{BASE}}$$

$$Z_{BASE} = \frac{254.031184}{254.64\ \text{A}}$$

$$Z_{BASE} = 0.9976206348\ \Omega$$

RTDS Electrical parameters

$$r_a = r_{1pu} = \frac{r_1}{Z_{BASE}} = \frac{0.007755}{0.9976206348} = 0.01086318844\text{pu}$$

$$jx_a = X_{Epu} = \frac{X_E/2}{Z_{BASE}} = \frac{0.1808852015/2}{0.9976206348} = 0.09065830998\ \text{pu}$$

$$jx_{mdO} = \frac{X_M}{Z_{BASE}} = \frac{4.284960031}{0.9976206348} = 4.295179832\text{pu}$$

$$r_{fd} = \frac{r_2}{Z_{BASE}} = \frac{0.04232093158}{0.9976206348} = 0.0424218687\text{pu}$$

RTDS Mechanical parameters

$$H = \frac{5.48x10^{-9} \text{ x J x } N_S{}^2}{MVA_{rating}}$$

$$H = \frac{5.48x10^{-9} \text{ x } 3 \text{ x } 1800^2}{0.1940312597}$$

$$H = 0.3385755476 \text{ s}$$

RTDS pu Torque

$$\text{RTDS Torque} = \frac{\text{Calculated VA}}{N_S}$$

$$\text{RTDS Torque} = \frac{194\ 031.2597}{188.4955592} = 1029.367803 \text{N. m}$$

$$1\text{pu} = 1029.367803 \text{ N. m}$$

$$\text{Rated Torque} = 863.2161766 \text{ N. m}$$

Rated pu RTDS Torque at full load current = 0.8385886695 pu

Appendix D

Pump 3 motor parameters

Name plate data:

P = 450 kW

V = 440 V

I = 690.6 A

pf = 0.81

N_R = 1786RPM & N_S = 1800RPM

CALCULATIONS

S = √3 VI

S = √3 x 440 x 690.6

S = 526 307.8866 VA

S = 0.5263078866 MVA

$$P_m = T\omega_R$$

$$\omega_s = \frac{2\pi N}{60}$$

$$\text{Slip} = N_s - \frac{N_r}{N_s}$$

$$\text{Slip} = 1800 - \frac{1786}{1800} = 0.00777778 = 0.77777778\%$$

$$\omega_s = \frac{2\pi \text{ x } 1800}{60} = 188.4955592 \text{ rad/s}$$

Slip is 0.77777778%, so the motor is running at 99.2222222% of synchronous speed

$$\omega_r = 188.4955592 \text{ x } 0.992222222 = 187.0294826 \text{ rad/s}$$

$$Torque(\tau) = \frac{450\ 000}{187.0294826} = 2406.037774 \text{ N.m}$$

No Load Test Calculations

No Load current = 175.42 A

$$P_{losses} = 8941 \text{ W}$$

$$P_O = \frac{3{V_o}^2}{R_L}$$

$$R_L = \frac{3{V_o}^2}{P_o}$$

$$R_L = \frac{3 \text{ x } (\frac{440}{\sqrt{3}})^2}{8941}$$

$$R_L = 21.65305894\ \Omega$$

$$I_L = \frac{V_O}{R_L}$$

$$I_L = \frac{440/\sqrt{3}}{21.65305894\ \Omega}$$

$$I_L = 11.7320199 \text{ A}$$

$${I_O}^2 = {I_L}^2 + {I_M}^2$$

$$I_M = \sqrt{(175.42^2 - 11.7320199^2)}$$

$$I_M = 175.0272439 \text{ A}$$

$$X_M = \frac{V_O}{I_M}$$

$$X_M = \frac{440/\sqrt{3}}{175.0272439\ A}$$

$$X_M = 1.451397581\ \Omega$$

Locked Rotor Test Calculations

$$I_{SC} = 689.90\ A$$

$$V_{SC} = \frac{75.89V}{\sqrt{3}} = 43.81511193\ V$$

$$P_{SC} = 25860\ W$$

$$P_{SC} = 3{I_{SC}}^2 R_E$$

$$R_E = \frac{P_{SC}}{3{I_{SC}}^2}$$

$$R_E = \frac{25860}{3\ x\ 689.90^2}$$

$$R_E = \ 0.01811068913\ \Omega$$

$$Z_E = \frac{V_{SC}}{I_{SC}}$$

$$Z_E = \frac{43.81511193}{689.90}$$

$$Z_E = 0.06350936647\ \Omega$$

$$X_E = \sqrt{(0.06350936647^2 - 0.01811068913^2)}$$

$$X_E = 0.0608723465\ \Omega$$

DC Resistance Test Calculations

Assume Star Connection for the motor windings

$$R_{DC} = 0.003674\ \Omega$$

$$2r_1 = \mathrm{R_{DC}}$$

$$r_1 = \frac{\mathrm{R_{DC}}}{2}$$

$$r_1 = \frac{0.003674\ \Omega}{2}$$

$$r_1 = \ 0.001837\ \Omega$$

$$\mathrm{r_2 = R_E - r_1}$$

$$\mathrm{r_2 = 0.01811068913 - \ 0.001837}$$

$$\mathrm{r_2 = 0.01627368913\ \Omega}$$

Per Unit System

$$V_{BASE} = \frac{440}{\sqrt{3}} = 254.0341184\mathrm{V}$$

$$I_{BASE} = 690.6\ \mathrm{A}$$

$$Z_{BASE} = \frac{V_{BASE}}{I_{BASE}}$$

$$Z_{BASE} = \frac{254.031184}{690.6}$$

$$Z_{BASE} = \ 0.3678455234\ \Omega$$

RTDS Electrical parameters

$$\mathrm{r_a = r_{1pu} = \frac{r_1}{Z_{BASE}} = \frac{0.001837}{0.3678455234} = 0.004993944151pu}$$

$$\mathrm{jx_a = X_{Epu} = \frac{X_E/2}{Z_{BASE}} = \frac{0.0608723465/2}{0.3678455234} = 0.0827417253\ pu}$$

$$\mathrm{jx_{mdO} = \frac{X_M}{Z_{BASE}} = \frac{1.451397581}{0.3678455234} = 3.945671454pu}$$

$$\mathrm{r_{fd} = \frac{r_2}{Z_{BASE}} = \frac{0.01627368913}{0.3678455234} = 0.04424055234pu}$$

RTDS Mechanical parameters

$$H = \frac{5.48x10^{-9} \text{ x J x } N_S{}^2}{MVA_{rating}}$$

$$H = \frac{5.48x10^{-9} \text{ x } 15 \text{ x } 1800^2}{0.5263078866}$$

$$H = 0.5060307983 \text{ s}$$

RTDS pu Torque

$$\text{RTDS Torque} = \frac{\text{Calculated VA}}{N_S}$$

$$\text{RTDS Torque} = \frac{526\ 307.8866}{188.4955592} = 2792.150058 \text{ N. m}$$

$$1\text{pu} = 2792.150058 \text{ N. m}$$

$$\text{Rated Torque} = 863.2161766 \text{ N. m}$$

Rated pu RTDS Torque at full load current = 0.8617150654 pu

Appendix E

Simplified Drillship network Distribution Transformer parameters

11kV/440V system Transformer parameters

NAME	DESCRIPTION	VALUE
Trf:	Transformer Name:	TRF1
YD1:	Winding #1 connection:	Delta
YD2:	Winding #2 connection:	Y
type:	Transformer Model Type:	Linear
Tmva:	Transformer rating (3phase)	2.8MVA
f:	Base frequency:	60Hz
xl:	Leakage inductance of Tx:	0.1412pu
VL1:	Base primary voltage (L-L RMS)	11kV
VL2:	Base primary voltage (L-L RMS)	0.45kV

11kV/725V/725V Drilling Drive system Transformer parameters

NAME	DESCRIPTION	VALUE
Trf:	Transformer Name:	Drilling Transformer (T1)

YD1:	Winding #1 connection:	Delta
YD2:	Winding #2 connection:	Delta
YD3:	Winding #3 connection:	Star
type:	Transformer Model Type:	Linear
Tmva:	Transformer rating (3phase)	6.5MVA
f:	Base frequency:	60Hz
xl:	Leakage inductance of Tx:	0.1pu
VL1:	Base primary voltage (L-L RMS)	11kV
VL2/3:	Base primary voltage (L-L RMS)	0.725kV

11kV/1725V/1725V Thruster Drive system Transformer parameters

NAME	**DESCRIPTION**	**VALUE**
Trf:	Transformer Name:	Drilling Transformer (T1)
YD1:	Winding #1 connection:	Delta
YD2:	Winding #2 connection:	Delta
YD3:	Winding #3 connection:	Star
type:	Transformer Model Type:	Linear
Tmva:	Transformer rating (3phase)	6.5MVA
f:	Base frequency:	60Hz
xl:	Leakage inductance of Tx:	0.1pu
VL1:	Base primary voltage (L-L RMS)	11kV
VL2/3:	Base primary voltage (L-L RMS)	1.725kV

Appendix F

Generator Parameters

Data Sheet:

Apparent Output Power (S) = 8750 kVA

Output Voltage = 11 000 V

Output Current = 459 A

Output Frequency = 60 Hz

Power Factor (pf) = 0.80

Calculations

Base MVA = 100MVA

Base Voltage = 11kV

Real Power (P) = S x pf

Real Power (P) = 8750 kVA x 0.80 = 7 000 kW

Reactive Power (Q) = $\sqrt{(8750^2 - 7000^2)}$ = 5 250 kVAr

Zero Sequence Impedance (Z0)

$Z0_{pu}$ = 0.053 + j0.9368 pu = 0.93834∟86.72°

$Z_{pu} = \frac{kVAbase\ x\ Z}{1000\ x\ kV^2}$

$0.93834 = \frac{100000\ x\ Z}{1000\ x\ 11\text{^}2}$

Z0 = 1.1353914 Ω

Positive Sequence Impedance (Z1)

Z1 = 0.1143 + j1.63

Z1 = 1.63∟85.99°

Z_{pu} = $\frac{kVAbase\ x\ Z}{1000\ x\ kV^2}$

1.63 = $\frac{100000\ x\ Z}{1000\ x\ 11\text{^}2}$

Z1 = 1.9723 Ω

Generator selected parameters

NAME	DESCRIPTION	VALUE
Name:	Source Name:	ENGINE1/ENGINE2
Type:	Source Impedance Type:	R-R//L
ZSeq:	Zero Sequence Included:	Yes
ZType:	Zero Sequence Impedance Type:	R-L
Es:	Initial Source Mag (L-L, RMS):	11kV
F0:	Initial Frequency:	60Hz
Ph:	Initial Phase:	0 deg.
Pt:	Specified Initial Real power (+ve=out)	7MW
Qt:	Specified Initial Reactive power (+ve=out)	5.25MVAR
Z1:	Positive Sequence Impedance:	1.979Ω
Phi1:	Positive Sequence Impedance phase angle:	85.94 degrees
Z0:	Zero Sequence Impedance:	1.137Ω
Phi0:	Zero Sequence Impedance phase angle:	86.63 degrees

Appendix G

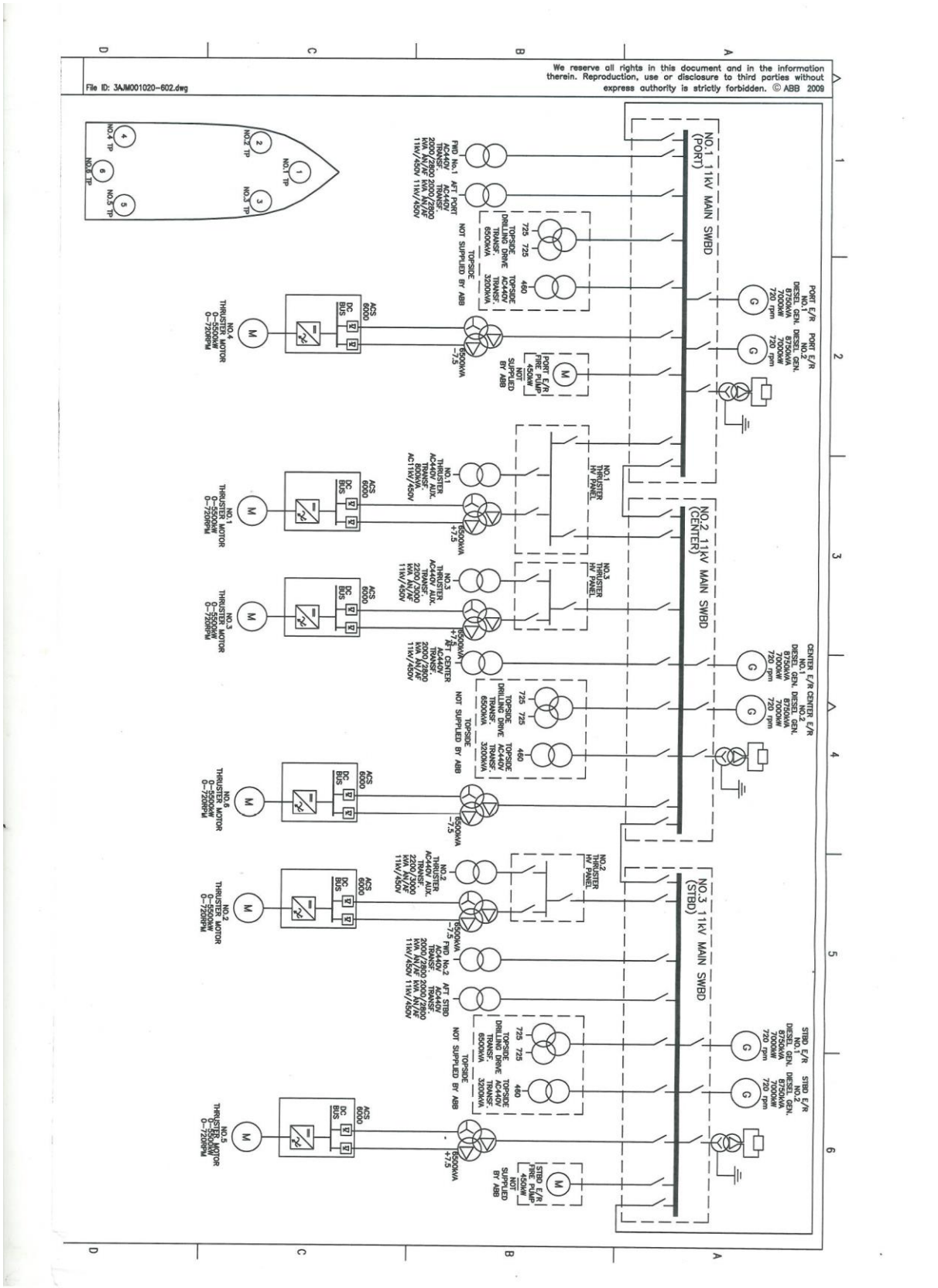
We reserve all rights in this document and in the information therein. Reproduction, use or disclosure to third parties without express authority is strictly forbidden. © ABB 2009
File ID: 3AJM001020-602.dwg
NO.1 11KV MAIN SWBD (PORT)
NO.2 11KV MAIN SWBD (CENTER)
NO.3 11KV MAIN SWBD (STBD)
PORT E/R NO.1 DIESEL GEN. 8750kVA 7000kW 720 rpm
PORT E/R NO.2 DIESEL GEN. 8750kVA 7000kW 720 rpm
CENTER E/R NO.1 DIESEL GEN. 8750kVA 7000kW 720 rpm
CENTER E/R NO.2 DIESEL GEN. 8750kVA 7000kW 720 rpm
STBD E/R NO.1 DIESEL GEN. 8750kVA 7000kW 720 rpm
STBD E/R NO.2 DIESEL GEN. 8750kVA 7000kW 720 rpm
FWD No.1 AFT PORT AC440V TRANSF. 2200/2800 kVA AN/AF 11kV/450V
TOPSIDE DRILLING DRIVE TRANSF. 8500kVA
TOPSIDE AC440V TRANSF. 3200kVA
NOT SUPPLIED BY ABB
PORT E/R FIRE PUMP 450kW
NO.1 THRUSTER HV PANEL
NO.1 THRUSTER AC440V AUX. TRANSF. AC110V/450V
NO.3 THRUSTER HV PANEL
NO.3 THRUSTER AC440V AUX. TRANSF.
FWD CENTER AFT CENTER TRANSF. 2000/2800 kVA AN/AF 11kV/450V
NO.2 THRUSTER HV PANEL
NO.2 THRUSTER AC440V AUX. TRANSF.
FWD No.2 AFT STBD TRANSF. 2200/3000 kVA AN/AF 11kV/450V
STBD E/R FIRE PUMP 450kW
ACS 6000 DC BUS
NO.1 THRUSTER MOTOR 0~5500kW 0~720RPM
NO.2 THRUSTER MOTOR 0~5500kW 0~720RPM
NO.3 THRUSTER MOTOR 0~5500kW 0~720RPM
NO.4 THRUSTER MOTOR 0~5500kW 0~720RPM
NO.5 THRUSTER MOTOR 0~5500kW 0~720RPM
NO.6 THRUSTER MOTOR 0~5500kW 0~720RPM
NO.1 TP
NO.2 TP
NO.3 TP
NO.4 TP
NO.5 TP
NO.6 TP

Appendix H

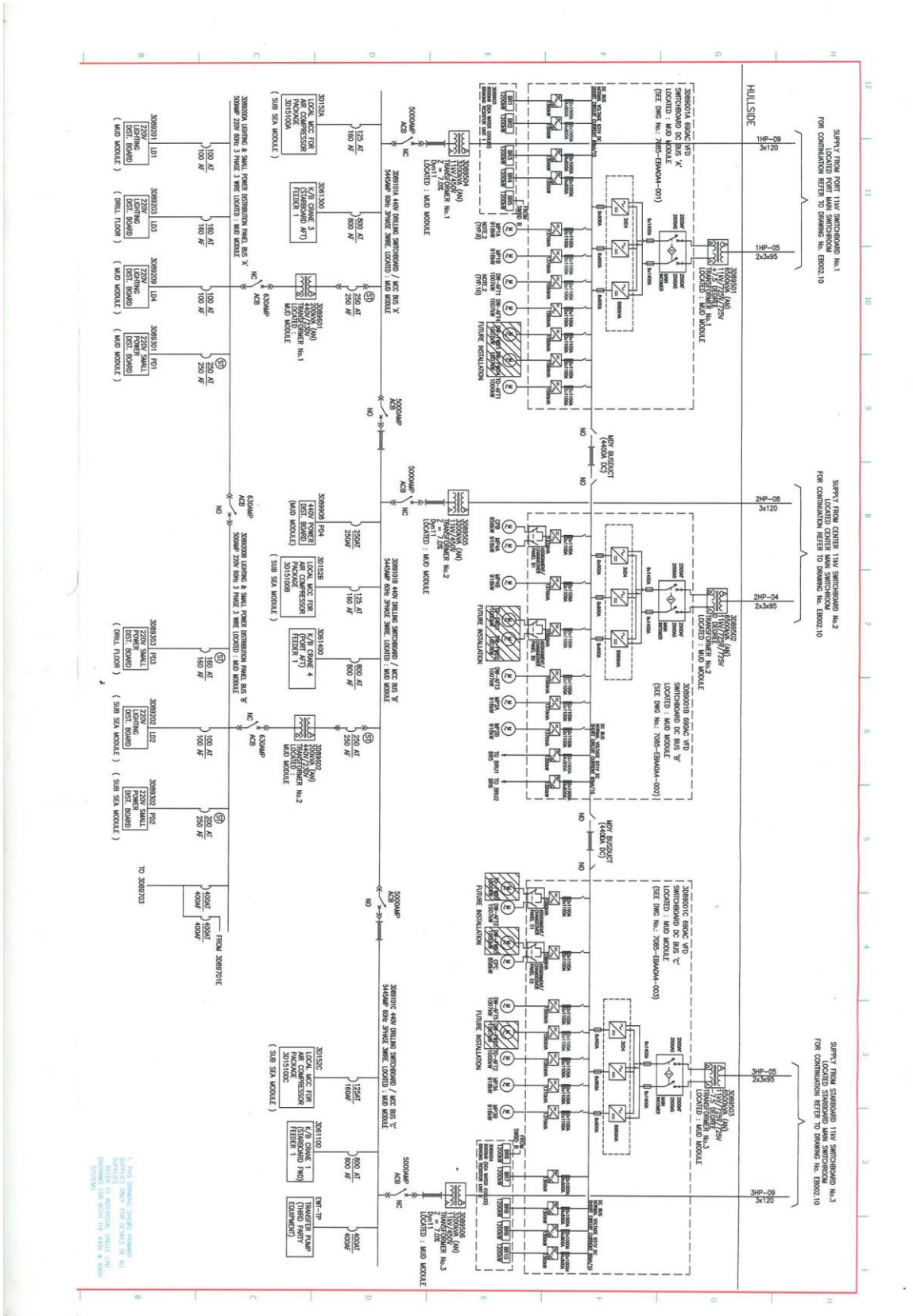

Appendix I

Schematic diagram of the Research Methodology – Steps of investigation

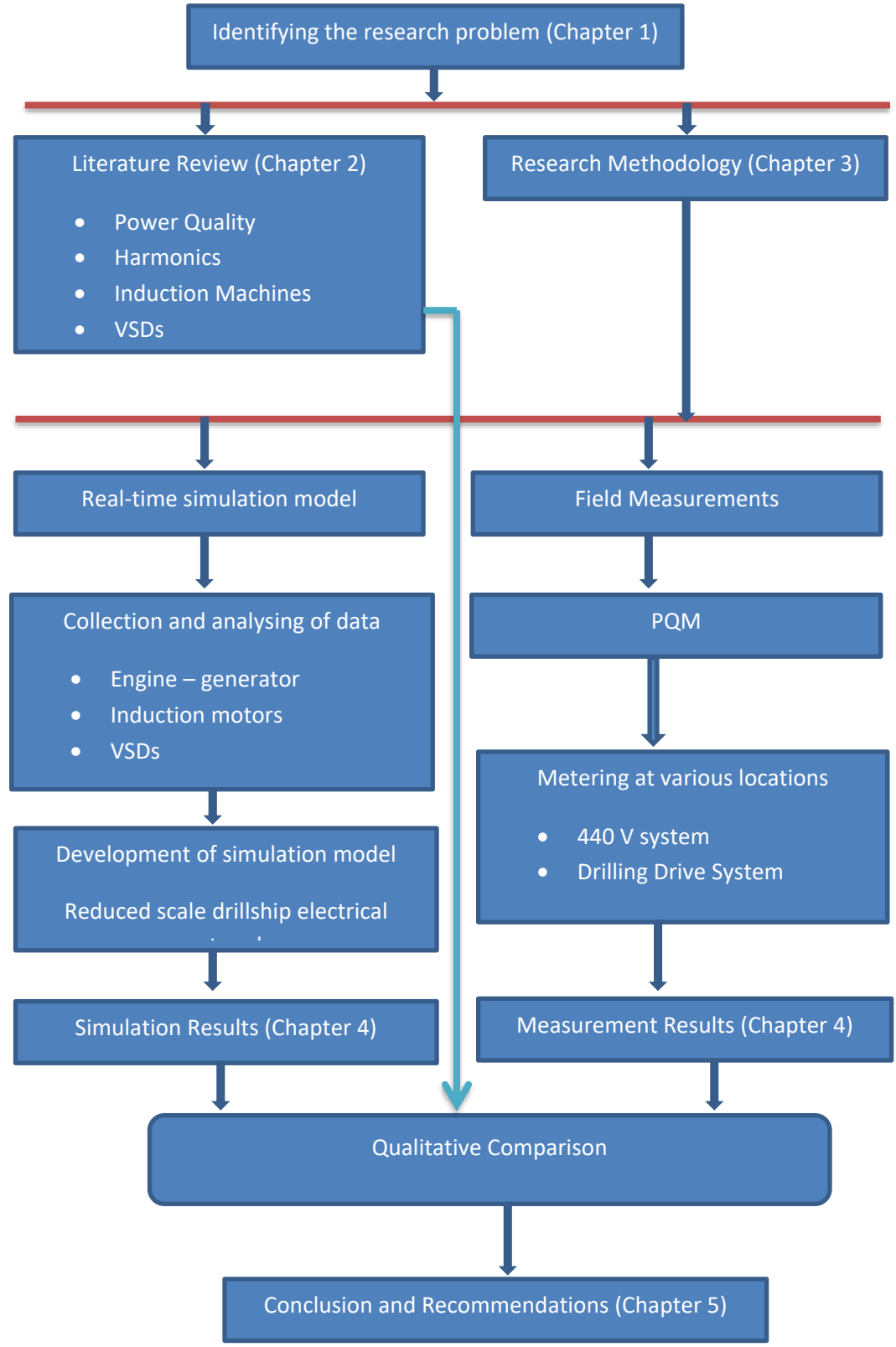

Appendix J

Summary of steps taken during simulation:

Drillship equipment	**Parameters**	**Action**	**Measured variables**
Engine 1	Generator sliders – Figure 4.1. Phase, frequency and voltage	Set the phase slider to 0.0°, the frequency to 60Hz and the generator output voltage to 11kV. This generator output is fixed so that it has no influence on power quality issues. Run the generator to measure open circuit voltage.	Voltage The shape of the waveform – even though it is not a measured variable.
Pump motors (P1 to P3) and inverter motor	Simulation model switches and sliders of Figure 4.2 and 4.3. Switches = BRK1MB, BRK2MB, BRK3MB and BLKinvVCI. Sliders = Load Torque and SetPtFreq.	• Start P1 using switch BRK1MB. • Start P2 using switch BRK2MB. • Start P3 using switch BRK3MB. Set the inverter sliders to 0. • Start the inverter using switch BLKinvVCI. Set the load torque slider to 0.74 and the frequency slider to 60Hz.	Voltage Current harmonics Voltage harmonics The shape of the waveform – even though it is not a measured variable.